Title
Entanglement, Complexity, and Holography

Author
Moosa, Mudassir

Publication Date
2018

Peer reviewed|Thesis/dissertation

Entanglement, Complexity, and Holography

by

Mudassir Moosa

A dissertation submitted in partial satisfaction of the

requirements for the degree of

Doctor of Philosophy

in

Physics

in the

Graduate Division

of the

University of California, Berkeley

Committee in charge:

Professor Raphael Bousso, Chair
Professor Yasunori Nomura
Professor K. Birgitta Whaley

Spring 2018

Entanglement, Complexity, and Holography

Abstract

Entanglement, Complexity, and Holography

by

Mudassir Moosa

Doctor of Philosophy in Physics

University of California, Berkeley

Professor Raphael Bousso, Chair

It was found, by studying black holes, that the compatibility of the theory of gravity and the laws of quantum mechanics demands that the universe must act like a hologram. That is, all the information inside a region of the universe should be encoded on a so-called holographic screen of one-lesser dimension. This is termed the holographic principle. In a generic spacetime, such as an expanding universe, holographic screens depend on the choice of an observer, which is consistent with the notion that the observer is part of the system in cosmology. In the first part of this dissertation, we study the observer-dependence of holographic screens. This will help us understand how the fundamental description of the universe depends on the choice of the observer. Furthermore, we study the dynamics of the holographic screens and their geometry in the first part of this dissertation.

An example where the holographic principle is manifest is the AdS-CFT correspondence. This correspondence connects quantum information quantities, like entanglement and complexity, to geometric quantities, like area and volume, respectively. In the second and the third part of this dissertation, we use the AdS-CFT correspondence as a tool to calculate the entanglement entropy and the computational complexity of a quenched CFT state. Studying the time evolution of the entanglement entropy following a quantum quench teaches us how a CFT state thermalizes. On the other hand, studying the time evolution of the computational complexity allows us to check the validity of various recent conjectures involving black holes and complexity.

To my parents,

Bilqis Moosa
&
Muhammad Moosa,

for their constant support
and encouragement.

Contents

Contents **ii**

List of Figures **iv**

1 Introduction **1**
1.1 Holography in General Spacetimes 3
1.2 Entanglement, Quantum Fields, and Geometry 4
1.3 Complexity and Geometry 7

I Holography in General Spacetimes **9**

2 Dynamics and Observer-Dependence of Holographic Screens **10**
2.1 Introduction 10
2.2 Kinematics of Holographic Screens 14
2.3 Dynamics and Observer-Dependence 18
2.4 Examples of Holographic Screens 23

3 Non-relativistic Geometry of Holographic Screens **34**
3.1 Introduction 34
3.2 Holographic Screens 36
3.3 Newton-Cartan Geometry 39
3.4 Newton-Cartan Geometry on Holographic Screens 42
3.5 Derivation of P_A, Θ_{AB}, and $\mathcal{E}^0$ from Gravitational Action 46
3.6 Discussion 48

II Entanglement and Holography **50**

4 Entanglement Tsunami in (1+1)-Dimensions **51**
4.1 Introduction 51
4.2 Setup and Review 52
4.3 Large-c CFT Calculation 58

4.4 Entanglement Tsunami 63
4.5 Discussion 66

5 Dynamics of the Area Law of Entanglement Entropy 68
5.1 Introduction 68
5.2 Holographic Calculation 71
5.3 Field Theory Calculation 78
5.4 Conclusions 87

III Computational Complexity and Holography 89

6 Evolution of Complexity Following a Global Quench 90
6.1 Introduction 90
6.2 Setup 92
6.3 Calculations 94
6.4 Discussion 102

7 Divergences in the Rate of Complexification 104
7.1 Introduction 104
7.2 Holographic Setup 106
7.3 Complexity using CA Conjecture 109
7.4 Complexity using CV Conjecture 114
7.5 Discussion 115

A Parallel Transport of Null Vectors 117

B Cross-focusing Equations 118

C Derivation of Screen Equations 120
C.1 $T_{ab}n^a k^b$ Equation 120
C.2 $T_{ab}n^a h^b$ Equation 120
C.3 $T_{ab}n^a q^b{}_c$ Equations 121

D Details of the Holographic Calculations in Ch. (5) 123
D.1 HRT Surface Calculation 123
D.2 Perturbative Solution of Einstein-Scalar Equations 124

E Useful Integral for Ch. (5) 127

Bibliography 128

List of Figures

2.1 *Left:* a future holographic screen, H (blue line). Points represent topological spheres. The dashed lines are 2+1 dimensional null slices N orthogonal to the leaves σ of H (blue dots), along the direction k^a. H can be constructed leaf by leaf, using a "zig-zag" procedure. First, deform the leaf $\sigma(R)$ along the other orthogonal null vector, l, by an infinitesimal step $\alpha(R, \vartheta, \varphi)l^a$ (green downward arrow). The function $\alpha < 0$ can be chosen arbitrarily; it reflects a kind of observer-dependence of the holographic screen. Thus one obtains a new surface $\bar{\sigma}(R+dR)$ (red), and from it, a new null slice $N(R + dR)$ orthogonal to $\bar{\sigma}$. The next leaf $\sigma(R + dR)$ is the surface of maximal area on $N(R + dR)$, at some infinitesimal distance βk^a along N from $\bar{\sigma}$ (orange arrow). *Right:* a past holographic screen (same color coding). In this case, $\alpha > 0$; the area of the leaves grows towards the future. We show the same construction, with only one spatial direction suppressed to offer a different visualization. The leaves $\sigma(R)$ are by definition the maximal area cross-sections of $N(R)$, despite what the figure shows. 12

2.2 Penrose diagrams for a spatially flat FRW universe dominated by matter (left) and radiation (middle). The right diagram is an approximation to de Sitter spacetime; it contains a fluid with positive energy and equation of state close to that of vacuum energy. To construct a past holographic screen H, we consider the past light-cones (dotted lines) of a comoving observer at $r = 0$ (left edge). The surfaces of maximum area on each of these light cones (black dots) are the leaves of the screen H (blue curve). Note that H approaches the event horizon (red line) at late times, in the near-de Sitter case. We find that the surface gravity κ approaches that of de Sitter space in the limit. 25

2.3 Penrose diagram for collapsing dust. The dark-shaded region is the dense region, $r < r_*$. The light shaded region contains arbitrarily dilute matter to satisfy the generic condition. We construct a holographic screen H using the future light-cones (dotted lines) of an observer at $r = 0$. Note that H changes signature and approaches the event horizon (red line) from the inside. We find that κ approaches the Schwarzschild surface gravity there. 27

2.4 Collapsing dust cloud: plots of the radial mass profile (left), the slope parameter β (middle), the surface gravity κ (right), for $r_* = 1$, $q = 1/20$, and $M = 1/100$. The region $r < r_*$ is the dense region. The change in the sign of β indicates the change in of signature of H from timelike to spacelike. The surface gravity saturates to $1/4M$ in the dilute region. 28
2.5 The Penrose diagram for Vaidya solution. We show the uncharged case, $e(v) = 0$. The mass function is $m(v) = 0$ for $v < v_0$ and $\dot{m}(v) \geq 0$ for $v > v_0$. The green dashed lines are the ingoing null shells. The red line is the event horizon. The blue line is the future holographic screen constructed from future light-cones centered at $r = 0$. 29
2.6 Two past holographic screens in the same expanding universe, associated with two different observers (thick black worldlines). *Left:* spherically symmetric screen constructed from a comoving observer at $r = 0$. *Right:* screen constructed from the past light-cones of a non-comoving observer. 31

4.1 The entropy production as a function of time for a region consisting of two disjoint intervals of length L, separated by a distance $R > L$. The quasiparticle model (left) shows decreasing behavior between $2\mathfrak{t} = R$ and $2\mathfrak{t} = L+R$. The holographic calculation (right) is monotonically increasing before saturation at $2\mathfrak{t} = L$, after which the entropy remains constant. 54
4.2 An EPR pair produced at the points marked as green at the bottom of the figure. When the constituent particles are at the positions marked as red at the intermediate time, they contribute to the entanglement entropy. At the later time when the particles are at the positions marked as blue, they do not contribute to the entanglement entropy. This process leads to a decrease in the entanglement entropy in the quasiparticle picture. 54
4.3 Penrose diagram of the time-dependent geometry following the quench. The red vertical line on the right is the AdS boundary ($z = 0$ in Poincare patch). The green diagonal line is the infalling shell, and the blue diagonal line is the horizon. The dashed curve is a late time extremal surface, which asymptotes to the critical surface, indicated by the solid curve. The linear growth of entanglement entropy comes from the portion of the extremal surface lying along the critical surface behind the horizon. 55
4.4 Here we display the extremal surfaces for two intervals. The first candidate HRT surface is the union of the two smaller arcs (marked in red and labeled $\mathcal{A}_1$ and $\mathcal{A}_2$). The second candidate is the union of the two larger arcs (marked in green and labeled $\mathcal{A}_3$ and $\mathcal{A}_4$). 57
4.5 The quench for two intervals of length L separated by a distance R when $L > R$. On the left, we show the entanglement tsunami wavefront as a function of time (jagged black line.) The region A is marked as red. The intervals between the disconnected components of A are marked as blue. On the right, we show the entanglement entropy as a function of time. 64

4.6 Entanglement tsunami for many intervals. The region A is marked as red. The intervals between the disconnected components of A are marked as blue. Note that at time $\mathfrak{t}_1$, $E(\mathfrak{t})$ consists of four disconnected components (orange solid lines) separated by the entanglement tsunami wavefront (jagged black line). But at time $\mathfrak{t}_2$, the first pair and second pair have merged, leaving two disconnected regions. At time $\mathfrak{t}_3$, there is only a single connected region. 66

5.1 Two dimensional cross-section of our setup illustrating equation Eq. (5.67). The entangling surface, ∂B, is at $\mathfrak{t}' = 0$ and $x_\perp = 0$ (marked as the black dot). The modular Hamiltonian of the unperturbed state lives entirely in the region B at $\mathfrak{t}' = 0$, indicated by the red line. We first compute the correlation function of K_0 with the relevant operator, $\mathcal{O}$, inserted at the blue line, and then integrate over the shaded region. The dashed line at $\mathfrak{t}' = -\delta$ serves as the UV cutoff. 80

6.1 The Penrose diagram of the time-dependent geometry as a result of a collapse of a null shell (shown as a double line). The dashed line is the event horizon, and the shaded region denotes the WDW patch corresponding to boundary time $\mathfrak{t}$. The intersection of the past null boundary of the WDW patch and the collapsing null shell is denoted by a black dot and is labeled by P. 93

6.2 The Penrose diagrams for AdS-Schwarzschild black hole (left) and vacuum AdS (right). The shaded region on the left/right corresponds to the part of the WDW inside/outside the collapsing null shell in Fig. (6.1). We have also included a cut-off surface at $z = \delta$ (shown as a blue line) in the Penrose diagram of AdS-Schwarzschild. The intersections of the WDW patch with the cut-off surface are labeled A and B, whereas the intersection of the past null boundary of the WDW patch and the collapsing null shell is denoted by a black dot and is labeled P. . 94

6.3 The plots showing the position of the plane P as a function of time for $d = \{3, 4, 5, 6\}$. It is evident from these plots that $z_P(\mathfrak{t}) \to z_h$ when $\mathfrak{t} \sim z_h$. 102

Acknowledgments

I am grateful to my research advisor, Raphael Bousso, for his support, guidance, and encouragement during the course of my graduate school. It was a pleasure to be benefitted from his insightful feedback and to be inspired by his passion for his work. Collaborating with him was an enjoyable and rewarding experience. I also thank him for giving me the freedom to explore different independent research projects. I also like to express my gratitude to Stefan Leichenauer and Michael Smolkin for their collaboration during the earlier stages of my graduate program. I would like to thank Yasunori Nomura and Birgitta Whaley to be on my dissertation committee, and to Holger Muller to be on my qualifying exam committee.

I have learned a lot through various discussion with my colleagues including Chris Akers, Ning Bao, Venkatesa Chandrasekaran, Zach Fisher, Illan Halpern, Jason Koeller, Adam Levine, Pratik Rath, Grant Remmen, Vladimir Rosenhaus, Fabio Sanchez, Arvin Shahbazi, Sean Jason Weinberg, Ziqi Yan, and Claire Zukowski. I would also like to thank Adam Brown, John Cardy, Netta Engelhardt, Tom Faulkner, Mark Mezei, Rob Myers, Niels Obers, Mukund Rangamani, and Leonard Susskind, for discussions that were helpful for the research covered in this dissertation.

I appreciate the support and help of Kathy Lee, Joelle Miles, Lavern Navarro, Donna Sakima, Claudia Trujillo, and especially Anne Takizawa, with administrative matters in the physics department.

My time in school would have been unendurable without my friends including Mohammad Ahmad, Ammar Amjad, Halleh Balch, Zach Fisher, Azeem Hassan, Alamdar Hussain, Aroosa Ijaz, Unab Javed, Abdul Rafay Khaled, Osama Khan, Stephanie Mack, Leigh Martin, Usama Javed Mirza, Saad Qadeer, Rabeet Rao, Paul Riggins, Fabio Sanchez, Saad Shaukat, Aaron Szasz, Ziqi Yan.

I am indebted to all of my teachers. They have inspired me and have kindled in me a thirst for knowledge. I would not be writing this dissertation if it was not owing to the hard work of Yawar Abbas, Mina Aganagic, Ehud Altman, Kashif Amin, Sabieh Anwar, Ata-ul-Haq, Pervez Hoodbhoy, Petr Horava, Fakhar-ul Inam, Amer Iqbal, Dung-Hai Lee, Hitoshi Murayama, Abdul Hameed Nayyar, Shabana Nisar, Babar Qureshi, Mumtaz Sheikh, Zeeshan Umer, Aneela Waseem, Martin White, Yasunori Yomura, and Imran Younus.

Finally, I feel fortunate to have the love and support of my family. I would like to thank my siblings, Mehreen Asif, Yameen Moosa, Yaseen Moosa, Huma Qassim, and Farhat Sohail. Above all, I am in debt to my parents, Bilqis Moosa and Muhammad Moosa, to whom this dissertation is dedicated, for providing me with an excellent education.

The research work in this dissertation was supported in part by the Berkeley Center for Theoretical Physics, by Berkeley Connect Fellowship, by the National Science Foundation (award numbers 1521446 and 1316783), by FQXi, and by the US Department of Energy under Contract DE-AC02-05CH11231.

Chapter 1

Introduction

The theory of quantum gravity holds the key to many of our fundamental questions of physics that can never be answered just using quantum mechanics or general relativity separately. Some progress in this field was made by studying black holes. Bekenstein noticed that the second law of thermodynamics loses its operational meaning in the presence of black holes [1]. For instance, the entropy of an object, like this dissertation, can be destroyed by throwing it into a black hole. Motivated by Hawking's area law - area of a horizon of a black hole can never decrease assuming certain energy conditions [2] - Bekenstein conjectured that the black holes have a finite entropy which is proportional to the area of their event horizon [3, 4]. That is,

$$S_{\rm BH} = \frac{A}{4}\,, \tag{1.1}$$

in Planck units. This allowed him to rescue the second law of thermodynamics by proposing what is known as the generalized second law: the entropy of a black hole plus the entropy of the matter outside the black hole never decreases in a physical process [3, 4]. That is, throwing this dissertation into a black hole will increase the entropy of a black hole by an amount more than the entropy of this dissertation.

The origin of Eq. (1.1) can only be explained using the theory of quantum gravity. Though it is still not clear how to formulate a theory of quantum gravity that is valid for all energy scales, we can still learn a great deal about quantum properties of black holes by treating the gravitational degrees of freedom as classical. By studying quantum field theory in a black hole background, Hawking verified Bekenstein's conjecture by deriving Eq. (1.1). Moreover, he showed that a black hole is a thermal object that emits purely thermal radiation [5, 6, 7], known as Hawking radiation.

The proportionality of entropy of a black hole to the area rather than the volume suggests that the degrees of freedom of a black hole 'live' on its horizon. This was promoted by 't Hooft [8] and Susskind [9] to a principle of quantum gravity - the degrees of freedom of quantum gravity inside any region can be encoded on the boundary of that region, at a density of no more than one bit per Planck area. This is known as the holographic principle. This implies that a theory of quantum gravity cannot be a local field theory.

The covariant formulation of the holographic principle is given by Bousso [10]. The covariant entropy bound, or the Bousso bound, states that the area of a closed spacelike codimension-2 surface, B, bounds the entropy of a quantum state on any light-sheet of B [10, 11, 12, 13]. That is,

$$S_{L[B]} \leq \frac{A[B]}{4}\,, \tag{1.2}$$

where $A[B]$ is the area of B and $L[B]$ is its light-sheet. A light-sheet emitted from B is a codimension-1 null hypersurface that is orthogonal to B and whose expansion along each generator is everywhere non-positive [10]. In other words, a light-sheet of B is a null hypersurface orthogonal to B as long as its cross-sectional area does not increase as one moves away from B.

The best working example of a holographic principle is Maldacena's AdS-CFT correspondence [14]. This correspondence conjectures that a theory of quantum gravity in $d+1$-dimensional asymptotically local Anti-de Sitter (AdS) spacetime is dual to a conformal field theory (CFT) in a d-dimensional conformal boundary of the AdS. More precisely, this conjecture makes the following two claims:

1. The quantum gravity state on each slice of AdS is described by the data on the boundary of that slice.

2. The unitary evolution of the boundary data from one slice to another is generated by the Hamiltonian of the boundary CFT.

Note that only the first of these two claims is demanded by the holographic principle. To generalize the first statement for generic spacetime, such as an expanding universe, we need to identify what codimension-1 surface is analogous to the conformal boundary of the AdS. Bousso showed that there exists 'observer-dependent' codimension-1 surfaces in a generic spacetime which can store the information of the spacetime, slice by slice [15, 16]. We review this construction in Sec. (1.1) and study the properties of these surfaces in part. (I) of this thesis.

The AdS-CFT correspondence provides a definition of a theory of quantum gravity in an asymptotically locally AdS spacetime in terms of the boundary CFT. However, it is still not very clear how to use this theory of quantum gravity. Instead, for certain CFTs with large central charge and sparse spectrum of light operators, the gravitational theory reduces to the classical general relativity [17]. This semiclassical approximation of the AdS-CFT correspondence can be used to study various properties of the quantum states of the boundary CFT and its deformation. Two of these properties are entanglement entropy and quantum complexity which we review in Sec. (1.2) and Sec. (1.3) respectively.

1.1 Holography in General Spacetimes

Though we have learned a good deal about quantum gravity in asymptotically locally AdS spacetimes from the AdS-CFT correspondence, a complete understanding still eludes us as asymptotically locally AdS spacetimes do not describe the universe that we live in. The difficulty in generalizing the holography in a generic spacetime is that it is not clear where the holographic information resides. That is, what hypersurface in a generic spacetime is a generalization of the conformal boundary of the AdS. Utilizing his covariant entropy bound, Eq. (1.2), Bousso presented a candidate for such hypersurfaces in a spacetime satisfying the null curvature condition,

$$R_{ab}k^a k^b \geq 0\,, \tag{1.3}$$

where R_{ab} is the Ricci tensor and k^a is any null vector. In particular, he demonstrated the existence of codimension-1 hypersurfaces, called holographic screens, which could holographically store the information of the spacetime [15, 16]. In this sense, holographic screens are a generalization of the conformal boundary of AdS to general spacetimes. Bousso's construction of a holographic screen can be summarized as follows:[15, 16]

1. Foliate the spacetime (or some region of it) by a one-parameter family of null hypersurfaces, $N(r)$. One way to do this is to choose an observer and shoot past (or future) light cones from her worldline.

2. On each null hypersurface, find a cross-section, $\sigma(r)$, of maximum area. The Raychaudhri equation together with the null curvature condition, Eq. (1.3), imply that the cross-sectional area of the null hypersurface, $N(r)$, does not increase as we move away from $\sigma(r)$ in either direction. Therefore, by definition, the segments of $N(r)$ inside and outside of $\sigma(r)$ are two separate light-sheets of $\sigma(r)$. The Bousso bound, Eq. (1.2), then bounds the entropy of the quantum state on $N(r)$ by the area of $\sigma(r)$.

3. Find a codimension-1 surface which is foliated by $\sigma(r)$.

The codimension-1 surface constructed in this way bounds the entropy of the spacetime (or some region of it), null slice by null slice. This surface is called the holographic screen, and its cross-sections, $\sigma(r)$, are called its *leaves*. In an asymptotically locally AdS spacetime, the maximum area cross-sections, $\sigma(r)$, coincide with the cross-sections of the conformal boundary of the AdS for any choice of null foliation. As a result, the holographic screen in an asymptotically locally AdS spacetime is the conformal boundary. In this sense, holographic screens are a generalization of the conformal boundary of AdS to general spacetimes. However, there are various properties of holographic screens in a generic spacetime that are not shared by the conformal boundary of AdS. First, holographic screens can lie inside the spacetime. Secondly, they are dynamical objects. For example, the area of the leaves increases as we move from one leaf to another [18, 19]. Thirdly, they depend on a choice of null slicing, $N(r)$, and hence are not unique. This non-uniqueness can be interpreted as an observer-dependence. It is, therefore, instructive to study the dynamics and

observer-dependence of the holographic screens to get more insights in our search for the quantum gravity in general spacetimes, such as cosmology. This is the subject matter of the part. (I) of this thesis.

In Ch. (2), we study the evolution of holographic screens, both generally and in explicit examples, including cosmology and gravitational collapse. If a holographic theory exists, the evolution of these variables should capture the behavior of course-grained quantities in quantum gravity. This will give us valuable information about the structure of the theory. We also discuss how this evolution depends on the observer used to construct the screen. We find that this ambiguity corresponds precisely to the free choice of a single function on the screen. We also consider the background-free construction of the screen, where the spacetime is not given. The evolution equations then constrain aspects of the full spacetime and the screen's embedding in it. This chapter is based on a paper written in collaboration with Raphael Bousso [20].

In Ch. (3), we propose that the intrinsic geometry of holographic screens should be described by the Newton-Cartan geometry. As a test of this proposal, we show that the evolution equations of the screen can be written in a covariant form in terms of a stress tensor, an energy current, and a momentum one-form. We derive the expressions for the stress tensor, energy density, and momentum one-form using Brown-York action formalism. This chapter is based on [21].

1.2 Entanglement, Quantum Fields, and Geometry

Entanglement is one of the most fundamental properties of quantum mechanics. Suppose we have a two-partite system (system A and system B) whose Hilbert space can be factorized as

$$\mathcal{H}_{AB} = \mathcal{H}_A \otimes \mathcal{H}_B \,. \tag{1.4}$$

A pure state $|\psi_{AB}\rangle \in \mathcal{H}_{AB}$ is said to be entangled if the reduced state of any subsystem is a mixed state [22]. The reduced state of any subsystem is given by starting with the global state and tracing over the Hilbert space of the complement of that subsystem. That is, the reduced state of the system A is given by

$$\rho_A = \mathrm{Tr}_B \, |\psi_{AB}\rangle \langle \psi_{AB}| \,. \tag{1.5}$$

The calculation of thermal radiation from a black hole was generalized by Unruh for an accelerating observer in a flat spacetime [23]. In particular, he showed that an observer with constant acceleration, also known as a Rindler observer, in a vacuum state of a Lorentz invariant quantum field theory detects particles obeying a thermal probability distribution with a temperature proportional to her acceleration. Since the Hamiltonian for a Rindler observer is a boost operator, H_R, the thermal state that she observes is given by

$$\rho_R = \frac{1}{Z_R} e^{-2\pi H_R} \,, \tag{1.6}$$

where $Z_R \equiv \mathrm{Tr}\, e^{-2\pi H_R}$ is the normalization constant. The significance of Unruh's calculation is that it implies that the vacuum state of a quantum field theory is entangled. To see this, let's consider a scalar field theory. In this case, the full Hilbert space can be factorized as

$$\mathcal{H} = \bigotimes_x \mathcal{H}_x \,, \tag{1.7}$$

where $\mathcal{H}_x$ is the Hilbert space at a point x on a Cauchy slice. Now note that a Rindler observer has access to the domain of dependence of only the half of a Cauchy slice and hence, to only half of the Hilbert space. The reduced state on this half-space is given in Eq. (1.6). Since this reduced state is a mixed state, we deduce that the global pure state must be entangled.

This entanglement structure of the vacuum state of a QFT is more general than Unruh's result. Suppose we take a closed spacelike codimension-2 surface, called entangling surface, that splits a codimension-1 Cauchy slice into a region, B, and its complement, B^c. This provides a 'bipartite' factorization of the Hilbert space. The reduced state of either region will then be a mixed state [24, 25]. Hence, the vacuum state of a field theory is entangled for any spatial factorization of the Hilbert space.

A useful measure of the entanglement of a pure state is the entanglement entropy. The entanglement entropy of system A is defined as the von Neumann entropy of the reduced state ρ_A. That is, [22]

$$S_A = -\mathrm{Tr}_A\, \rho_A \log \rho_A \,. \tag{1.8}$$

Note that S_A vanishes if the reduced state ρ_A is a pure state, which would be the case if the pure state $|\psi_{AB}\rangle$ is unentangled. Though it is not clear a priori, one can show for a pure state $|\psi_{AB}\rangle$, $S_A = S_B$ [22].

The spatial entanglement entropy for a vacuum state of an arbitrary QFT is a UV divergent quantity. This UV divergence can be attributed to the infinite short distance entanglement between nearby modes residing on either side of the entangling surface. This further implies that the UV divergences in the entanglement entropy should scale as the area of the entangling surface rather than the volume of the region bounded by the entangling surface. Therefore, the leading divergence in the entanglement entropy for an arbitrary entangling surface in a d-dimensional curved spacetime is of the form

$$S \sim \frac{A}{\delta^{d-2}} + \dots \,, \tag{1.9}$$

where A is the area of the entangling surface and δ is a short distance UV cutoff. The proportionality constant depends on the details of the field theory, entangling surface, and the choice of regularization scheme. The similarity of the 'area law' of entanglement entropy, Eq. (1.9), and the Bekenstein-Hawking entropy, Eq. (1.1), motivates the study of the entanglement entropy.

The calculation of the entanglement entropy for a general entangling surface is not an easy task. This involves first finding the reduced density matrix and then diagonalizing it.

For field theories with a classical holographic dual, the AdS-CFT correspondence provides an alternative prescription. This holographic method was first conjectured in [26] for time-independent states and was generalized later in [27, 28] for general states. These conjectures were later proven in [29, 30]. The holographic formula for the entanglement entropy of any spatial region A is

$$S_A = \frac{A(\Sigma_A)}{4}\,, \tag{1.10}$$

where $A(\Sigma_A)$ is the area of a codimension-2 spacelike stationary area surface, Σ_A, in the bulk subject to the conditions that it is anchored on the boundary at the entangling surface, ∂A, and that it is homologous to the boundary region A. If there are several such surfaces, we choose the one with the minimum area.

In addition to providing an analytical tool to compute the entanglement entropy for a general entangling surface, this holographic formula connects a quantum information quantity to a geometric quantity. This connection has led to many new insights about the emergence of classical spacetime [31, 32]. Moreover, it has been shown that the holographic entanglement entropy satisfies several inequalities that are not valid in general [33]. Therefore, these inequalities can be used to determine what CFTs have a classical gravitational bulk dual.

The part. (II) of this dissertation is devoted to studying of the entanglement in a time-dependent setting. In Ch. (4), we study the time dependence of the entanglement entropy of disjoint intervals following a global quantum quench in (1+1)-dimensional CFTs at large-c with a sparse spectrum. We find the result agrees with a holographic calculation but differs from the free field theory answer. In particular, a simple model of free quasiparticle propagation is not adequate for CFTs with a holographic dual. We elaborate on the entanglement tsunami proposal of Liu and Suh and show how it can be used to reproduce the holographic answer. This chapter is based on a paper written in collaboration with Stefan Leichenauer [34].

In Ch. (5), we study the evolution of the universal area law of entanglement entropy when the Hamiltonian of the system undergoes a time-dependent perturbation. In particular, we derive a general formula for the time-dependent first order correction to the area law under the assumption that the field theory resides in the vacuum state when a small time-dependent perturbation of a relevant coupling constant is turned on. Using this formula, we carry out explicit calculations in free field theories deformed by a time-dependent mass, whereas for a generic QFT we show that the time-dependent first order correction is governed by the spectral function defining the two-point correlation function of the trace of the energy-momentum tensor. We also carry out holographic calculations and find qualitative and, in certain cases, quantitative agreement with the field theory calculations. This chapter is based on a paper written in collaboration with Stefan Leichenauer and Michael Smolkin [35].

1.3 Complexity and Geometry

The interior of a black hole keeps 'stretching' even after the scrambling time. According to the AdS-CFT correspondence, this phenomenon should have a dual description in terms of the boundary CFT. This raises the question if there is any CFT quantity that has the property that it could keep growing after the scrambling time. Susskind argued that the quantum complexity of the CFT state has this property [36]. The computational complexity of a quantum state is defined as the minimum number of quantum gates to map a simple state to that state [36, 37]. That is, the complexity of a state is the size of the smallest circuit that is required to prepare that state. The size of a circuit is proportional to the time that the circuit runs. Therefore, the complexity of any quantum state grows linearly with time until the classical recurrence time [36], which is much larger than the scrambling time.

Based on these observations, Susskind conjectured that the growth of the complexity of the CFT state is holographically dual to the growth of the size of the black hole. More precisely, he characterized the size of a black hole by the volume of an extremal bulk Cauchy slice [38]. In particular, the original conjecture states that the complexity, $\mathcal{C}$, of a CFT state at any time is proportional to the volume, $\mathcal{V}_{\text{ext}}$, of an extremal bulk Cauchy surface anchored on the boundary at that time [38]

$$\mathcal{C} \equiv \frac{\mathcal{V}_{\text{ext}}}{G\,\ell}\,, \tag{1.11}$$

where ℓ is an appropriate length scale. This conjecture is known as *complexity equals volume* conjecture. A more recent conjecture relates the size of a black hole, and hence the complexity of the boundary state, to the on-shell action, $\mathcal{A}$, of the domain of dependence of a bulk Cauchy slice [39, 40]

$$\mathcal{C} \equiv \frac{\mathcal{A}}{\pi}\,. \tag{1.12}$$

This proposal is called the *complexity equals action* conjecture.

The quantum complexity has been a topic of interest for classical and quantum computational scientists for reasons independent of quantum gravity. Let's consider a 'classical' circuit which is made up of gates that take a quantum state in the computational basis (that is a classical state) into an orthogonal state in the computational basis. The Margolus-Levitin theorem [41] states that the time that a logical gate takes to map a state into an orthogonal state is bounded from below by the inverse of the energy of the state. This implies that the number of gates that are implemented per unit time is bounded from above by the energy of the system. Based on this reasoning, Lloyd conjectured that the rate of increase of a complexity of a state is bounded from above by the energy, E, of that state. That is,

$$\frac{d}{dt}\mathcal{C} \leq \frac{2}{\pi}E\,. \tag{1.13}$$

This is known as the Lloyd bound [42]. Even though this bound is supposed to be true only for gates that map a state into an orthogonal state, it is conjectured in [39, 40] that holographic complexities satisfy this universal bound.

We allocate the part. (III) of this dissertation to test the consistency of these holographic conjectures. In Ch. (6), we use the *complexity equals action* conjecture to study the time evolution of the complexity of the CFT state after a global quench. We find that the rate of growth of complexity is not only consistent with the conjectured bound, but it also saturates the bound soon after the system has achieved local equilibrium. This chapter is based on [43].

In Ch. (7), we perturb a holographic CFT by a relevant operator with a time-dependent coupling, and study the complexity of the time-dependent state using the *complexity equals action* and the *complexity equals volume* conjectures. We find that the rate of complexification according to both of these conjectures has UV divergences, whereas the instantaneous energy is UV finite. This implies that neither the *complexity equals action* nor *complexity equals volume* conjecture is consistent with the conjectured bound on the rate of complexification. This chapter is based on [44].

Part I

Holography in General Spacetimes

Chapter 2

Dynamics and Observer-Dependence of Holographic Screens

2.1 Introduction

In the search for a quantum theory of gravity in general spacetimes, the study of holographic screens [15] has recently led to interesting new results. An area theorem was proven for past and future holographic screens in any spacetime satisfying the null curvature condition [18, 19]. The semiclassical extension of this theorem led to the first rigorous formulation of a universal Generalized Second Law [45], applicable in cosmology and other highly dynamical spacetimes. In the present chapter, we will study the classical evolution of holographic screens in more detail.

A *holographic screen* H can be associated to a null foliation of a spacetime M, i.e., a foliation of M into 2+1 dimensional hypersurfaces $N(R)$, each with two spatial and one light-like direction. (See Fig. (2.1).) The screen consists of a sequence of two-dimensional surfaces $\sigma(R)$ called *leaves*. Each leaf is the spatial cross-section of the largest area on the corresponding slice $N(R)$. A holographic screen is called *future* (*past*) if the area of each leaf is decreasing (increasing) in the opposite light-like direction, i.e., if every $\sigma(R)$ is marginally trapped (anti-trapped). Future screens appear inside black holes or near a big crunch. Past holographic screens exist in an expanding universe, for example in ours.

The covariant entropy bound (Bousso bound) [10, 11] implies that all of the information about the quantum state on each null slice $N(R)$ can be stored on the corresponding leaf $\sigma(R)$, at a density of no more than one bit per Planck area. This suggests that the holographic principle [8, 9, 46] applies in all spacetimes. (Several precise semiclassical versions of this conjecture have recently been formulated, and in some cases, proven rigorously [12, 13, 47, 48, 49].) The holographic relation between quantum information and geometry substantially involves both G_N and $\hbar$, Newton's and Planck's constants. Its origin can only lie in a quantum theory of gravity, so one expects the structure of holographic screens to reflect aspects of the underlying theory.

In spacetimes with conformal boundaries, all or parts of the screen lie on it [15, 16]. For example, in asymptotically Anti-de Sitter spacetimes, the screen is located on the conformal boundary at spatial infinity. This is consistent with the AdS/CFT correspondence providing a full quantum description. It is therefore of interest to study holographic screens in more realistic spacetimes, where quantum gravity remains a mystery. (An interesting recent approach explores a generalization of the stationary-surface conjecture [26, 27] for computing entanglement entropy [50, 51, 52].) In particular, it is important to understand the dynamics of holographic screens in cosmology and in the collapsing regions inside of black holes.

Future holographic screens have already been studied in some detail under the guise of "dynamical horizons" [53] or "future outer-trapped horizons" [54], as interesting candidates for quasi-local boundaries of black holes. Strictly, the latter objects are more restrictive: dynamical horizons correspond only to the *spacelike* portions of future holographic screens. For the purposes of proving an area theorem, the restriction to spacelike portions is significant: the area theorem is trivial for dynamical horizons, but highly nontrivial for future holographic screens. This is because without the spacelike assumption, the area theorem relies on a global property that is hard to prove: the (unique) foliation of a given screen H into leaves $\sigma(R)$ uniquely defines a foliation of a (portion of) the spacetime M into null slices $N(R)$.

Here we will be interested in studying the evolution of local quantities, the metric and extrinsic curvature of the leaves. For this purpose, the spacelike assumption yields no significant simplification. In fact, a number of authors have studied the local evolution problem for dynamical horizons [53, 55, 56, 57, 58, 59], and some noted that the spacelike assumption is not required for the validity of the evolution equations. For completeness, we offer a simplified derivation of the evolution equations in the Appendix (C). In the main text, our focus will be on their interpretation. In particular, we will emphasize the role of a gauge choice which corresponds geometrically to a choice of null foliation, and which has a natural interpretation as reflecting a choice of observer.

In Sec. (2.2), we establish conventions, and we define the screen variables: local geometric quantities that can be associated to a holographic screen. They include the metric and null extrinsic curvatures of the leaves, a tangent vector field to the leaves describing the relative evolution of the two null normals, and a tangent vector field normal to the leaves describing the "slope" and "rate" of the screen's progress through the spacetime it is embedded in. We also identify one "global" and one "gauge" transformation, which leave the screen invariant but act nontrivially on some of the above variables.

In Sec. (2.3), we present the evolution equations for the screen variables. We then analyze them from three different perspectives. First, we regard both the spacetime M and the screen H as given. This viewpoint has been examined previously, and it has led to suggestions that the screen evolution can be interpreted as fluid dynamics. We identify a number of problems with this interpretation.

Next, we regard the spacetime M as given but consider the evolution equations as a tool for constructing H. We find that the equations are underdetermined by one function α on H. We show that this function corresponds precisely to the ambiguity in choosing a null

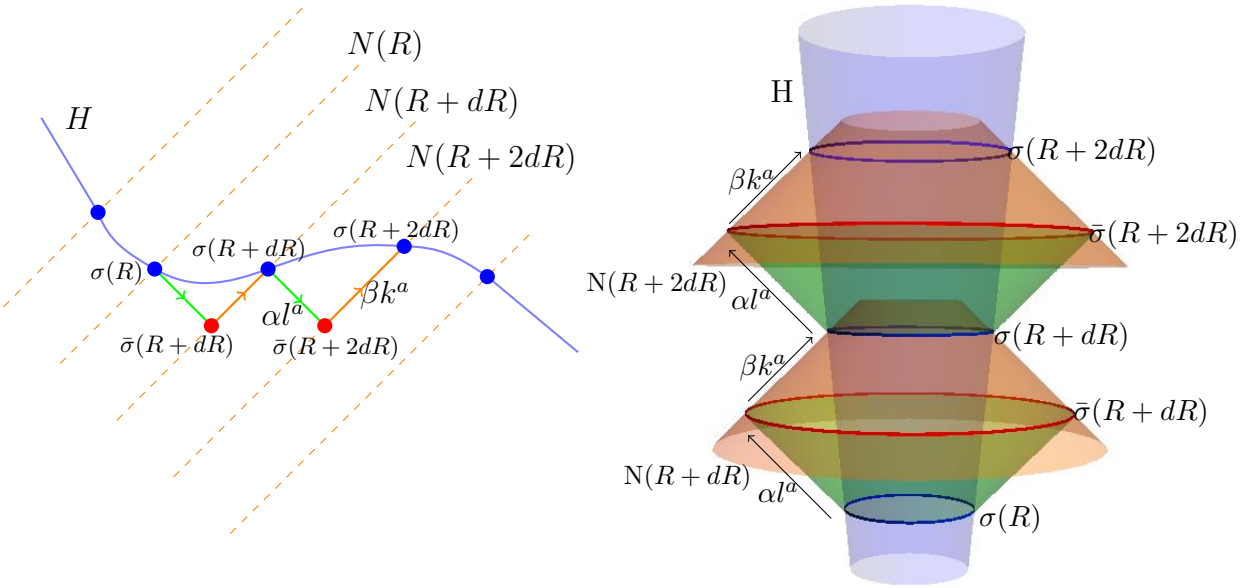

Figure 2.1: *Left:* a future holographic screen, H (blue line). Points represent topological spheres. The dashed lines are 2+1 dimensional null slices N orthogonal to the leaves σ of H (blue dots), along the direction k^a. H can be constructed leaf by leaf, using a "zig-zag" procedure. First, deform the leaf $\sigma(R)$ along the other orthogonal null vector, l, by an infinitesimal step $\alpha(R,\vartheta,\varphi)l^a$ (green downward arrow). The function $\alpha<0$ can be chosen arbitrarily; it reflects a kind of observer-dependence of the holographic screen. Thus one obtains a new surface $\bar\sigma(R+dR)$ (red), and from it, a new null slice $N(R+dR)$ orthogonal to $\bar\sigma$. The next leaf $\sigma(R+dR)$ is the surface of maximal area on $N(R+dR)$, at some infinitesimal distance βk^a along N from $\bar\sigma$ (orange arrow). *Right:* a past holographic screen (same color coding). In this case, $\alpha>0$; the area of the leaves grows towards the future. We show the same construction, with only one spatial direction suppressed to offer a different visualization. The leaves $\sigma(R)$ are by definition the maximal area cross-sections of $N(R)$, despite what the figure shows.

slicing; see Fig. (2.1). More precisely, given a partially constructed screen up to some leaf $\sigma(R)$, we show that α can be regarded as a lapse function that describes how much the infinitesimal step R advances the slicing away from each point on $\sigma(R)$. This defines a new null slice $N(R + dR)$ and ultimately, a new leaf $\sigma(R + dR)$, in an α-dependent way.

We can regard α as encoding a kind of generalized observer-dependence of the screen, in the following sense. Consider a worldline, and consider the future light-cone from each point on the worldline. If the worldline is in a collapsing region (e.g., inside a black hole), then there will be a cross-section of the maximum area on this light-cone: a marginally trapped surface. The sequence of such surfaces defined by the above construction yields a holographic screen, H.

Now consider a different observer, whose worldline coincides in some interval with the previous one, but then departs from it. The above construction still works, and in the region where the worldlines agree it, it will yield the same leaves. Therefore the holographic screens will also agree on those leaves. But the leaves constructed from the light-cones of points where the worldlines do not agree will differ. Therefore there is no unique future evolution for a holographic screen, even if we are given part of the screen and the entire spacetime M.

This mathematical description of the observer-dependence of holographic screens, as a choice of the function α, is the central result of this chapter. It would be nice to explore this further. For example, infinitesimally nearby screens encode nearly the same subset of M. The transformation relating them may correspond either to a change of variables in the underlying theory or to a change of the prescription for reconstructing spacetime from those variables.

Finally, we consider the evolution equations from a "background-free" perspective, where neither M nor H are given. In this case, we can regard the screen variables as given. What was previously regarded as their evolution equations now determines aspects of the spacetime M, and of how H is embedded in M. However, from this viewpoint, the equations are highly underdetermined. This is not surprising since the screen variables can at most represent a coarse grained subset of the information in the underlying quantum gravity theory.

In Sec. (2.4), we illustrate our general analysis with some examples. We construct screens explicitly for black holes and for cosmological solutions, and we compute the screen variables. In particular, we construct two different screens for the same cosmology, only one of which is spherically symmetric. This illustrates the observer-dependence associated with a choice of different worldlines and null slicings.

Relation to other work Our analysis builds on earlier studies of dynamical horizons and future outer-trapped horizons, such as [54, 53, 55, 60, 61, 62]. In many of these works, an analog of the first law of black hole thermodynamics was sought. (The second law holds trivially for dynamical horizons.) However, it is not clear that physically meaningful intrinsic and extrinsic variables, such as total energy and temperature, can be uniquely defined. We do not pursue this direction here, though we note in Sec. (2.4) that a certain local geometric quantity κ limits to the usual surface gravity of an event horizon, in all examples where a

sensible comparison can be made.

Here, we focus on local parameters that arise naturally from the geometry of holographic screens. In Sec. (2.3) we take as our starting point the evolution equations of Gourgoulhon and Jaramillo [57, 58, 59]. (For completeness, their derivation is given in the Appendix (C).) In Sec. (2.4), we make use of the work of Booth *et al.* [63], who explicitly constructed dynamical horizons for spherical dust collapse.

2.2 Kinematics of Holographic Screens

A *future (past) holographic screen*, H, is a hypersurface (not necessarily of definite signature) that is foliated by marginally trapped (anti-trapped) codimension-2 spatial surfaces called *leaves*. For simplicity, we will take spacetime to have four dimensions in what follows, and we consider future screens unless otherwise noted, but all results are easily generalized. By a *surface* we shall mean a smooth two-dimensional achronal surface. We will consider only regular screens, which satisfy a set of further mild technical conditions [19] such as the generic condition, Eq. (2.62) below. In this section, we will discuss the kinematic structure underlying holographic screens and establish a number of conventions.

Tangent and Normal Vectors

In a Lorentzian manifold, every two-dimensional spatial surface has two future-directed orthogonal null vector fields, k^a and l^a. It is convenient to choose their normalization such that

$$k^a l_a = -1 \ . \tag{2.1}$$

This allows for arbitrary rescalings $l \to \gamma l$, $k \to \gamma^{-1} k$, where γ is an arbitrary positive function on the screen H. We show below that this gives rise to a $U(1)$ gauge symmetry.

A surface is marginally trapped if

$$\theta^{(k)} = 0 \ , \quad \theta^{(l)} < 0 \ . \tag{2.2}$$

By the above definition, a future holographic screen can be thought of as a one-parameter sequence of such surfaces, its leaves $\sigma(R)$. In principle, any parameter can be used. For example, the existence of an area theorem for holographic screens [18, 19] makes it possible to choose R to be a monotonic function of the area of the leaves.

Next we wish to define a vector field h which is tangent to H and normal to each leaf $\sigma(R)$. The latter condition implies that

$$h^a = \alpha l^a + \beta k^a \ . \tag{2.3}$$

A key intermediate result in the proof of the area theorem [19] is that $\alpha < 0$ everywhere on H (in our convention where l is future-directed). That is, the evolution of leaves of a future holographic screen is towards the past or the spatial exterior. The parameter β corresponds

to the "slope" of the holographic screen. By Eq. (2.3), the screen is past-directed if $\beta < 0$ and spatially outward-directed if $\beta > 0$. The generic condition of [19] prevents h from becoming collinear with k, so β is always finite. However, β has no upper bound. In the limit as $\beta \to \infty$, H approaches an isolated horizon. For example, H can approach the event horizon of a black hole from the inside.

Because β can have any sign, H need not be of definite signature. Thus we cannot require that h have unit norm:

$$h^a h_a = -2\alpha\beta \ . \tag{2.4}$$

Instead, we normalize h by requiring that

$$h(R) = h^a (dR)_a = 1 \ , \tag{2.5}$$

where R is the (arbitrary) foliation parameter. We also define a vector normal to H and to every leaf:

$$n^a = -\alpha l^a + \beta k^a \ , \tag{2.6}$$

which satisfies $h^a n_a = 0$ and $n^a n_a = 2\alpha\beta$.

There are two ways to think about this normalization, corresponding to different perspectives on screen evolution. In one viewpoint, we consider a given screen H in a given spacetime M. Then it is natural to choose a foliation parameter R, which fixes the product $\alpha\beta$ via the above two equations. The ratio β/α is fixed by the slope of the screen's embedding in M. Alternatively, we may consider only the spacetime M as given, and consider it our task to construct the screen H. In this case, the screen will not be unique. Even if some portion of the screen is known (as a set of leaves associated with a finite range of R), this does not determine the remainder of the screen. We shall see that the ambiguity is precisely associated with a choice of a negative function α on H (at a fixed choice of l). This corresponds to a choice of null foliation of M, or physically, to a choice of observer associated with the screen. We will later identify a constraint equation that determines β as a function of α and other data, Eq. (2.61) below. The parameter R is then determined by Eq. (2.5).

The induced metric on the screen H is not always well-defined:

$$\gamma_{ab} = g_{ab} - \frac{1}{2\alpha\beta} n_a n_b \ ; \tag{2.7}$$

This is ill-defined on null portions of H, i.e., when β vanishes; and it changes signature when β changes sign. But we will not need this metric below. By contrast, the induced spatial metric on a leaf $\sigma(R)$ is always well defined:

$$q_{ab} = g_{ab} + k_a l_b + l_a k_b \ . \tag{2.8}$$

Extrinsic Curvature and Acceleration

We are interested in the extrinsic curvature of the leaves $\sigma(r)$ in the spacetime, rather than the extrinsic curvature of the screen H. Since the leaves are of codimension 2, the full

extrinsic curvature data consists of the following objects: the null extrinsic curvatures in the k and l directions, respectively; and the so-called Weingarten map, which measures how the null normals vary with respect to each other.

The null extrinsic curvatures are defined by

$$B^{(k)}_{ab} = q^c_a q^d_b \nabla_c k_d \ , \tag{2.9}$$
$$B^{(l)}_{ab} = q^c_a q^d_b \nabla_c l_d \ . \tag{2.10}$$

The expansion and shear are given by

$$\theta^{(k)} = B^{(k)}_{ab} q^{ab} \tag{2.11}$$
$$\sigma^{(k)}_{ab} = B^{(k)}_{(ab)} - \frac{1}{2}\theta^{(k)} q_{ab} \ , \tag{2.12}$$

and similarly for l. We recall that by definition of a future holographic screen, $\theta^{(k)} = 0$ and $\theta^{(l)} < 0$.

Analagously one can define extrinsic curvature, expansion, and shear for any vector field orthogonal to σ, such as h^a or n^a. Since the definitions are linear, Eq. (2.3) implies, e.g.,

$$\theta^{(h)} = \alpha\theta^{(l)} + \beta\theta^{(k)} = \alpha\theta^{(l)} \ , \tag{2.13}$$
$$\theta^{(n)} = -\alpha\theta^{(l)} + \beta\theta^{(k)} = -\alpha\theta^{(l)} \ . \tag{2.14}$$

From the one-form $-l_b \nabla_a k^b$, one can construct the *normal one-form* by projection along the leaf,

$$\Omega_a \equiv q_a{}^c(-l_b \nabla_c k^b) \ , \tag{2.15}$$

and the *acceleration* $\tilde{\kappa}$ by projection along the evolution vector field,

$$\tilde{\kappa} \equiv h^c(-l_b \nabla_c k^b) \ . \tag{2.16}$$

This quantity is called "surface gravity" in [57, 58, 59] and is denoted κ there. We will reserve that term and notation for a different, closely related quantity defined in Eq. (2.18) below, because we find that it better matches the surface gravity of event horizons.

It is easy to see that the following expressions are equivalent to Eq. (2.16): $\tilde{\kappa} = k_b h^a \nabla_a l^b = h_b h^a \nabla_a k^b = -l_b h^a \nabla_a (h^b/\beta)$. Yet another equivalent expression for $\tilde{\kappa}$ can be given by extending the null vector fields k and l into a neighborhood of H (which was not needed above), according to the following prescription: l is parallel transported along itself, and k is parallel transported but rescaled so as to satisfy $k^a l_a = -1$ everywhere. With this choice, one finds

$$k^a \nabla_a k^b = \kappa k^b \ , \tag{2.17}$$

where

$$\kappa \equiv \frac{\tilde{\kappa}}{\beta} \ . \tag{2.18}$$

At points where $\beta = 0$, the above prescription fails to extend l into an open neighborhood of such points, leading to a divergence.

Notably, Eq. (2.17) takes the same form as the definition of the surface gravity of a Killing horizon. However, the acceleration κ is not invariant under certain allowed rescalings of k, which we will discuss shortly. For Killing horizons, there is a similar ambiguity, which would also rescale the surface gravity. But in some cases (e.g. asymptotically flat spacetimes), a preferred normalization of the Killing vector field $k_{\mathrm{K}H}$ exists [64]. In our case, by contrast, the normalization is set by the choice of evolution parameter R, which is ambiguous.

In Sec. (2.4) we will consider a particularly simple choice of parametrization. Remarkably, we will find for a large class of dynamical solutions that the acceleration defined in Eq. (2.17) agrees with the standard Killing surface gravity of the corresponding static solutions.

Gauge and Reparametrization Transformations

There are two kinds of transformations that do not change the screen and preserve the conventions of Eq. (2.1) and Eq. (2.5). The first transformation is analogous to a global symmetry, in that it does not depend on the position. The second is a $U(1)$ gauge symmetry.

The first symmetry is a trivial reparametrization of the label R of the leaves. There are certain geometrically motivated choices one could consider in order to fix R: for example, by linking it to the area A of the leaves, e.g. via $A = 4\pi R^2$ or $A = \exp(R)$. Here we will insist only that R grow monotonically with A. Then we can consider any transformation $R \to R'$ with

$$\exp[\gamma(R)] \equiv \frac{dR'}{dR} > 0 \ . \tag{2.19}$$

Note that γ can only depend on R, not on the angular position on each leaf. The above conventions and definitions imply the following transformation properties:

$$\begin{aligned}
h &\to e^{-\gamma} h && (2.20)\\
n &\to e^{-\gamma} n && (2.21)\\
l &\to e^{-\gamma} l && (2.22)\\
k &\to e^{\gamma} k && (2.23)\\
\beta &\to e^{-2\gamma} \beta && (2.24)\\
\Omega_a &\to \Omega_a && (2.25)\\
\tilde{\kappa} &\to e^{-\gamma}(\tilde{\kappa} + \gamma'(R)) \ . && (2.26)
\end{aligned}$$

The extrinsic curvature tensors, $B_{ab}^{(h,n,k,l)}$, and their components (expansion and shear), transform like h, k, n, l, respectively.

A second symmetry arises from rescaling α by an arbitrary positive function of R and of the angular position, while holding h, n, and R fixed. This requires taking $l \to e^{-\Gamma} l$, and by

Eq. (2.1), $k \to e^{\Gamma} k$. The remaining screen parameters transform as[1]

$$\begin{aligned} \alpha &\to e^{\Gamma}\alpha && (2.27)\\ \beta &\to e^{-\Gamma}\beta && (2.28)\\ \tilde{\kappa} &\to \tilde{\kappa} + \dot{\Gamma} && (2.29)\\ \Omega_a &\to \Omega_a + D_a\Gamma \ . && (2.30) \end{aligned}$$

Note that the combination

$$\begin{aligned} \widehat{\Omega}_a &\equiv h^b q_a{}^c \nabla_c n_b \, , && (2.31)\\ &= -2\alpha\beta\Omega_a + \beta D_a\alpha - \alpha D_a\beta \, . && (2.32) \end{aligned}$$

is invariant under the gauge symmetry.

Again, it is possible to gauge-fix this symmetry. For example, we can insist that $\alpha = -1$ everywhere, or that $\theta^{(l)} = -1$. Below we find that different choices are convenient for different applications. However, the most general evolution equations we display in the next section will be invariant under any of the above transformations.

2.3 Dynamics and Observer-Dependence

A holographic screen is a codimension-one hypersurface in spacetime. Hence, it must obey the constraint equations of General Relativity,

$$G_{ab} n^b = 8\pi T_{ab} n^b \ . \qquad (2.33)$$

These four equations are usually expanded in a $3+1$ formalism, as one energy constraint plus three momentum constraints on the 3-metric and 3-extrinsic curvature.

Here we are dealing with a hypersurface of indefinite signature, but with the additional structure of a 2+1 decomposition, the foliation into leaves. Thus it is natural to express Eq. (2.33) in terms of the kinematic quantities defined in the previous section, which are adapted to this foliation. One finds

$$\begin{aligned} \alpha(\widehat{\mathcal{L}}_h + \tilde{\kappa})\theta^{(l)} + D_a\widehat{\Omega}^a &= 8\pi T_{ab} n^a h^b + B^{(h)}_{ab} B^{ba}_{(n)} && (2.34)\\ (\widehat{\mathcal{L}}_h + \theta^{(h)})\Omega_c - D_c\tilde{\kappa} + \alpha D_c\theta^{(l)} &= 8\pi T_{ab} n^a q^b_c - D_a B^{(n)a}_c && (2.35)\\ -\frac{\alpha}{2}\mathcal{R} + \alpha\Omega_a\Omega^a - \alpha D_a\Omega^a - 2\Omega^a D_a\alpha + D_a D^a\alpha &= 8\pi T_{ab} n^a k^b + \beta\sigma^{(k)}_{ab}\sigma^{ab}_{(k)} \ , && (2.36) \end{aligned}$$

where we have used $\theta^{(k)} = 0$ to simplify the equations. Recall that $\widehat{\Omega}_a$ is not an independent variable but given by Eq. (2.32). Here $\mathcal{R}$ is the Ricci scalar associated with the leaf metric, q_{ab}. In addition, there is a dynamical equation for the metric on the leaves,

$$\widehat{\mathcal{L}}_h q_{ab} = B^{(h)}_{ab} \ . \qquad (2.37)$$

[1]Note that $(\tilde{\kappa}, \Omega_a)$ transform like $(A_0, \mathbf{A})$, the electric and magnetic potential, under a gauge transformation Γ. It would be nice to relate this to a shift by Γ in the phase of a nonrelativistic wavefunction ψ [65, 66, 67] that is part of the quantum gravity theory on the screen.

The evolution operator $\widehat{\mathcal{L}}_h$ acts on the tensors which are purely tangent to the leaf as [57]

$$\widehat{\mathcal{L}}_h A_{ab\ldots c} \equiv \; q_a^{\;a'} q_b^{\;b'} \ldots q_c^{\;c'} \, \mathcal{L}_h A_{a'b'\ldots c'} \, , \tag{2.38}$$

where we consider $\mathcal{L}_h$ as an operator on H.

This system of equations is invariant under the symmetries described in Sec. (2.2). We have displayed intrinsic quantities associated with the screen on the left side. Extrinsic quantities that act like sources appear on the right hand side. We will now describe three ways in which one might interpret this system of equations, using different gauge choices.

Viscous Fluid Analogy

We begin by regarding both the spacetime M and the screen H as fixed. In this case, we are merely expressing the 3D intrinsic and extrinsic curvatures of H as the evolution of 2D screen variables along H. This may nevertheless be interesting if it throws new light on the system. In fact, the evolution equations bear some similarity to fluid equations. We will identify a number of problems with the fluid interpretation, however.

To obtain fluid-like equations, we will set $\alpha = -1$ to gauge-fix the $U(1)$ symmetry. We do not gauge-fix the screen parameter R. Equations (2.34-2.37) become

$$(\widehat{\mathcal{L}}_h + \theta^{(h)})\theta^{(h)} + (\tilde{\kappa} - \theta^{(h)})\theta^{(h)} - B^{(h)}_{ab} B^{ba}_{(n)} + D_a \widehat{\Omega}^a \;=\; 8\pi T_{ab} n^a h^b \tag{2.39}$$

$$(\widehat{\mathcal{L}}_h + \theta^{(h)})\Omega_c - D_c(\tilde{\kappa} - \theta^{(h)}) + D_a B^{(n)a}_{c} \;=\; 8\pi T_{ab} n^a q^b_c \tag{2.40}$$

$$\frac{1}{2}\mathcal{R} - \Omega_a \Omega^a + D_a \Omega^a - \beta \sigma^{(k)}_{ab} \sigma^{ab}_{(k)} \;=\; 8\pi T_{ab} n^a k^b \, , \tag{2.41}$$

$$\widehat{\mathcal{L}}_h q_{ab} \;=\; B^{(h)}_{ab} \, . \tag{2.42}$$

We expand the extrinsic curvature terms using Eq. (2.11) and Eq. (2.12), to obtain[2]

$$\widehat{\mathcal{L}}_h \theta^{(h)} + \theta^{(h)2} \;=\; -\tilde{\kappa}\theta^{(h)} + \frac{1}{2}\theta^{(h)2} + \sigma^{(h)}_{ab}\sigma^{(n)ba} - D_a \widehat{\Omega}^a + 8\pi T_{ab} h^a n^b \tag{2.43}$$

$$\widehat{\mathcal{L}}_h \Omega_c + \theta^{(h)} \Omega_c \;=\; D_c(\tilde{\kappa}) - D_a \sigma^{(n)a}_{c} - \frac{1}{2} D_c \theta^{(h)} + 8\pi T_{ab} n^a \tilde{q}^b_c \tag{2.44}$$

$$-\frac{1}{2}\mathcal{R} + \Omega_a \Omega^a - D_a \Omega^a \;=\; 8\pi T_{ab} n^a k^b + \beta \sigma^{(k)}_{ab} \sigma^{ab}_{(k)} \, , \tag{2.45}$$

$$\widehat{\mathcal{L}}_h q_{ab} \;=\; \frac{1}{2}\theta^{(h)} q_{ab} + \sigma^{(h)}_{ab} \, . \tag{2.46}$$

[2]The equations appear slightly simpler than in [57, 58, 59] due to a difference in conventions. There, the evolution vector h satisfies $h_a l^a = 1$ (in our notation). This convention is not well-defined when $\beta = 0$, i.e., at points where the screen changes signature. The convention we adopt in this subsection, $h_a k^a = 1$, is everywhere well-defined; this follows from the area theorem [18].

With the definitions

$$\Pi_c \equiv -\frac{1}{8\pi}\Omega_c \qquad \text{momentum density} \tag{2.47}$$

$$\epsilon \equiv \frac{1}{8\pi}\theta^{(h)} \qquad \text{energy density} \tag{2.48}$$

$$P \equiv \frac{1}{8\pi}(\tilde{\kappa} - \theta^{(h)}) \qquad \text{pressure} \tag{2.49}$$

$$Q_c \equiv \frac{1}{8\pi}\widehat{\Omega}_c \qquad \text{heat current} \tag{2.50}$$

$$\zeta \equiv \frac{1}{16\pi} \qquad \text{bulk viscosity} \tag{2.51}$$

$$\mu \equiv \frac{1}{8\pi} \qquad \text{shear viscosity} \tag{2.52}$$

$$f_c \equiv -T_{ab}n^a\tilde{q}^b_c \qquad \text{external force density} \tag{2.53}$$

$$q \equiv T_{ab}n^a h^b \qquad \text{external heat source} \tag{2.54}$$

Eq. (2.44) resembles the Navier-Stokes equation for the momentum density

$$\widehat{\mathcal{L}}_h\Pi_c + \theta^{(h)}\Pi_c = -D_cP + \mu D_a\sigma^{(n)a}_c + \zeta D_c\theta^{(n)} + f_c \ ; \tag{2.55}$$

and Eq. (2.43) resembles an equation governing the flux of the internal energy:

$$\widehat{\mathcal{L}}_h\epsilon + \theta^{(h)}\epsilon = -P\theta^{(h)} + \zeta\theta^{(h)}\theta^{(n)} + \mu\sigma^{(h)}_{ab}\sigma^{(n)ba} - D_aQ^a + q \tag{2.56}$$

First, let us note that the bulk viscosity is positive. This contrasts with the negative (hence unstable) bulk viscosity of the event horizon fluid in the membrane paradigm of Price and Thorne [68]. This is simply because we absorbed an additional term proportional to $\theta^{(h)}$ into the definition of the pressure. With an analogous definition of pressure, one would also find a positive bulk viscosity in [68]. We do not regard this as a success, however. Rather, the fact that pressure and bulk viscosity terms cannot be uniquely identified is a first sign that the fluid analogy fails. We will discuss additional problems below.

Note that a positive bulk viscosity was also obtained in [57, 58, 59], but for a different reason: by defining the pressure to be $\tilde{\kappa}$, and taking $\theta^{(h)}$ rather than $\theta^{(n)}$ to be the expansion rate relevant to the bulk viscosity. However, the same tensor should define both the expansion and the shear. Since $\sigma^{(n)}$ appears in the shear viscosity term of Eq. (2.55), we require that $\theta^{(n)}$, and not $\theta^{(h)}$, appear in the bulk viscosity term. Yet, this requirement, too, appears inconsistent, since the expansion that controls the dilution of the energy and momentum densities is $\theta^{(h)}$.

These ambiguities and contradictions lead us to recognize that the viscous fluid analogy has multiple, serious shortcomings:

- There is no equation of state that would determine the pressure $\tilde{\kappa}$ from other dynamical parameters intrinsic to the fluid.

- There is no dynamical equation for the number density or mass density of fluid particles, analogous to the continuity equation.
- Therefore, there is no well-defined velocity vector field ("v^b").
- Therefore, the rate of shear and expansion cannot be computed from the dynamical equations (via "$D_a v^b$"). Rather, these rates are an arbitrary external input variable.
- The dissipation term $\mu\sigma^{(h)}_{ab}\sigma^{(n)ba}$ in Eq. (2.56) corresponds neither to a Newtonian, nor properly to a non-Newtonian fluid. $\sigma^{(h)}_{ab}$ is entirely independent of $\sigma^{(n)}_{ab}$, so the viscous stresses are not a function of fluid variables alone.

Some of this criticism also applies to the fluid description of event horizons in the membrane paradigm [69, 68], as has also been noted by Strominger and collaborators [70].

Finally, it is not clear what the interpretation of Eq. (2.45) and Eq. (2.46) is, in the fluid picture. They state that not all external input parameters are completely independent, such as $\sigma^{(k)}_{ab}$ and $\sigma^{(h)}_{ab}$, q_{ab} and T_{nk}. Alternatively we may regard Eq. (2.45) as a constraint equation determining the parameter β.

To conclude, we do not find the interpretation of screen evolution as fluid dynamics to be plausible. Moreover, the above analysis, with M and H fixed, actually ignores a crucial degree of freedom, as we shall see next.

Observer-Dependence

An instructive way to think about the evolution equations is to consider only the 4D spacetime M as given. Our task is to construct a holographic screen, H. Once we have started, the equations tell us how to find the (infinitesimally) next leaf. This task is ambiguous because each leaf is associated with a null slice and there are many ways of picking a null foliation of M. We can regard $\alpha < 0$ as a free parameter that determines a choice of a null foliation (for a fixed, arbitrary choice of null vector field l at every leaf). There is no equation determining α, because it is a genuine ambiguity, corresponding to the "observer-dependence" of holographic screens.

Let us define an effective stress tensor

$$8\pi\bar{T}_{ab} \equiv 8\pi T_{ab} + k_a k_b B^{cd}_{(l)} B^{(l)}_{cd} + l_a l_b B^{cd}_{(k)} B^{(k)}_{cd} \tag{2.57}$$

$$= 8\pi T_{ab} + k_a k_b \left(\frac{\theta^2_{(l)}}{2} + \sigma^{cd}_{(l)}\sigma^{(l)}_{cd} \right) + l_a l_b \sigma^{cd}_{(k)}\sigma^{(k)}_{cd} \ . \tag{2.58}$$

This takes a form similar to the effective stress-energy of gravitational radiation in linearized gravity. In general no local definition of energy can be given for gravitational degrees of freedom, but here the holographic screen provides additional structure analogous to a preferred background. Thus, $\bar{T}_{ab}$ can be interpreted as incorporating stress energy associated

with gravitational radiation crossing the leaf orthogonally.[3] Thus Eqs. (2.34)-(2.36) become

$$\alpha(\widehat{\mathcal{L}}_h + \tilde{\kappa})\theta^{(l)} + D_a(-2\alpha\beta\Omega^a + \beta D^a\alpha - \alpha D^a\beta) = 8\pi\bar{T}_{ab}n^a h^b \tag{2.59}$$

$$(\widehat{\mathcal{L}}_h + \theta^{(h)})\Omega_c - D_c\tilde{\kappa} + \alpha D_c\theta^{(l)} = 8\pi\bar{T}_{ab}n^a q^b_c - D_a B^{(n)a}_c \tag{2.60}$$

$$-\frac{\alpha}{2}\mathcal{R} + \alpha\Omega_a\Omega^a - \alpha D_a\Omega^a - 2\Omega^a D_a\alpha + D_a D^a\alpha + 8\pi\alpha\bar{T}_{ab}k^a l^b = 8\pi\beta\bar{T}_{ab}k^a k^b \ , \tag{2.61}$$

Eq. (2.37) is trivial from this viewpoint, so we have not listed it again.

Geometrically, we can think of the role of α and β by considering the forward evolution of the screen by an infinitesimal "time" step dR (see Fig. (2.1)). In order to find the next leaf after $\sigma(R)$, we transport the leaf $\sigma(R)$ infinitesimally along αl to a nearby surface $\bar{\sigma}(R+dR)$. In general this surface will not be marginally trapped, but it does define a new null slice, $N(R+dR)$, generated by the k-lightrays orthogonal to $\bar{\sigma}(R+dR)$. Then we find the cut with $\theta^{(k)} = 0$ on $N(R+dR)$. This gives the new leaf $\sigma(R+dR)$.

Eq. (2.61) can be regarded as a constraint equation that allows us to short-circuit this construction. It can be solved for β, because the generic condition of [18, 19] requires that

$$\bar{T}_{ab}k^a k^b > 0 \ . \tag{2.62}$$

Then $\sigma(R+dR)$ can be obtained directly, by transporting the surface $\sigma(R)$ along the vector $h = \alpha l + \beta k$. Thus, the parameter β tells us how far to slide up or down $N(R+dR)$ from the "wrong" surface $\bar{\sigma}(R+dR)$ to get to the correct new leaf $\sigma(R+dR)$.

The remaining Eq. (2.59) and Eq. (2.60) describe the evolution of the vector fields k and l which are linked by the condition $k^a l_a = -1$. They provide additional structure beyond the given spacetime M, associated with the screen H. As shown in Appendix (A), the failure of k and l to be parallel-transported into themselves along H by h is captured by $\tilde{\kappa}$, α, β, and the vector field Ω_c:

$$h^b\nabla_b k_a = \tilde{\kappa}k_a + D_a\alpha - \alpha\Omega_a \tag{2.63}$$

$$h^b\nabla_b l_a = -\tilde{\kappa}l_a + D_a\beta + \beta\Omega_a \tag{2.64}$$

Note that both $\theta^{(l)}$ and its derivative are fully determined by the arbitrary choice of the "length" of l at each leaf. Here we take the "length" of l as input, so Eq. (2.59) acts as a constraint that determines $\tilde{\kappa}$. [Alternatively, we could specify $\tilde{\kappa}$ and thus fix the length of l via Eq. (2.59).] Finally, Eq. (2.60) is a dynamical evolution equation for Ω_c.

Background-Free Description

Finally, we consider an interpretation where neither M nor H are given. Then we may regard Eqs. (2.34)-(2.37) as a nonrelativistic system evolving with the time variable R. The

[3] In [71], Hayward derives a stress tensor for the gravitational radiation in a "quasi-spherical" approximation. We do not work in this approximation, but we not that his result takes the same form as our definition in Eq. (2.58).

advantage of this viewpoint is that it makes no reference to the spacetime that the screen is embedded in, or even to an induced 2+1 metric on the screen. This minimal approach may be appropriate if we regard the screen as a (partially) pre-geometric object that arises from an underlying quantum gravity theory in an appropriate regime. It may be natural for the screen to be constructed as a first step, before reconstructing the entire 4D geometry and fields. Eqs. (2.34)-(2.37) constrain this construction.

In this case it is convenient to choose a gauge in which $\theta^{(l)} = -1$, so that Eqs. (2.34)-(2.37) reduce to

$$-\alpha\tilde{\kappa} - D_a\left[\alpha\beta\left(2\Omega^a + D^a \log\frac{\beta}{\alpha}\right)\right] = 8\pi\bar{T}_{ab}n^a h^b \tag{2.65}$$

$$\dot{\Omega}_c - \alpha\Omega_c - D_c\tilde{\kappa} + \frac{1}{2}D_c\alpha = 8\pi\bar{T}_{ab}n^a q^b_c - D_a\sigma^{(n)a}_c \tag{2.66}$$

$$\alpha\left[\Omega_a\Omega^a - D_a\Omega^a - 2\Omega^a D_a \log\alpha - \frac{\mathcal{R}}{2} + \alpha^{-1}D_a D^a\alpha\right] = 8\pi\bar{T}_{ab}n^a k^b \tag{2.67}$$

$$\dot{q}_{ab} = -\frac{\alpha}{2}q_{ab} + \alpha\sigma^{(l)}_{ab} + \beta\sigma^{(k)}_{ab}\,. \tag{2.68}$$

We have replaced the Lie-derivatives with dots, since in this viewpoint they are simple time derivatives. Objects such as k, l, h, n are now considered to emerge in the reconstruction of the geometry. For example, the length of integral curves of h is related to the evolution parameter R by $(dL/dR)^2 = -2\alpha\beta$, where positive values correspond to a spacelike signature. Similarly, $\tilde{\kappa}$ and Ω allow us to reconstruct the null vector fields k and l by integration of Eq. (2.63) and Eq. (2.64). None of these geometric concepts are intrinsic to the above equations, but they can be reconstructed from them.

We may regard $\alpha, \beta, \kappa, \Omega_c$, and the 2D metric q_{ab} as intrinsic quantities of the holographic screen, but they are highly underdetermined. It is not clear whether $\sigma^{(k,l)}_{ab}$ and $T_{ab}n^b$ are best regarded as input (which happens to correspond to the matter stress tensor and gravitational waves in the reconstructed 4D spacetime); or rather whether the above equations should be viewed as determining certain components of the stress tensor and the shear, given arbitrary input for the screen quantities $\alpha, \beta, \kappa, \Omega_c$. One parameter (most naturally α) is associated with a null foliation of the 4D spacetime. For each leaf of the screen, microscopic data should determine the quantum state on the associated null slice.

2.4 Examples of Holographic Screens

In this section, we work out a number of detailed examples of physical interest. Several of the holographic screens we will construct are spherically symmetric. Therefore, we will begin by listing general results that apply to all spherical screens, before specializing further.

Implications of Spherical Symmetry

Consider a screen H embedded in a spacetime M, such that both are invariant under spherical symmetry. In this case we shall choose the area radius as the evolution parameter R,

$$A = 4\pi R^2 \ . \tag{2.69}$$

We shall further choose the convention that

$$\alpha = -1 \ , \tag{2.70}$$

which can be regarded as gauge-fixing the rescaling symmetry of l. The metric q_{ab} is of the form

$$q_{ab} = R^2 s_{ab} \tag{2.71}$$

where s_{ab} is the metric on the unit two-sphere. Using the above conventions of R and α, one finds

$$\theta^{(l)} = \theta^{(n)} = -\theta^{(h)} = -\frac{d}{dR}\log A = -\frac{2}{R} \ . \tag{2.72}$$

The shears and the normal one form would break spherical symmetry and so must vanish,

$$\sigma_{cd}^{(k,l,h,n)} = 0 \ , \quad \Omega_c = 0 \ . \tag{2.73}$$

Since $h^a h_a = 2\beta$, the induced 3-metric on H is

$$ds_H^2 = 2\beta dR^2 + R^2 d\Omega^2 \ ; \tag{2.74}$$

Again, this is only well-defined piecewise on portions with definite sign of β, and we will not consider this metric further.

The only nontrivial intrinsic quantities associated with screen evolution are the slope, β, and the acceleration, κ. They are determined entirely by certain stress tensor components and by R, since Eq. (2.34) and Eq. (2.36) reduce to

$$\tilde{\kappa} \ = \ 4\pi R \ T_{ab} n^a h^b \tag{2.75}$$

$$\beta \ = \ \frac{(8\pi R^2)^{-1} - T_{ab} k^a l^b}{T_{ab} k^a k^b} \ . \tag{2.76}$$

We have used $\mathcal{R} = 2/R^2$. The former equation is somewhat reminiscent of a first law, if we write it as

$$\frac{\tilde{\kappa}}{2\pi}\frac{d(A/4)}{dR} = \oint d^2\vartheta \sqrt{q} \ T_{ab} n^a h^b \ . \tag{2.77}$$

The equation for β can also be written as a constraint linking the radius to a stress tensor component:

$$\frac{1}{8\pi R^2} = T_{ab} n^a k^b \ . \tag{2.78}$$

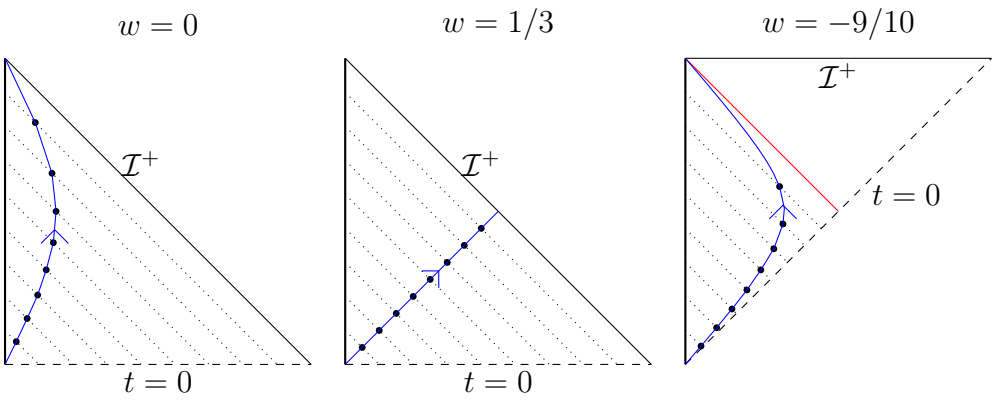

Figure 2.2: Penrose diagrams for a spatially flat FRW universe dominated by matter (left) and radiation (middle). The right diagram is an approximation to de Sitter spacetime; it contains a fluid with positive energy and equation of state close to that of vacuum energy. To construct a past holographic screen H, we consider the past light-cones (dotted lines) of a comoving observer at $r = 0$ (left edge). The surfaces of maximum area on each of these light cones (black dots) are the leaves of the screen H (blue curve). Note that H approaches the event horizon (red line) at late times, in the near-de Sitter case. We find that the surface gravity κ approaches that of de Sitter space in the limit.

Expanding Universe

Let M be a flat Friedmann-Robertson-Walker universe with fixed equation of state $p = w\rho$, $-1 < w \leq 1$; see Fig. (2.2). The stress tensor is

$$T_{ab} = \rho t_a t_b + p(g_{ab} + t_a t_b)\,. \tag{2.79}$$

The metric is

$$ds^2 = -dt^2 + a^2(t)\left(dr^2 + r^2 d\Omega^2\right) \tag{2.80}$$

with

$$a(t) = t^q \tag{2.81}$$

and

$$q = \frac{2}{3}\frac{1}{1+w}\,. \tag{2.82}$$

To generate a null foliation of M, we consider the past light-cone of each point on the worldline $r = 0$; see Fig. (2.6)). On each cone, there is a cross-section of maximal area (since $A \to 0$ as the big bang is approached). This surface has vanishing expansion, $\theta^{(k)} = 0$, by construction. The relevant spheres lie at (r, t) subject to the condition [15, 16]

$$r\dot{a}(t) - 1 = 0. \tag{2.83}$$

The proper area radius is $R = ra(t)$. The future-directed outgoing congruence from any sphere in this geometry is obviously expanding, so this is a past holographic screen. Therefore [18], we have $\alpha > 0$.

In order for the screen to stay centered on the comoving worldline $r = 0$, we must take α to be independent of angle, for example

$$\alpha = 1 \ . \tag{2.84}$$

We will make a different, angle-dependent choice below, corresponding to the construction of a nonspherical screen in the same spacetime (see Sec. (2.3)).

The null normals k, l satisfying $k^a l_a = -1$, $\theta^{(l)} = 2/R$ are

$$k^a = \left(\frac{\partial}{\partial t}\right)^a - \frac{1}{a(t)}\left(\frac{\partial}{\partial r}\right)^a , \tag{2.85}$$

$$l^a = \frac{1}{2}\left(\frac{\partial}{\partial t}\right)^a + \frac{1}{2a(t)}\left(\frac{\partial}{\partial r}\right)^a . \tag{2.86}$$

The vectors normal and tangent to the screen are $n = -l + \beta k$ and $h = l + \beta k$ with

$$\beta = q - \frac{1}{2} = \frac{1}{6}\frac{1-3w}{1+w} \tag{2.87}$$

This implies, for example, that the screen is timelike in a matter-dominated universe ($q = 2/3$, $w = 0$, $\beta = 1/6$) and null for a radiation-dominated universe ($q = 1/2$, $w = 1/3$, $\beta = 0$). For stiffer fluids the screen will be spacelike.

The screen acceleration is

$$\tilde{\kappa} = \frac{q-1}{R} \ . \tag{2.88}$$

The "surface gravity" defined in Eq. (2.18) is

$$\kappa \equiv \frac{\tilde{\kappa}}{\beta} = \frac{2q-2}{2q-1}\frac{1}{R} \ . \tag{2.89}$$

For example, $\kappa = -2/R$ for the matter dominated universe. Notably, in the limit as $w \to -1$ ($q \to \infty$), this approaches the surface gravity of the de Sitter Killing horizon: $\kappa \to 1/R$.

Collapsing Star

One can model a collapsing star by a finite, spherical, homogeneous dust ball. This is described by the Oppenheimer-Snyder solution [72]; see Fig. (2.3). It can be constructed as a portion $r < r_*$ of a time-reversed Friedmann-Robertson-Walker cosmology, glued to a portion of the vacuum Schwarzschild solution. However, in order to satisfy the generic condition, Eq. (2.62), we will study the more general collapse of spherically symmetric dust with density $\rho(r)$. We can take $\rho(r)$ to become arbitrarily small outside some characteristic

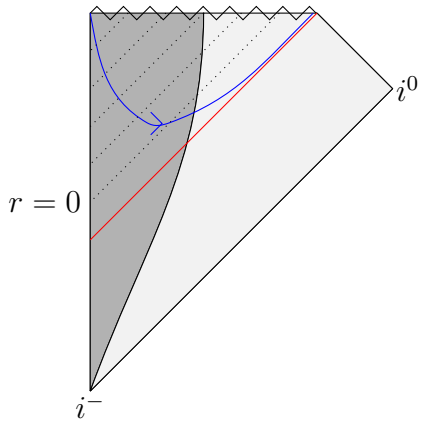

Figure 2.3: Penrose diagram for collapsing dust. The dark-shaded region is the dense region, $r < r_*$. The light shaded region contains arbitrarily dilute matter to satisfy the generic condition. We construct a holographic screen H using the future light-cones (dotted lines) of an observer at $r = 0$. Note that H changes signature and approaches the event horizon (red line) from the inside. We find that κ approaches the Schwarzschild surface gravity there.

radius r_*. The holographic screens in such collapse scenarios were computed by Booth *et al.* in [63]. Here we reproduce the relevant analysis and compute the screen quantities β and $\tilde{\kappa}$.

The metric describing the collapse is

$$ds^2 = -d\tau^2 + \frac{R'(\tau,r)^2}{1-2m(r)/r}dr^2 + R^2\left(d\theta^2 + \sin^2\theta d\phi^2\right) , \tag{2.90}$$

where τ is the proper time along the dust particles, and

$$m(r) = 4\pi\int_0^r dr' r'^2 \rho(r') . \tag{2.91}$$

The stress tensor is

$$T_{ab} = \frac{r^2\rho(r)}{R^2(\tau,r)R'(\tau,r)}(d\tau)_a(d\tau)_b . \tag{2.92}$$

The future holographic screen satisfies [63]

$$R(\tau,r) = 2m(r). \tag{2.93}$$

The null normals such that $k^a l_a = -1$ and $\theta^{(l)} = -2/R$ are

$$k^a \cong \sqrt{1-\frac{2m(r)}{r}}\left(\frac{\partial}{\partial\tau}\right)^a + \frac{1-\frac{2m(r)}{r}}{R'(\tau,r)}\left(\frac{\partial}{\partial r}\right)^a , \tag{2.94}$$

$$l^a \cong \frac{1}{2}\frac{1}{\sqrt{1-\frac{2m(r)}{r}}}\left(\frac{\partial}{\partial\tau}\right)^a - \frac{1}{2R'(\tau,r)}\left(\frac{\partial}{\partial r}\right)^a , \tag{2.95}$$

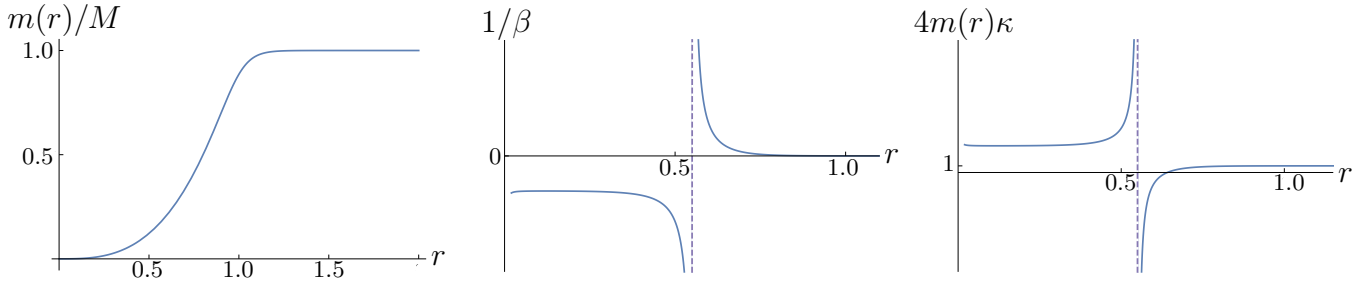

Figure 2.4: Collapsing dust cloud: plots of the radial mass profile (left), the slope parameter β (middle), the surface gravity κ (right), for $r_* = 1$, $q = 1/20$, and $M = 1/100$. The region $r < r_*$ is the dense region. The change in the sign of β indicates the change in of signature of H from timelike to spacelike. The surface gravity saturates to $1/4M$ in the dilute region.

where $\cong$ means that we impose the constraint Eq. (2.93) while evaluating the right hand side. The slope β, and the surface gravity κ are

$$\beta \cong \frac{1}{2m'(r)} \frac{R' - m'(r)}{1 - 2m(r)/r}, \tag{2.96}$$

$$\kappa \cong \frac{1}{2m(r)} \frac{m'(r)}{R'(\tau, r)} \left(\frac{4\beta^2 (1 - 2m(r)/r)^2 - 1}{4\beta(1 - 2m(r)/r)} \right). \tag{2.97}$$

As an example, we consider the 'Fermi-Dirac distribution' for $\rho(r)$

$$\rho(r) = \frac{\mathrm{M}}{-8\pi q^3 \mathrm{Li}_3\left(-e^{r_*/q}\right)} \frac{1}{\exp^{\left(\frac{r-r_*}{q}\right)} + 1}, \tag{2.98}$$

where the overall normalization is such that M is the ADM mass. This reduces to the standard Oppenheimer-Synder solution in the limit $q \to 0$. In the following, we fix $r_* = 1$ and $q = 1/20$.

The profile of the mass is shown in Fig. (2.4). It shows that the most of the mass is in $r < r_*$. We call this region dense region. Fig. (2.4) also shows the plots of $1/\beta$ and $4m(r)\kappa$. Note that β is negative for small r and then becomes positive. This implies a change in the signature of the screen. From the plot of $4m(r)\kappa$, we learn that the surface gravity quickly saturates to the Schwarzschild value in the near-vacuum region:

$$\kappa \to \frac{1}{4M}. \tag{2.99}$$

Charged Black Holes

Next, we consider the Vaidya-Bonnor solution [73, 74], which describes the formation of a black hole by an arbitrary sequence of charged spherical null shells:

$$ds^2 = -f\,dv^2 + 2dv\,dr + r^2\,d\Omega^2 \tag{2.100}$$

where

$$f(r,v) = 1 - \frac{2m(v)}{r} + \frac{e^2(v)}{r^2} \tag{2.101}$$

and $m(v) \geq |e(v)|$ are integrable differentiable functions with

$$\dot{m} \equiv \frac{\partial m}{\partial v} > 0\ , \quad m(\infty) < \infty\ . \tag{2.102}$$

An example is shown in Fig. (2.5). The stress tensor is

$$T_{ab} = -\frac{1}{8\pi r}\dot{f}(r,v)(dv)_a(dv)_b + T^{(EM)}_{ab}\ , \tag{2.103}$$

where

$$T^{(EM)}_{ab} = -\frac{1}{8\pi}\frac{e^2(v)}{r^4}\left(g_{ab} - 2r^2 s_{ab}\right) \tag{2.104}$$

is the stress tensor of the point charge of magnitude $e(v)$, and s_{ab} is the metric on the unit two-sphere.

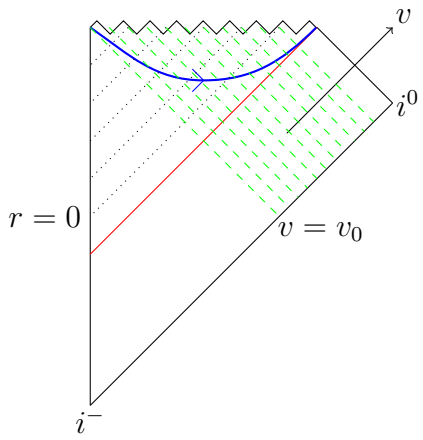

Figure 2.5: The Penrose diagram for Vaidya solution. We show the uncharged case, $e(v) = 0$. The mass function is $m(v) = 0$ for $v < v_0$ and $\dot{m}(v) \geq 0$ for $v > v_0$. The green dashed lines are the ingoing null shells. The red line is the event horizon. The blue line is the future holographic screen constructed from future light-cones centered at $r = 0$.

The holographic screen, H, consists of marginally trapped surfaces, with k the future and outward directed null vector. The condition $\theta^{(k)} = 0$ implies $r = R$ and $f(R, v) = 0$, and thus

$$R = m(v) + \sqrt{m^2(v) - e^2(v)} \ . \tag{2.105}$$

The null vectors normal to the leaves are found to be

$$k^a = \left(\frac{\partial}{\partial v}\right)^a , \tag{2.106}$$

$$l^a = -\left(\frac{\partial}{\partial r}\right)^a . \tag{2.107}$$

Their linear combinations tangent and normal to H, $h = -l + \beta k$, $n = l + \beta k$ are determined by

$$\beta = \frac{dv}{dR} = \frac{R - m(v)}{R\dot{m}(v) - e(v)\dot{e}(v)} \ . \tag{2.108}$$

The acceleration is

$$\tilde{\kappa} = \frac{(R - m(v))^2}{R^2(R\dot{m}(v) - e(v)\dot{e}(v))} \ ; \tag{2.109}$$

the surface gravity, $\tilde{\kappa}/\beta$, is

$$\kappa = \frac{m(v)}{R^2} - \frac{e^2(v)}{R^3}, \tag{2.110}$$

Note that this result has the same form as the surface gravity of a Reissner-Nordstrom black hole with mass m and charge e. Moreover, let us define an electric potential in the usual way,

$$\Phi = \frac{e(v)}{R} \ . \tag{2.111}$$

Then Eq. (2.77) takes a form similar to the first law of thermodynamics for a Reissner-Nordstrom black hole:

$$\frac{\kappa}{8\pi}\frac{dA}{dR} = \frac{dm}{dR} - \Phi \ \frac{de}{dR} \ , \tag{2.112}$$

where we have used Eq. (2.108) and the chain rule, $\beta\dot{f} = v'(R)\dot{f} = f'$.

Nonspherical Screen in Cosmology

We again consider the expanding universe and specialize to the matter dominated universe: $p = 0$. The metric is

$$ds^2 = a^2(\eta)\left(-d\eta^2 + dx^2 + dy^2 + dz^2\right) \ , \tag{2.113}$$

with

$$a(\eta) = \eta^2/9 \ . \tag{2.114}$$

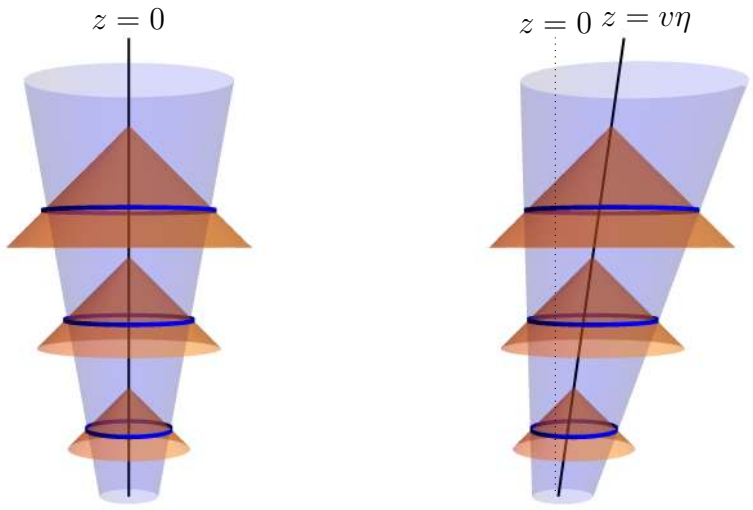

Figure 2.6: Two past holographic screens in the same expanding universe, associated with two different observers (thick black worldlines). *Left:* spherically symmetric screen constructed from a comoving observer at $r = 0$. *Right:* screen constructed from the past light-cones of a non-comoving observer.

We pick an observer whose worldline is given by

$$z = v\eta \ , \tag{2.115}$$

for $-1 < v < 1$. To construct the past screen, we shoot past light cones from each point on this worldline, and find the cross-section of maximal area on each of these light cones; see Fig. (2.6). The collection of all these cross-section, that is the past screen, satisfies the condition

$$\left(z - \frac{3}{2}\eta\right)^2 + x^2 + y^2 - \frac{\eta^2}{4} = 0. \tag{2.116}$$

We choose to work in the coordinate system

$$\begin{aligned} z &= \frac{3}{2}v\eta + r\cos\theta \,, && (2.117)\\ x &= r\sin\theta\cos\phi \,, && (2.118)\\ y &= r\sin\theta\sin\phi \,, && (2.119)\\ \eta &= \eta \,. && (2.120) \end{aligned}$$

In these coordiante system, Eq. (2.116) simplifies to

$$r - \frac{\eta}{2} = 0. \tag{2.121}$$

The area-radius of the leaf of the screen is

$$R = ra(\eta) = \frac{\eta^3}{18}. \tag{2.122}$$

We pick an orthogonal basis for the one-forms tangent tn the leaf:

$$\hat{e}^{(1)}_a = -\frac{3v\sin\theta}{\eta}(d\eta)_a + (d\theta)_a\,, \tag{2.123}$$

$$\hat{e}^{(2)}_a = (d\phi)_a\,, \tag{2.124}$$

where $q_a{}^b\hat{e}^{(i)}_b = \hat{e}^{(i)}_a$ for $i = \{1,2\}$, and $\hat{e}^{(1)}\cdot\hat{e}^{(2)} = 0$. Similarly, we pick an orthogonal basis for vectors normal to the leaf:

$$\chi^a_{(1)} = \left(\frac{\partial}{\partial\eta}\right)^a - \frac{3v\cos\theta}{2}\left(\frac{\partial}{\partial r}\right)^a + \frac{3v\sin\theta}{\eta}\left(\frac{\partial}{\partial\theta}\right)^a\,, \tag{2.125}$$

$$\chi^a_{(2)} = \left(\frac{\partial}{\partial r}\right)^a\,. \tag{2.126}$$

where $q^a{}_b\chi^b_{(i)} = 0$ for $i = \{1,2\}$, and $\chi_{(1)}\cdot\chi_{(2)} = 0$. The null vectors normal to the leaf, normalized such that $k^a l_a = -1$ and $\theta^{(l)} = 2/R$, are

$$k^a = \frac{1}{a(\eta)}\left(\chi^a_{(1)} - \chi^a_{(2)}\right)\,, \tag{2.127}$$

$$l^a = \frac{1}{2a(\eta)}\left(\chi^a_{(1)} + \chi^a_{(2)}\right)\,. \tag{2.128}$$

The tangent and normal vectors to the screen are $h^a = \alpha l^a + \beta k^a$ and $n^a = -\alpha l^a + \beta k^a$, where

$$\alpha = 1 + v\cos\theta\,, \tag{2.129}$$

$$\beta = \frac{1}{6}\left(1 - 3v\cos\theta\right)\,. \tag{2.130}$$

The normal one-form and the acceleration are

$$\Omega_a = 0\,, \tag{2.131}$$

$$\widehat{\Omega}_a = -\frac{2v\sin\theta}{3}\,\hat{e}^{(1)}_a\,, \tag{2.132}$$

$$\tilde{\kappa} = -\frac{1}{3R}\left(1 + 3v\cos\theta\right)\,. \tag{2.133}$$

One can easily combine this construction with that of the spherically symmetric screen in an expanding universe. For example, we can use the worldline $r = 0$ up to some conformal time η_* to construct a portion of the screen which is centered at $r = 0$. We can then

consider continuing this worldline to that of a moving observer, by substituting $\eta \to \eta - \eta_*$ in Eq. (2.116) and below. This corresponds to choosing α as in Eq. (2.129), instead of $\alpha = 1$, for $\eta > \eta_*$. We thus obtain a nonspherical screen (above η_*), corresponding to the fact that the observer's worldline (and the associated null foliation) violates the spherical symmetry, above η_*. This illustrates how the observer-dependence of H is captured by a choice of α, as advertised in Sec. (2.3).

Chapter 3

Non-relativistic Geometry of Holographic Screens

3.1 Introduction

The holographic principle [8, 9], loosely speaking, asserts that the physical degrees of freedom of quantum gravity in a region of area A cannot be more than $\frac{A}{4G\hbar}$. This principle was presented in a more formal setting in terms of covariant entropy bound, or Bousso bound [10, 11, 16, 12, 13], which bounds the entropy on the light-sheets of any spatial codimension-2 surface by the area of this surface. The AdS-CFT correspondence [14] provides an example of this principle. The correspondence states that the quantum state on a slice of AdS is described by the state of the CFT on the boundary of that slice.

Despite the success of the AdS-CFT correspondence, not much progress has been made in generalizing it to general spacetimes. The reason behind the lack of progress in this direction is that it is not clear where the information of the state of the bulk theory on a given slice of the spacetime lives. That is, it is not clear what codimension-1 surface plays the role of the conformal boundary of the AdS. Holographic screens [15] are believed to be a candidate for this surface.

A holographic screen is constructed by starting with a null foliation, $N(R)$, of the spacetime. On each null hypersurface, we choose a spatial cross-section of largest area. This cross-section, $\sigma(R)$, called *leaf*, is a codimension-2 spatial surface with vanishing expansion. That is,

$$\theta^{(k)} = 0\,, \tag{3.1}$$

where k^a is the null generator of the null slice, $N(R)$. Assuming the null energy condition, the Raychaudhri equation (see for *e.g.* [75]) guarantees that the portions of $N(R)$ 'outside' and 'inside' of $\sigma(R)$ are two separate light-sheets of $\sigma(R)$. The covariant entropy bound then implies that the entropy of the quantum state on the null slice is bounded by the area of the corresponding leaf. The codimension-1 hypersurface foliated by these leaves, by construction,

bounds the entropy of the spacetime, slice by slice. This codimension-1 hypersurface is called holographic screen.

Recently it has been shown that the area of the leaves obeys an area law in the spacetimes which satisfy few generic conditions [18, 19]. The area law states that the area of the leaves is monotonic as we translate from one leaf to another. The fact that the area of leaves is not constant seems problematic, as it indicates that the degrees of freedom of the dual theory vary with time. This suggests that the dual theory might not be a unitary QFT.

Some progress has been made in developing the holographic theory of the general spacetimes. In [50], the holographic entropy formula of [26, 27] has been generalized beyond AdS-CFT correspondence. They proposed that the entanglement entropy of the reduced quantum state on some subregion of the leaf is related to the area of the stationary surface anchored on the boundary of that subregion. This proposal has been used in [52, 76] to study the Hilbert space structure of the holographic theory.

In Ch. (2), we have studied the dynamical equations of holographic screen. These are actually the constraints equations of GR (see Eqs. (3.13)), but we have decomposed them in $2+1$ equations, using the additional structure of the screen in terms of foliation into leaves. We will review these equations in Sec. (3.2). These $2+1$ equations are invariant under the foliation preserving diffeomorphism, but not under arbitrary coordinate transformation on the screen. One of the main results of this chapter is to write a covariant version of these equations.

The goal of this chapter is to understand the intrinsic geometry of holographic screen, H. The motivation behind this is that if we hope to put a holographic field theory on H, then we need to understand how to couple this theory with the geometry of H. For instance, we have to define the notion of parallel transport and covariant derivative on H. If H were a hypersurface which is nowhere null, with the normal vector normalized such that $\hat{n}^a\hat{n}_a = \pm 1$, then the induced metric on the screen would have been

$$\gamma_{ab} = g_{ab} \mp \hat{n}_a\hat{n}_b \,. \tag{3.2}$$

In this chapter, we assume the following index notation: The first half of the Latin letters (a, b, c) denote the directions in the full 4-dimensional spacetime. The second half of the Latin letters (i, j, k) denote the directions on the codimension-1 hypersurface (such as H). The upper case Latin letters (A, B, C) denote the directions on the codimenison-2 surface (such as $\sigma(R)$). Let e^a_i be the pull-back operator that pull backs an one-form from the spacetime to the codimension-1 hypersurface. Similarly, we define e^a_A and e^i_A. The pull-back of the spacetime metric on H is

$$\gamma_{ij} = g_{ab}e^a_i e^b_j \,, \tag{3.3}$$

$$= \gamma_{ab}e^a_i e^b_j \,. \tag{3.4}$$

This metric would have completely described the intrinsic geometry of H. For instance, if we were only given H with this metric, and had no information of the geometry of background

spacetime, we could have used this metric to define various geometric quantities on H, like connection and intrinsic Riemann curvature for example.

However, there are known examples where H does not have a fixed signature. As a result, the induced metric becomes degenerate at the points where the hypersurface changes its signature. Therefore, we can not invert this metric, which means we can not use the standard formula of various geometric quantities, such as Christoffel symbols.[1] This concludes that the metric in Eq. (3.2) is not suitable to describe the intrinsic geometry of H.

Furthermore, holographic screens are not arbitrary hypersurfaces of indefinite signature. Rather they have an additional structure of foliation into leaves. It was shown in [19] that this foliation is unique. This hints at the non-relativistic structure of holographic screen. Another reason to expect the non-relativistic structure of holographic screen comes from the fact that the quantization on the light front is non-relativistic (see for *e.g.* [77])[2].

Motivated by these observations, we propose that the geometry of holographic screen should be described by a non-relativistic geometry. In Sec. (3.3), we will review the Newton-Cartan (NC) geometry, an example of a non-relativistic geometry. In Sec. (3.4), we will argue that the Riemannian metric on the leaves, the foliation structure of the screen, and the existence of the vector field normal to the leaves but tangent to the screen, allow us to define NC data on H, which we can use to define connection and curvature on H.

In Sec. (3.4), we will use the diffeomorphism invariance of the screen to derive a covariant version of the dynamical equations of the holographic screens. This will be a test of our proposal that the geometry of the screen is described by the NC formalism. These covariant equations will be in terms of a screen 'stress tensor', 'energy current', and 'momentum one-form'. We will make an ansatz of these tensors in Sec. (3.4). Finally, we will follow [62] to perform the treatment similar to that of Brown and York [78] to verify our ansatz.

3.2 Holographic Screens

A *future/past* holographic screen [18, 19] is constructed by starting with the world line of an observer and shooting future/past light cones from it [15]. These light cones provide us with a one-parameter null foliation, $N(r)$, of some region of the spacetime. On each null hypersurface, we choose the spatial cross-section of maximum area. These spatial surfaces are called leaves, $\sigma(r)$. The Bousso bound [10, 16] guarantees that entropy on $N(r)$ is bounded by the area of $\sigma(r)$. The union of these leaves is called the future/past holographic screen.

By construction, a holographic screen is a codimension-1 hypersurface, which is foliated by the codimension-2 spacelike surfaces, $\sigma(r)$, where r is the foliation parameter. Since the background manifold is Lorentzian, there are two future directed null vectors normal to the

[1] Of course, one can still define various quantities as the pullback of their analogs from the full spacetime. However, this would require the knowledge of the background spacetime, whereas we want to study the geometry of H assuming we know nothing about the metric of the spacetime.

[2] We thank R. Bousso for emphasizing these points.

leaves, l^a and k^a. We fix their relative normalization by demanding $k^a l_a = -1$. The defining property of holographic screen is that the expansion of the null congruence in k^a direction vanishes, that is

$$\theta^{(k)} \equiv \tilde{q}^{ab}\nabla_a k_b = 0\,, \tag{3.5}$$

where

$$\tilde{q}^{ab} = g^{ab} + k^a l^b + l^a k^b\,, \tag{3.6}$$

$$= e^a_A e^b_B \tilde{q}^{AB}\,, \tag{3.7}$$

is the induced (inverse) metric on the leaves. For future/past holographic screens, the leaves are marginally trapped/anti-trapped [18, 19]. This means that the expansion in the l^a direction is negative for future holographic screens,

$$\theta^{(l)} < 0\,, \tag{3.8}$$

where as the opposite inequality holds for past holographic screen.

Given an arbitrary codimension-1 hypersurface of indefinite signature, one might ask what data is required to describe the intrinsic geometry of the hypersurface. One candidate is to use the induced metric on the hypersurface, defined as the pull-back of the spacetime metric

$$\gamma_{ij} = e^a_i e^b_j g_{ab}\,. \tag{3.9}$$

Though this works for the hypersurfaces that are nowhere null, it is not suitable for the hypersurfaces which do not have a fixed signature. For these hypersurfaces, the metric in Eq. (3.9) becomes degenerate, and hence non-invertible, wherever the signature changes. As a result, we can not define the connection, curvature, or any other intrinsic quantity that requires the inverse metric, on these hypersurfaces.

As holographic screens do not have a definite signature, it is interesting to understand how to describe their intrinsic geometry. In this section, we will review some properties of the holographic screens that were proven in [19]. We will see in Sec. (3.4) that these properties allow us to propose that the intrinsic geometry of the holographic screens can be described by the Newton-Cartan geometry. We will also review the evolution equations of the holographic screens, that were studied in Ch. (2), in the current section.

Let h^i be the vector tangent to the screen, but normal to the leaves. This means that we can write it as a linear combination [18, 19]

$$e^a_i h^i = h^a = \alpha l^a + \beta k^a\,. \tag{3.10}$$

Since the signature of the screen is not fixed, we can not normalize the vector h^a by fixing its norm. Instead, we normalize it by demanding that $h^a(dr)_a = h^i(dr)_i = 1$. Similarly, we fix the length of the normal vector, n^a, to the holographic screen by demanding $n^a n_a = -h^a h_a$. This implies that the normal vector can be written as

$$n^a = -\alpha l^a + \beta k^a\,. \tag{3.11}$$

Assuming some mild generic conditions, an area law for the holographic screens was proven in [18, 19]. An important ingredient in the proof of this area law in [19] was the proof of the fact that α in Eq. (3.10) does not vanish. In particular, it was shown that $\alpha < 0$ for future holographic screens, while $\alpha > 0$ for past screens. This important result, together with Eq. (3.5) and Eq. (3.10), immediately yields the area law: "the area of the leaves always increases as we move along the screen". That is,

$$\theta^{(h)} = \alpha\theta^{(l)} > 0\,. \tag{3.12}$$

The result $\alpha \neq 0$ is important to us for one another reason. We will see in Sec. (3.4) that this result plays a significant role in the consistency of our proposal to describe the intrinsic geometry of the screen using Newton-Cartan geometry.

Another important theorem proven in [19] guarantees the uniqueness of the foliation of a holographic screen into leaves. In particular, it was shown that if we take a screen and choose a different foliation into codimension-2 closed surfaces, these surfaces will not have vanishing null expansion. This implies that the foliation into leaves is important for the defining property of the holographic screens, as was also emphasized in [62]. Without this foliation, $\theta^{(k)} = 0$ condition is not well-defined.

Imposing Einstein equations on the spacetime puts constraints on the extrinsic geometry of a codimension-1 hypersurface,

$$G_{ab}n^a e^b_i = 8\pi T_{ab}n^a e^b_i\,. \tag{3.13}$$

For hypersurfaces with fixed signature, Gauss-Codazzi equations (see for *e.g.* [79]) can be used to write these constraint equations as

$$\widehat{D}_j(\widehat{K}^j_i - \gamma^j_i\widehat{K}) = T_{ab}\hat{n}^a e^b_i\,, \tag{3.14}$$

where $\widehat{D}_j$ is the covariant derivative compatible with the metric γ_{ij} in Eq. (3.9), and $\widehat{K}_{ij}$ is the extrinsic curvature of the hypersurface. However, Eq. (3.14) is not well-defined for the holographic screens as both the covariant derivative compatible with γ_{ij} and the extrinsic curvature tensor are defined using the inverse induced metric, γ^{ij}. To resolve this problem, it was suggested in Ch. (2) to use the foliation structure of the screen, and to use the geometric quantities defined using the (Riemannian) metric on the leaves, such as the extrinsic curvature of the leaves

$$B^{(h)}_{AB} = e^a_A e^a_B B^{(h)}_{ab}\,, \tag{3.15}$$

$$B^{(n)}_{AB} = e^a_A e^a_B B^{(n)}_{ab}\,, \tag{3.16}$$

with

$$B^{(h)}_{ab} = \frac{1}{2}\,\tilde{q}^c_a\tilde{q}^d_b\mathcal{L}_h\tilde{q}_{cd}\,, \tag{3.17}$$

$$B^{(n)}_{ab} = \frac{1}{2}\,\tilde{q}^c_a\tilde{q}^d_b\mathcal{L}_n\tilde{q}_{cd}\,. \tag{3.18}$$

The extrinsic geometry of the screen is not completely fixed by that of the leaves, as $B^{(n)}_{AB}$ has only three components while there are six components of $\widehat{K}_{ij}$. The rest of the information of the extrinsic geometry of the screen is given in terms of the *normal one-form*,

$$\omega_i \equiv -e^a_i l^b \nabla_a k_b \,, \tag{3.19}$$

which can be decomposed into a scalar and a one-form on the leaf,

$$\tilde{\kappa} = h^i \omega_i = -l^b h^a \nabla_a k_b \,, \tag{3.20}$$

$$\Omega_A = e^i_A \omega_i = -e^a_A l^b \nabla_a k_b \,. \tag{3.21}$$

In terms of these geometric quantities, and using the foliation structure of the screen, Eq. (3.13) can be decomposed in $2+1$ 'evolution' equations of the holographic screens (also see [57, 58, 59] for similar equations for dynamical or trapping horizons [54, 53, 55, 56])

$$\alpha \mathcal{L}_h \theta^{(l)} + \theta^{(h)2} - B^{(h)AB}\left(B^{(n)}_{AB} - \theta^{(n)}\tilde{q}_{AB} - \tilde{\kappa}\tilde{q}_{AB}\right) + \widetilde{D}_A \widehat{\Omega}^A = 8\pi T_{ab} n^b h^a \,, \tag{3.22}$$

$$\tilde{q}^B_A \mathcal{L}_h \Omega_B + \theta^{(h)}\Omega_A + \widetilde{D}_B\left(B^{(n)B}_A - \theta^{(n)}\tilde{q}^B_A - \tilde{\kappa}\tilde{q}^B_A\right) - \theta^{(l)}\widetilde{D}_A \alpha = 8\pi T_{ab} n^b e^a_A \,, \tag{3.23}$$

where $\widetilde{D}_A$ is the covariant derivative compatible with $\tilde{q}_{AB}$, and $\widehat{\Omega}_A \equiv e^a_A \widehat{\Omega}_a$ is defined as,

$$\widehat{\Omega}_a \equiv h^b \tilde{q}^c_a \nabla_c n_b \,. \tag{3.24}$$

These evolution equations are invariant under diffeomorphisms on the screen that preserve the foliation structure of the screen. These diffeomorphisms include the diffeomorphism on the leaves, plus the reparameterization of the foliation parameter. In Sec. (3.4), we will use the Newton-Cartan structure on the screen to write these equations in a covariant form, that is in a form which is invariant under the full diffeomorphism on the screen.

3.3 Newton-Cartan Geometry

The Newton-Cartan geometry is an example of a non-relativistic geometry, originally developed by Cartan as the geometric formulation of Newtonian gravity [80, 81]. This has gained popularity in the recent years owing to its many applications. For instance, it has been used to write the effective field theory and to study the covariant Ward identities of the quantum Hall effect in [65, 82]. It has also been used to couple non-relativistic field theories with the background spacetime in [83, 66, 84, 67, 85], and to present the covariant formulation of non-relativistic hydrodynamics in [86, 67, 87]. It was shown in [88] that making the Newton-Cartan geometry dynamical gives rise to Hořava-Lifshitz gravity [89], and it has been used to study Lifshitz holography in [90, 91, 92, 84].

In this section, we present a review of the Newton-Cartan (NC) geometry. There are different conventions used in the literature when describing NC geometry. We will be using

the conventions used in [65]. Consider a 2+1-dimensional manifold $\mathcal{M}$ such that $\mathcal{M} = R \times \Sigma$, where Σ are 2-dimensional Riemannian manifolds (generalization to higher dimensions is trivial). The NC structure on $\mathcal{M}$ means that there is a one-form field τ_i such that

$$\tau \wedge d\tau = 0\,, \tag{3.25}$$

a degenerate inverse metric h^{ij} such that

$$h^{ij}\tau_j = 0\,, \tag{3.26}$$

and a vector field v^i such that

$$v^i\tau_i = 1\,. \tag{3.27}$$

The condition in Eq. (3.25) implies that τ is hypersurface orthogonal. The volume element on $\mathcal{M}$ is given by

$$\widehat{\epsilon} = \tau \wedge \widetilde{\epsilon}\,, \tag{3.28}$$

where $\widetilde{\epsilon}$ is the volume element on Σ.

Note that we are not provided with a metric on $\mathcal{M}$. This means that the connection, and hence covariant derivative, on $\mathcal{M}$ cannot be defined using the standard formulae from any textbook of GR, such as [75]. To remedy this, we first define a unique tensor h_{ij} by demanding

$$h_{ij}v^j = 0\,, \qquad\qquad h^{ik}h_{kj} = \delta^i_j - v^i\tau_j \equiv P^i_j\,. \tag{3.29}$$

Demanding 'metric compatibility' conditions

$$D_i\tau_j = 0\,, \qquad\qquad D_ih^{jk} = 0\,, \tag{3.30}$$

and 'curl-freeness' of v^i

$$D^iv^j - D^jv^i = 0\,, \tag{3.31}$$

yields the unique connection [82]

$$\widehat{\Gamma}^i_{\ jk} = v^i\partial_j\tau_k + \frac{1}{2}h^{il}\left(\partial_jh_{kl} + \partial_kh_{jl} - \partial_lh_{jk}\right)\,. \tag{3.32}$$

Note that this connection has torsion unless τ_i is closed:

$$T^i_{jk} \equiv \widehat{\Gamma}^i_{\ jk} - \widehat{\Gamma}^i_{\ kj}\,, \tag{3.33}$$

$$= v^i(d\tau)_{jk}\,. \tag{3.34}$$

The Lie derivative of h_{ij} along v^i

$$B^{(v)}_{ij} \equiv \frac{1}{2}\mathcal{L}_vh_{ij}\,, \tag{3.35}$$

is transverse, that is $v^iB^{(v)}_{ij} = 0$.

Global-time Coordinates on $\mathcal{M}$

All the tensors and equations in the last section holds in any coordinate system on $\mathcal{M}$. However, we may choose a coordinate system , $x^i = \{t, x^A\}$, where x^A are coordinates on Σ, and $x^0 = t$ is the foliation parameter. These system of coordinates are called *'global-time coordinates'* (GTC) in [65, 82]. In these coordinate systems, τ_i is of the form

$$\tau_i = N(dt)_i \,, \tag{3.36}$$

for some lapse function $N \neq 0$, where we have used the fact that τ is hypersurface orthogonal. The condition $h^{ij}\tau_i = 0$ means $h^{00} = h^{0A} = 0$, and $h^{AB} = \tilde{q}^{AB}$, where $\tilde{q}^{AB}$ is the inverse Riemannian metric on Σ. That is

$$h^{ij} = \begin{pmatrix} 0 & 0 \\ 0 & \tilde{q}^{AB} \end{pmatrix} . \tag{3.37}$$

The condition $v^i\tau_i = 1$ means that

$$v^i = \begin{pmatrix} N^{-1} \\ N^{-1}s^A \end{pmatrix} . \tag{3.38}$$

Eq. (3.29) implies that h_{ij} is of the form

$$h_{ij} = \begin{pmatrix} s^2 & -s_A \\ -s_B & \tilde{q}_{AB} \end{pmatrix} , \tag{3.39}$$

where $s_A = \tilde{q}_{AB}s^B$, and $s^2 = s_A s^A$. The volume element in Eq. (3.28) then becomes

$$\widehat{\epsilon} = dt \wedge d^2x \, N\sqrt{\tilde{q}} \,. \tag{3.40}$$

Currents as Response to the Geometry

For a relativistic field theory, the energy-momentum tensor is defined as the variation of the action with respect to the metric to which the theory is coupled. Similarly, the currents in a non-relativistic theory can be defined as the variation of the action with respect to the NC geometry [65, 82, 66, 84, 67]. Assume that we have an action as a functional of the NC data, $I_{NC}[\tau, h, v]$, and we want to compute its variation under a diffeomorphism generated by the vector field ξ^i. The variations of τ_i, v^i, and h^{ij} are

$$\begin{aligned} \delta\tau_i = \mathcal{L}_\xi \tau_i &= \tau_j D_i \xi^j - T^k_{ij}\tau_k\xi^j \,, && (3.41)\\ &= \tau_j D_i \xi^j - (d\tau)_{ij}\xi^j \,, && (3.42)\\ \delta v^i = \mathcal{L}_\xi v^i &= \xi^j D_j v^i - v^j D_j \xi^i + T^i_{jk} v^j \xi^k \,, && (3.43)\\ \delta h^{ij} = \mathcal{L}_\xi h^{ij} &= D^i\xi^j + D^j\xi^i + (T^{i\ j}_{\ k} + T^{j\ i}_{\ k})\xi^k \,. && (3.44) \end{aligned}$$

Note that only those variations are allowed for which $\delta(v^i\tau_i) = 0$ and $\delta(h^{ij}\tau_j) = 0$. This means that we can keep $\delta\tau_i$ unconstrained, but demand that [82]

$$\delta v^i = - v^i v^j \delta\tau_j + \delta u^i \,, \tag{3.45}$$

$$\delta h^{ij} = - v^i \delta\tau^j - v^j \delta\tau^i - \delta H^{ij} \,, \tag{3.46}$$

where $\tau_i \delta u^i = 0$ and $\tau_i \delta H^{ij} = 0$. The energy current $\mathcal{E}^i$, the stress tensor Θ^{ij}, and the momentum one-form P_i, are then defined in terms of the variation of the action, $I_{NC}[\tau, h, v]$,

$$\delta I_{NC} \equiv \int dt d^2x \, N\sqrt{\tilde{q}} \left\{ \frac{1}{2}\Theta^{ij}\delta H_{ij} - \mathcal{E}^i \delta\tau_i - P_i \delta u^i \right\} . \tag{3.47}$$

Note that the stress tensor and momentum one-form are transverse:

$$\Theta^{ij}\tau_i = 0 \,, \qquad\qquad P_i v^i = 0 \,. \tag{3.48}$$

Inserting the variations from Eqs. (3.41)-(3.46) in Eq. (3.47), and performing the integration by parts lead to [82, 66, 67]

$$\delta I_{NC} = \int dt d^2x \, N\sqrt{\tilde{q}} \; \xi^j \left\{ -D_i(P_j v^i) - P_i D_j v^i - (D_i - T^k_{ki})\Theta^i_j + \tau_j (D_i - T^k_{ki})\mathcal{E}^i + (d\tau)_{ij}\mathcal{E}^i \right\} . \tag{3.49}$$

This is an important result that we will use in Sec. 3.4 to write the covariant form of the screen equations, Eqs. (3.22)-(3.23). We will also use the general form of the variation in Eq. (3.47) to identify the currents on holographic screens.

3.4 Newton-Cartan Geometry on Holographic Screens

This section is the most important part of this chapter. In this section, we will combine the ideas from the last two sections to propose that the geometry of the holographic screen, H, can be described by the NC geometry. In particular, we suggest that the Riemannian metric on the leaves, $\sigma(r)$, the vector field, h^i, normal to the leaves, and a non-vanishing scalar α in Eq. (3.10), play the role of NC data on H.

The foliation structure of H into leaves allows us to pick a coordinate system on H: $\{r, x^A\}$, where r is the foliation parameter, and x^A are angular coordinates on $\sigma(r)$. These are the GTC of Sec. (3.3). The foliation parameter, r, acts as the '*screen time*'. One can always define a one-form, $(dr)_i$, which is normal to the leaves. We use this to write a one-form

$$\tau_i = \alpha(dr)_i \,. \tag{3.50}$$

This means that α plays the role of the lapse function, N. This proposal would have been inconsistent if α were allowed to vanish anywhere. Recall that α is indeed non-vanishing, as was proven in [19] assuming certain generic conditions.

The second ingredient in the NC data is the vector field v^i, such that $v^i\tau_i = 1$. We use the vector field h^i to define $v^i \equiv \alpha^{-1}h^i$. The coordinate representation of this vector field in the GTC, $\{r, x^A\}$, is

$$v^i = \begin{pmatrix} \alpha^{-1} \\ 0 \end{pmatrix} . \tag{3.51}$$

Finally, we use the metric on the leaves, $\tilde{q}_{AB}$, and its inverse $\tilde{q}^{AB}$, to construct a $(2,0)$ symmteric tensor on H, whose coordinate representation is

$$h^{ij} = \begin{pmatrix} 0 & 0 \\ 0 & \tilde{q}^{AB} \end{pmatrix} . \tag{3.52}$$

We combine τ_i in Eq. (3.50), v^i in Eq. (3.51), and h^{ij} in Eq. (3.52) to put a NC structure on the screen. This allows us to define geometric quantities like connection and covariant derivatives on H. The non-zero components of the connection in Eq. (3.32) are

$$\widehat{\Gamma}^0_{i0} = \partial_i \log\alpha \,, \tag{3.53}$$

$$\widehat{\Gamma}^A_{B0} = \widehat{\Gamma}^A_{0B} = \frac{1}{2}\tilde{q}^{AC}\partial_0\tilde{q}_{BC} \,, \tag{3.54}$$

$$\widehat{\Gamma}^A_{BC} = \widetilde{\Gamma}^A_{BC} \equiv \frac{1}{2}\tilde{q}^{AD}\left(\partial_B\tilde{q}_{CD} + \partial_C\tilde{q}_{BD} - \partial_D\tilde{q}_{BC}\right) , \tag{3.55}$$

where $\widetilde{\Gamma}^A_{BC}$ are the Christoffel symbols of the metric $\tilde{q}_{AB}$.

Note that we have only presented the NC data in the GTC. The representation of τ_i, v^i, and h^{ij} in any arbitrary coordinate system can be determined using the transformation law of tensors. This is an important result, as this allows us to describe the geometry of H without using the foliation structure of H.

Also note that the scalar β in Eq. (3.10), unlike α, does not appear in Eqs. (3.50)-(3.52). This means that the intrinsic geometry of H is not dependent on β. This is consistent with the interpretation of β as the "slope" of H in Ch. (2). That is, it tells us how much the screen bends in the spacetime it is embedded in. Therefore, β is an extrinsic quantity.

To finish this section, we want to compare the NC geometry with the geometry described by the induced metric for screens which are nowhere null. The advantage of NC geometry is that the foliation structure of screen is implicit in it through one-form field τ. Another advantage of using NC geometry will be apparent in Sec. (3.5), where we will find that the boundary conditions on NC data are more suitable for holographic screens than the boundary conditions on the induced metric.

Covariant Screen Equations

The evolution equations of holographic screen, Eqs. (3.22)-(3.23), are the decomposition of constraint equations, Eq. (3.13), into directions normal and transverse to the leaves. These equations are invariant under the foliation-preserving diffeomorphisms. In this section, we will show that we can use the NC geometry to write a covariant version of these equations.

Before we derive the covariant screen equations, recall how the constraint equations, Eq. (3.14), for the hypersurface of a fixed signature arise from diffeomorphism invariance. Imagine taking the spacetime and truncating it at the hypersurface. As a result, the Einstein-Hilbert (EH) action has to be compensated with the Gibbons-Hawking-York (GHY) boundary term living on the hypersurface,

$$I = I_{EH}[g] + I_{GHY}[g,\gamma]\,. \tag{3.56}$$

The variation of this action is [78]

$$\delta I = \frac{1}{16\pi}\int_M d^4x\,\sqrt{g}\,G_{ab}\delta g^{ab} + \frac{1}{16\pi}\int_{\partial M} d^3x\,\sqrt{\gamma}\,\left(\widehat{K}_{ij} - \widehat{K}\,\gamma_{ij}\right)\,\delta\gamma^{ij}\,. \tag{3.57}$$

Now we take a vector field tangent to the hypersurface, ξ^i, and generate diffeomorphism by it. The variation of the total action under this transformation is

$$\delta I = -\frac{1}{8\pi}\int_M d^4x\,\sqrt{g}\,G_{ab}\nabla^a\xi^b - \frac{1}{8\pi}\int_{\partial M} d^3x\,\sqrt{\gamma}\,\left(\widehat{K}_{ij} - \widehat{K}\,\gamma_{ij}\right)\,\widehat{D}^i\xi^j\,, \tag{3.58}$$

where $\xi^a = e^a_i\xi^i$ is the push-back of the vector field on the full spacetime. Performing the integration by parts yields

$$\delta I = \frac{1}{8\pi}\int_M d^4x\,\sqrt{g}\,\xi^b\,\nabla_a G^{ab} - \frac{1}{8\pi}\int_{\partial M} d^3x\,\sqrt{\gamma}\,\xi^i\left[G_{ab}n^a e^b_i - \widehat{D}_j\left(\widehat{K}_{ij} - \widehat{K}\,\gamma_{ij}\right)\right]. \tag{3.59}$$

Demanding that the action is invariant under diffeomorphisms generated by ξ^i gives us Bianchi identity and Gauss-Codazzi constraint. The latter, when combined with the Einstein equations, becomes Eq. (3.14).

Now we repeat the similar analysis for holographic screens, H. That is, we take a spacetime in which the holographic screen is embedded in, and truncate it at H. The variational principle requires that we add a boundary action on H, whose variation cancels the boundary term in the variation of the EH action. In the next section, we will follow [62] and study this variational problem. For now, simply assume that there exists a screen action as a functional of NC data such that the combination

$$I = I_{EH}[g] - I_H[g,\tau,h,v]\,. \tag{3.60}$$

has a well-defined variation, and is given by

$$\delta I = \frac{1}{16\pi}\int_M d^4x\,\sqrt{g}\,G_{ab}\delta g^{ab} - \int_H dr d^2x\,\alpha\,\sqrt{\tilde{q}}\,\left\{\frac{1}{2}\Theta^{ij}\delta H_{ij} - \mathcal{E}^i\delta\tau_i - P_i\delta u^i\right\}\,, \tag{3.61}$$

where we have used Eq. (3.47). If we take the variation to be a diffeomorphism generated by a vector field ξ^i on H, then we get

$$\begin{aligned}\delta I = &-\frac{1}{8\pi}\int_M d^4x\,\sqrt{g}\,G_{ab}\nabla^a\xi^b \\ &-\int_H dr d^2x\,\alpha\sqrt{\tilde{q}}\,\xi^j\left\{-D_i(P_jv^i) - P_iD_jv^i - (D_i - T^k_{ki})\Theta^i_j + \tau_j(D_i - T^k_{ki})\mathcal{E}^i + (d\tau)_{ij}\mathcal{E}^i\right\}\,,\end{aligned} \tag{3.62}$$

where we have used Eq. (3.49) in the second term. Performing the integration by parts, and demanding $\delta I = 0$ leads to a Bianchi identity, and a constraint equation which when combined with Einstein equations becomes

$$D_i(P_j v^i) + P_i D_j v^i + (D_i - T^k_{ki})\Theta^i_j - \tau_j(D_i - T^k_{ki})\mathcal{E}^i - (d\tau)_{ij}\mathcal{E}^i = \alpha^{-1}\, T_{ab} n^a e^b_j \,. \tag{3.63}$$

In the following, we will show that this tensor equation is a covariant version of the screen equations, Eqs. (3.22)-(3.23). In particular, we will show that this equation reduces to Eqs. (3.22)-(3.23) when we expand it in the GTC. Note that Eq. (3.48) implies that the momentum one-form P_i, stress tensor Θ^{ij}, and energy current $\mathcal{E}^i$ have the following representation in the GTC

$$P_i = \big(0, P_A\big)\,, \tag{3.64}$$

$$\Theta^{ij} = \begin{pmatrix} 0 & 0 \\ 0 & \Theta^{AB} \end{pmatrix}\,, \tag{3.65}$$

$$\mathcal{E}^i = \begin{pmatrix} \mathcal{E}^0 \\ \mathcal{E}^A \end{pmatrix}\,. \tag{3.66}$$

The contraction of Eq. (3.63) with v^i is

$$\alpha^{-1}\, T_{ab} n^a v^b = -(D_i - T^k_{ki})\mathcal{E}^i + T^k_{ki}\mathcal{E}^i - \Theta^j_i D_j v^i \tag{3.67}$$

$$= -D_i\mathcal{E}^i + 2T^k_{ki}\mathcal{E}^i - \Theta^{ij} B^{(v)}_{ij}\,. \tag{3.68}$$

By writing this equation in the GTC, and using the relation $v^i = \alpha^{-1} h^i$, we get

$$T_{ab} n^a h^b = -\alpha \mathcal{L}_h(\alpha\mathcal{E}^0) - \alpha^2\mathcal{E}^0\theta^{(h)} - \widetilde{D}_A(\alpha^2\mathcal{E}^A) - \alpha\,\Theta^{AB} B^{(h)}_{AB}\,. \tag{3.69}$$

Similarly, the contraction of Eq. (3.63) with h^{ij} is

$$\alpha^{-1}\, T_{ab} n^a e^b_j h^{ij} = h^{ij}\,\mathcal{L}_v P_j + h^{ij} P_j \theta^{(v)} + (D_j - T^k_{kj})\Theta^{ij} - h^{ij}(d\tau)_{kj}\mathcal{E}^k\,. \tag{3.70}$$

Writing this equation in the GTC leads to

$$T_{ab} n^a e^b_A = \tilde{q}^B_A \mathcal{L}_h p_B + p_A\theta^{(h)} + \widetilde{D}_B(\alpha\Theta^B_A) + \alpha\mathcal{E}^0\widetilde{D}_A\alpha\,. \tag{3.71}$$

With the identifications

$$P_A = \frac{1}{8\pi}\,\Omega_A\,, \tag{3.72}$$

$$\mathcal{E}^0 = -\frac{1}{8\pi\,\alpha}\theta^{(l)} = -\frac{1}{8\pi\,\alpha^2}\theta^{(h)}, \tag{3.73}$$

$$\mathcal{E}^A = -\frac{1}{8\pi\,\alpha^2}\widehat{\Omega}^A\,, \tag{3.74}$$

$$\Theta_{AB} = \frac{1}{8\pi\,\alpha}\left(B^{(n)}_{AB} - \theta^{(n)}\tilde{q}_{AB} - \widetilde{\kappa}\tilde{q}_{AB}\right)\,. \tag{3.75}$$

Eq. (3.69) and Eq. (3.71) reduces to Eq. (3.22) and Eq. (3.23) respectively. This confirms our claim that Eq. (3.63) is a covariant generalization of the screen evolution equations. We view this as an application of the Newton-Cartan formalism to describe the geometry of the screen. However at this point, the identifications that we have made in Eqs. (3.72)-(3.75) seem arbitrary. In the next section, we will follow [62] to write the variation of the total action in a form similar to Eq. (3.61). This will allow us to verify the identifications that we have made for P_A, $\mathcal{E}^0$, and Θ_{AB}.

3.5 Derivation of P_A, Θ_{AB}, and $\mathcal{E}^0$ from Gravitational Action

In the spacetime with boundaries, the Einstein-Hilbert action has to be compensated with a boundary term which depends on the boundary conditions. For instance, Dirichlet conditions on a boundary of fixed signatures lead to Gibbons-Hawking-York term. Brown and York studied this problem in [78], where they assumed that the spacetime is bounded by four boundaries: an outer timelike, an inner timelike, a future spacelike, and a past spacelike boundary. This analysis was generalized in [93], where the corner contributions from the interaction of two different boundaries were also considered. This was further generalized in [62], where the inner timelike boundary was replaced with the codimension-1 hypersurface which

- is foliated by the codimension-2 marginally trapped or anti-trapped closed surfaces,
- is of indefinite signature.

Note that these are exactly the properties of holographic screens. In this section, we will follow the calculations of [62]. However, our analysis will be different from that of [62] in two ways. As we only care about the boundary contributions to the Einstein-Hilbert action coming from the holographic screen, we will assume that there are no other boundaries of the spacetime. The other, and more important, difference in the two analysis is that we will be assuming slightly different boundary conditions.

We now discuss the boundary conditions that we are imposing on the holographic screens. The Dirichlet condition on the induced metric is, of course, not suitable as the signature of screens is allowed to change. There is another reason for why Dirichlet conditions are inapplicable. Note that we are only allowed to impose six boundary conditions on the screen. If we fix the induced metric on the screen, then we cannot fix any other geometric data. However, holographic screens are special as the leaves have vanishing null-expansion, $\theta^{(k)} = 0$. Following [62], we do not impose any boundary conditions on the induced metric. Rather, we assume a Dirichlet condition on $\theta^{(k)}$. This boundary condition also fixes the foliation structure of the holographic screen.

We still need to choose five more boundary conditions. We fix three of those by imposing Dirichlet condition on the metric on the leaves, $\tilde{q}_{AB}$, which also fixes its inverse, $\tilde{q}^{AB}$. So far,

our four boundary conditions are same as those of [62]. Next, we choose to impose boundary conditions on the variation of the evolution vector field, h^i. Note that the normalization $h^i(dr)_i = 1$ implies that δh^i is transverse,

$$\delta h^i = e^i_A \, \delta s^A \,. \tag{3.76}$$

We now impose the Dirichlet conditions on s^A. These are our last two boundary conditions. Note that these conditions are different from those of [62] where they had imposed Dirichlet conditions on Ω_A. As we will see below, our boundary conditions not only result in the well-defined variation of the action, it will also help us to compare the variation of the total action with Eq. (3.61).

As emphasized in [62], we also have to fix the 'length' of the null vector k^a. Note that this is not an additional boundary condition. We need to impose this condition because the extrinsic quantities like $\widetilde{\kappa}$ and Ω_A depend on the 'length' of the null vectors. This is equivalent to the case of the boundary with a fixed signature, where we fix the norm of the normal vector to be ± 1. Without fixing the norm of the normal vector, the extrinsic curvature and hence the GHY boundary term have ambiguities and are not well defined. We can fix the 'length' of the null vectors by imposing the Dirichlet condition on α .

After discussing the boundary conditions in detail, we now consider the variation of EH action on the spacetime with the holographic screen as the boundary. We copy from [62]

$$\begin{aligned}\delta I_{EH}[g] = & \frac{1}{16\pi}\int_M d^4x\,\sqrt{g}\,G_{ab}\,\delta g^{ab} \\ & + \frac{1}{16\pi}\int_H drd^2x\,\sqrt{\tilde{q}}\,\left(-2(\delta\theta^{(n)}) - (\delta\tilde{q}_{AB})B^{(n)AB} - 2(\delta\alpha)\theta^{(l)} - 2(\delta\widetilde{\kappa}) + 2(\delta h^i)\omega_i\right)\,,\end{aligned} \tag{3.77}$$

which we re-write as [62]

$$\begin{aligned}\delta I_{EH}[g] = & \frac{1}{16\pi}\int_M d^4x\,\sqrt{g}\,G_{ab}\,\delta g^{ab} - \frac{1}{8\pi}\delta\left\{\int_H drd^2x\,\sqrt{\tilde{q}}\left(\widetilde{\kappa}+\theta^{(n)}\right)\right\} \\ & - \frac{1}{8\pi}\int_H drd^2x\,\sqrt{\tilde{q}}\,\left(\frac{1}{2}(\delta\tilde{q}_{AB})\Big(B^{(n)AB} - \theta^{(n)}\tilde{q}^{AB} - \widetilde{\kappa}\tilde{q}^{AB}\Big) - (\delta s^A)\Omega_A + (\delta\alpha)\theta^{(l)}\right)\,.\end{aligned} \tag{3.78}$$

Note that if we impose our boundary conditions, then the second line in the above equation vanishes. The second term in the first line is a total variation, and should be added to EH action as the boundary term. Therefore, the total gravitational action in the spacetime with holographic screen as the boundary is

$$I = \frac{1}{16\pi}\int_M d^4x\,\sqrt{g}\,R + \frac{1}{8\pi}\int_H drd^2x\,\sqrt{\tilde{q}}\,(\widetilde{\kappa}+\theta^{(n)})\,. \tag{3.79}$$

The variation of this total action follows from Eq. (3.78)

$$\delta I = \frac{1}{16\pi}\int_M d^4x\,\sqrt{g}\,G_{ab}\,\delta g^{ab} - \frac{1}{8\pi}\int_H drd^2x\,\alpha\,\sqrt{\tilde{q}}\,\left(\frac{1}{2}(\delta\tilde{q}_{AB})\frac{1}{\alpha}\Big(B^{(n)AB}-\theta^{(n)}\tilde{q}^{AB}-\widetilde{\kappa}\tilde{q}^{AB}\Big)-\frac{1}{\alpha}(\delta s^A)\Omega_A+(\delta\alpha)\frac{1}{\alpha}\theta^{(l)}\right). \tag{3.80}$$

By comparing the above expression for the total variation with Eq. (3.61) (or Eq. (3.47)), we can deduce the expressions for momentum one-form P_i, stress tensor Θ^{ij}, and energy current $\mathcal{E}^i$. However, all the calculation that we have done in this section are in the GTC gauge, Eq. (3.36)-(3.39). In this gauge, the variation $\delta\tau_i$, δu^i in Eq. (3.45), δH^{ij} in Eq. (3.46), are of the form

$$\delta\tau_0 = \delta\alpha\,, \tag{3.81}$$
$$\delta\tau_A = 0\,, \tag{3.82}$$
$$\delta u^i = \alpha^{-1}\,e^i_A\delta s^A \tag{3.83}$$
$$\delta H^{ij} = e^i_A e^i_B\,\delta\tilde{q}^{AB}\,. \tag{3.84}$$

With these variations, Eq. (3.61) becomes

$$\delta I = \frac{1}{16\pi}\int_M d^4x\,\sqrt{g}\,G_{ab}\delta g^{ab} - \int_H drd^2x\,\alpha\,\sqrt{\tilde{q}}\,\left\{\frac{1}{2}\Theta^{AB}\delta\tilde{q}_{AB}-\alpha^{-1}P_A\,\delta s^A-\mathcal{E}^0\,\delta\alpha\right\}. \tag{3.85}$$

Comparison of this expression with Eq. (3.80) leads us to conclude that

$$P_A = \frac{1}{8\pi}\,\Omega_A\,, \tag{3.86}$$
$$\mathcal{E}^0 = -\frac{1}{8\pi\,\alpha}\theta^{(l)} = -\frac{1}{8\pi\,\alpha^2}\theta^{(h)}, \tag{3.87}$$
$$\Theta_{AB} = \frac{1}{8\pi\,\alpha}\left(B^{(n)}_{AB}-\theta^{(n)}\tilde{q}_{AB}-\widetilde{\kappa}\tilde{q}_{AB}\right), \tag{3.88}$$

which agrees with the identifications that we made in Eqs. (3.72)-(3.73) and in Eq. (3.75). However, note that we have failed to derive the expression for $\mathcal{E}^A$ using the above formalism. The reason behind this failure is that we have been working in the GTC gauge, in which $\delta\tau_A = 0$. To derive the spatial components of the energy current, $\mathcal{E}^A$, we need to vary the action of the theory with respect to τ_A. This requires going away from the GTC at least to the first order. It is not clear how to perform the above analysis in a fully covariant way. We leave understanding this task to future work.

3.6 Discussion

We have seen that the induced metric on a holographic screen is degenerate, and is not applicable to define geometric structure such as connection and covariant derivative. We have

proposed that the intrinsic geometry should, instead, be described by the Newton-Cartan geometry. We have used some results from [19] to argue that this proposal is consistent. Using the NC connection on H, we have presented the screen evolution equations of Ch. (2) into a covariant form. There are many possible directions which we intend to pursue in the future. We briefly discuss these in the following.

The natural next step would be to couple a (non-relativistic) field theory to a holographic screen. The coupling of field theories to Newton-Cartan geometry has been studied in [66, 84, 67]. It would be interesting to know if there are any constraints on the field theory that we can define on the screen. One possible way to find these constraints might be to compare the entanglement structure of the field theory with the screen entanglement conjecture of [50].

In AdS spacetime, metric near the conformal boundary can be written as a power series in the bulk coordinate [94]. This type of expansion has also been studied in [90] for Lifshitz gravity, where the geometry of the boundary is Newton-Cartan. It would be fascinating if a metric of a spacetime can be expanded in a similar fashion near the screen. One-to-one correspondence between the screen and the null foliation of the spacetime suggests that the affine parameter on null slices can be used as a bulk coordinate.

As discussed in Sec. (3.5), we also plan to understand how to generalize the calculations of [62] without using the GTC gauge, Eq. (3.36)-(3.39). This would be important as this will allow us to derive the spatial components of the energy currents, $\mathcal{E}^A$, which we failed to do in Sec. (3.5).

Part II

Entanglement and Holography

Chapter 4

Entanglement Tsunami in (1+1)-Dimensions

4.1 Introduction

Computation of entanglement entropy in quantum field theory is a topic of growing interest. Unfortunately, in many situations, it is an extremely difficult quantity to compute. For strongly coupled systems, one of our best analytical tools is holography. In a holographic theory, entanglement entropy is evaluated as the area of an extremal surface in the dual geometry [26, 27]. In some cases, especially in (1+1)-dimensional CFTs, purely field-theoretical arguments can be given for the form of the entanglement entropy.

We will be using entanglement entropy to study the approach to equilibrium following a global quantum quench. Calabrese and Cardy [95, 96] famously showed that, in (1+1)-dimensions, the entanglement entropy of an interval increases linearly with time until it saturates at the thermal value. The field-theoretical results could be reproduced by a simple intuitive model: the growth and saturation of the entanglement entropy were effectively modeled by the free propagation of quasiparticle excitations, which we will review below.

This linear growth in (1+1)-dimensions was confirmed in holographic calculations, first numerically [97], and then analytically [98, 99], where it was also extended to higher dimensions (see also [100]). In [101, 102], it was noted that a free-streaming quasiparticle picture was inadequate to explain the rate of growth beyond the (1+1)-dimensional case and it was suggested that the linear growth could be thought of in terms of an "entanglement tsunami," represented by an effective wavefront which propagates into the region under consideration and entangles interior degrees of freedom with exterior degrees of freedom. An underlying free-streaming quasiparticle model for the entanglement tsunami yielded a wavefront velocity smaller than the velocity calculated holographically in dimensions higher than (1+1). In (1+1) dimensions, the holographic calculation and quasiparticle model both said that the effective wavefront moved at the speed of light. At this level, then, it seemed that quasiparticles were sufficient to explain the time dependence of the entanglement entropy of a single

interval in (1+1) dimensions, even for holographic CFTs which are strongly interacting.

However, when multiple disjoint intervals are considered, there is a qualitative difference between the holographic calculation and the quasiparticle model of Calabrese and Cardy (as noted in [103, 104], and also present in [105]): the holographic calculation gives a non-decreasing entropy, while the quasiparticle model has both increasing and decreasing behavior as a function of time. Therefore already in (1+1)-dimensions, there is a need to replace the quasiparticle picture. We will elaborate on the entanglement tsunami proposal, showing how it can be used as a rule to calculate the entanglement entropy of one or two intervals in holographic CFTs and provide a natural upper bound for more than two intervals. We will make no attempt to derive the entanglement tsunami from underlying physical excitations, quasiparticle-like or otherwise.

The remainder of this chapter is organized as follows. In Sec. (4.2) we will review the setup for the problem and the results from both the quasiparticle and holographic viewpoints. In Sec. (4.3) we will provide a CFT argument for the holographic result, showing how CFTs with large-c and a sparse spectrum differ from weakly coupled CFTs, and in particular do not follow the quasiparticle prediction. In Sec. (4.4) we will propose an entanglement tsunami prescription for the entanglement entropy as a function of time. Finally, in Sec. (4.5) we will describe how these results may be extended to higher dimensions, where there are still some unresolved issues, and speculate on possible derivations of the entanglement tsunami from interactions.

4.2 Setup and Review

Quasiparticle Model

We are interested in the entanglement entropy of a subregion A of the real line following a global quench in a CFT. Note that A is always the union of a collection of disjoint intervals. Let A^c denote the complement of A. Globally, the system is in a pure state $|\Psi\rangle$ and the entanglement entropy for the region A as given by

$$S = -\mathrm{Tr}\,\rho_A \log \rho_A, \qquad \text{with } \rho_A = \mathrm{Tr}_{A^c} |\Psi\rangle\langle\Psi| \,. \tag{4.1}$$

$|\Psi\rangle$ is a time-dependent state, and so S will be time-dependent. A global quench is defined by beginning in the vacuum state of one theory, and then suddenly changing the Hamiltonian to that of a different theory. The result is that the initial state from the point of view of the second theory (the CFT) is a highly excited state, but has a simple entanglement structure. We are interested in the time dependence of the finite part of the entanglement entropy, so we will assume that the UV-divergent parts can be subtracted in a consistent way, whether or not they are modified by the quench. Henceforth when we refer to the entropy we will mean the finite part of the entropy, or the vacuum-subtracted entropy. At $\mathfrak{t} = 0$, then, we have $S = 0$.

At late times, the system will effectively thermalize and we should find $S(\mathfrak{t} \to \infty) = S_{\text{therm}} = s_{\text{eq}}\text{Vol}(A)$. In (1+1)-dimensions $\text{Vol}(A)$ is just the sum of the lengths of the intervals that make up A, but we are emphasizing that the thermal entropy is extensive with the volume of the system. s_{eq} is the thermal entropy density, which is a property of the state. At intermediate times, either a CFT calculation or a holographic calculation can be used to describe the transition from zero entropy to the thermal result. We will discuss both of these calculations below, but for now, we will record the expected answer as predicted by the quasiparticle model.

Calabrese and Cardy showed [95, 96] that, following a global quench, the time-dependence of the entropy can be effectively modeled by the propagation of entangled quasiparticles, at least for weakly coupled CFTs. At the time of the quench, we imagine that a uniform density of EPR pairs of quasiparticles is produced, where each pair begins localized at a point and consists of a left-mover and right-mover. These quasiparticles move in opposite directions at the speed of light, and there are no interactions between pairs. To compute the entanglement entropy of A, we only have to count the number of unpaired particles in the region at any given time:

$$S(\mathfrak{t}) \propto \int_{x' \in A} dx' \int_{x'' \in A^c} dx'' \int_{-\infty}^{\infty} dx \left\{ \delta(x' - x - \mathfrak{t})\delta(x'' - x + \mathfrak{t}) + \delta(x' - x + \mathfrak{t})\delta(x'' - x - \mathfrak{t}) \right\}. \quad (4.2)$$

The constant of proportionality is related to the initial density of EPR pairs, which determines s_{eq}. When A consists of a single interval of length L, computing the above integral gives the following time dependence:

$$S(\mathfrak{t}) = 2s_{\text{eq}} \times \begin{cases} \mathfrak{t}, & \mathfrak{t} \leq \frac{L}{2}, \\ \frac{L}{2}, & \mathfrak{t} > \frac{L}{2}. \end{cases} \quad (4.3)$$

First there is a linear growth phase, and then saturation at the thermal value.

The behavior is a little more complicated when A consists of two disjoint intervals. For simplicity, consider the case where the two intervals have equal lengths L and are separated by a distance $R > L$. Then the quasiparticle model gives (see Fig. (4.1) for a plot)

$$S(\mathfrak{t}) = 2s_{\text{eq}} \times \begin{cases} 2\mathfrak{t}, & \mathfrak{t} \leq \frac{L}{2}, \\ L, & \frac{L}{2} < \mathfrak{t} < \frac{R}{2}, \\ L - \left(\mathfrak{t} - \frac{R}{2}\right), & \frac{R}{2} < \mathfrak{t} < \frac{L+R}{2}, \\ L + \left(\mathfrak{t} - L - \frac{R}{2}\right), & \frac{L+R}{2} < \mathfrak{t} < \frac{2L+R}{2}, \\ L, & \mathfrak{t} > \frac{2L+R}{2}. \end{cases} \quad (4.4)$$

In particular, this result tells us that the entanglement entropy is not monotonic in time. We can understand the drop in the entanglement entropy in the following way. Consider an EPR pair that started propagating from the region between the two intervals which make up

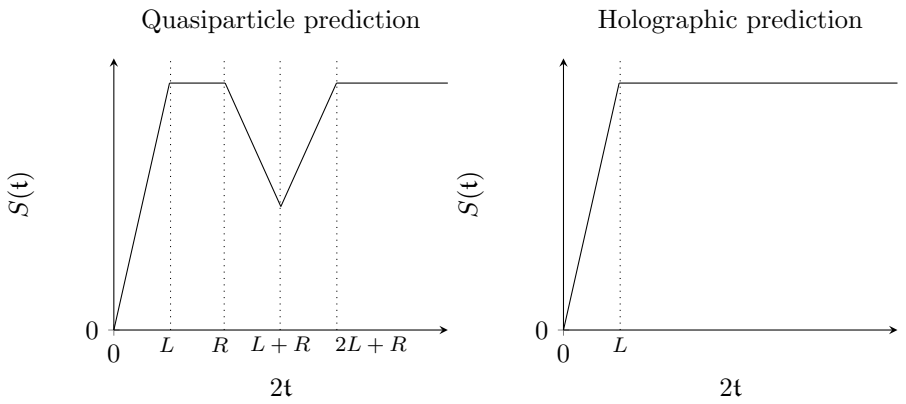

Figure 4.1: The entropy production as a function of time for a region consisting of two disjoint intervals of length L, separated by a distance $R > L$. The quasiparticle model (left) shows decreasing behavior between $2\mathfrak{t} = R$ and $2\mathfrak{t} = L + R$. The holographic calculation (right) is monotonically increasing before saturation at $2\mathfrak{t} = L$, after which the entropy remains constant.

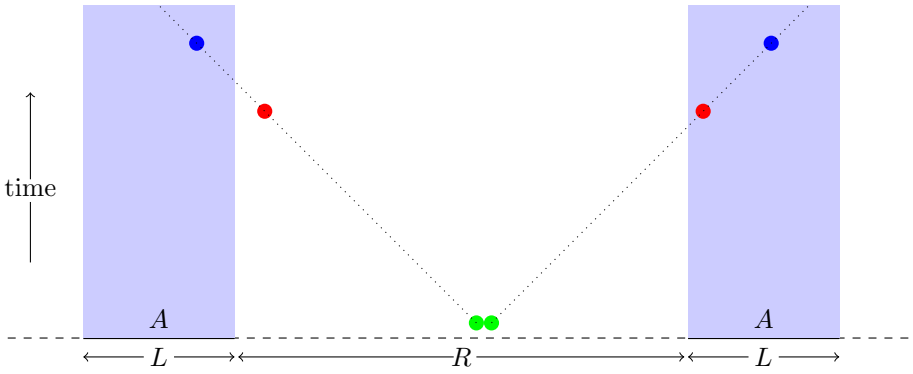

Figure 4.2: An EPR pair produced at the points marked as green at the bottom of the figure. When the constituent particles are at the positions marked as red at the intermediate time, they contribute to the entanglement entropy. At the later time when the particles are at the positions marked as blue, they do not contribute to the entanglement entropy. This process leads to a decrease in the entanglement entropy in the quasiparticle picture.

A at the time of quench, $\mathfrak{t} = 0$ (see Fig. (4.2)). At some time $\mathfrak{t} < R/2$, one of the particles will enter region A and while the other remains in the complement. At that time, and for times immediately following, this pair contributes one unit to the entanglement entropy. However, at a later time the second particle will enter the region A as well, and so there is an opportunity for both particles to be inside A at the same time. Then they will no longer contribute to the entanglement entropy. This results in decreased entanglement.

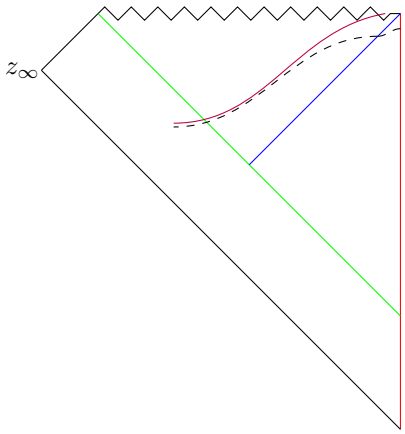

Figure 4.3: Penrose diagram of the time-dependent geometry following the quench. The red vertical line on the right is the AdS boundary ($z = 0$ in Poincare patch). The green diagonal line is the infalling shell, and the blue diagonal line is the horizon. The dashed curve is a late time extremal surface, which asymptotes to the critical surface, indicated by the solid curve. The linear growth of entanglement entropy comes from the portion of the extremal surface lying along the critical surface behind the horizon.

Holographic Calculation

The time evolution of entanglement entropy after a global quench can also be studied using the AdS-CFT correspondence [97, 98, 99, 101, 102]. According to the AdS-CFT dictionary, a global quench in the boundary theory is dual to throwing a spatially homogeneous and isotropic shell of matter into the bulk. This shell will eventually collapse to form a black hole, which is the gravity dual to a thermal state in the CFT.

After the quench, the geometry of the bulk is given by the time-dependent AdS-Vaidya geometry (displayed as a conformal diagram in Fig. (4.3)). As a result, the area of the boundary-anchored extremal surfaces, and hence the entanglement entropy of the boundary region, will depend on time. Though we are concerned with a (1+1)-dimensional CFT, and hence a 2+1-dimensional bulk, Liu and Suh were able to perform the calculation in arbitrary dimensions and with different types of black hole.

The local equilibrium length is given by the horizon radius, z_h. Consider a spatial interval on the boundary of length $L \gg z_h$. For times $\mathfrak{t} \gg z_h$, but smaller than $L/2$, the extremal surface in the bulk anchored to the endpoints of the interval has an area that grows linearly with time. Geometrically, the linear growth is tied to the existence of a critical extremal surface behind the black hole horizon. The extremal surface anchored to the boundary interval goes behind the horizon and approaches the critical surface. The length of the portion of the extremal surface lying along the critical surface increases linearly with $\mathfrak{t}$, which leads to a linear growth in the area. At $\mathfrak{t} \approx L/2$, there is a transition (the details of which do not concern us here), after which the extremal surface lies outside of the horizon

in the black hole portion of the geometry and is no longer influenced by the collapsing shell. The symmetries of this geometry ensure that the area is time-independent in this region, and so this represents thermal saturation of the entropy.

To summarize, the vacuum subtracted entropy for a single interval as computed holographically is given by

$$S(\mathfrak{t}) = 2s_{\rm eq} \times \begin{cases} \mathfrak{t}, & \mathfrak{t} \leq \frac{L}{2}, \\ \frac{L}{2}, & \mathfrak{t} > \frac{L}{2}. \end{cases} \tag{4.5}$$

where $s_{\rm eq}$ is related to the AdS-radius, $L_{\rm AdS}$, horizon radius, z_h, and Newton's constant, G_N, by

$$s_{\rm eq} = \frac{1}{4G_N} \frac{2L_{\rm AdS}}{z_h}. \tag{4.6}$$

This holographic result for a single interval agrees with the predictions of the quasiparticle picture Eq. (4.3).

We can deduce the holographic result for an arbitrary collection of intervals by using the answer for a single interval. For example, consider the case of a pair of intervals, $[x_1, x_2]$ and $[x_3, x_4]$. We need to find the bulk extremal surface with minimal area anchored to those intervals on the boundary. This is called the HRT surface [27]. There are two candidate HRT surfaces, which we display in Fig. (4.4). First, there is the union of the bulk extremal surfaces associated to the two intervals $[x_1, x_2]$ and $[x_3, x_4]$ individually ($\mathcal{A}_1$ and $\mathcal{A}_2$ in Fig. (4.4)). But the union of the bulk extremal surfaces associated to $[x_1, x_4]$ and $[x_2, x_3]$ is a second choice ($\mathcal{A}_3$ and $\mathcal{A}_4$ in Fig. (4.4)). The holographic prescription is to compute the total area in both cases and take the minimum value. But in each case, the extremal surfaces are just unions of extremal surfaces associated to intervals, and the time-dependence of those surfaces is given by Eq. (4.5).

Let $L_1 = x_2 - x_1$, $L_2 = x_4 - x_3$, and $R = x_3 - x_2$. Suppose $L_1 < L_2$. Then the first possible pair of extremal surfaces ($\mathcal{A}_1$ and $\mathcal{A}_2$ in Fig. (4.4)) would have a time-dependence given by

$$S^{(1)}(\mathfrak{t}) = 2s_{\rm eq} \times \begin{cases} 2\mathfrak{t}, & \mathfrak{t} < \frac{L_1}{2}, \\ \mathfrak{t} + \frac{L_1}{2}, & \frac{L_1}{2} < \mathfrak{t} < \frac{L_2}{2}, \\ \frac{L_1+L_2}{2}, & \mathfrak{t} > \frac{L_2}{2}, \end{cases} \tag{4.7}$$

while the second choice of extremal surfaces ($\mathcal{A}_3$ and $\mathcal{A}_4$ in Fig. (4.4)) has

$$S^{(2)}(\mathfrak{t}) = 2s_{\rm eq} \times \begin{cases} 2\mathfrak{t}, & \mathfrak{t} < \frac{R}{2}, \\ \mathfrak{t} + \frac{R}{2}, & \frac{R}{2} < \mathfrak{t} < \frac{L_1+L_2+R}{2}, \\ \frac{L_1+L_2+2R}{2}, & \mathfrak{t} > \frac{L_1+L_2+R}{2}. \end{cases} \tag{4.8}$$

At each time we take the minimum of $S^{(1)}(\mathfrak{t})$ and $S^{(2)}(\mathfrak{t})$ to get $S(\mathfrak{t})$. The interesting case is when R is the smallest of the three lengths, which means that our two disjoint intervals are

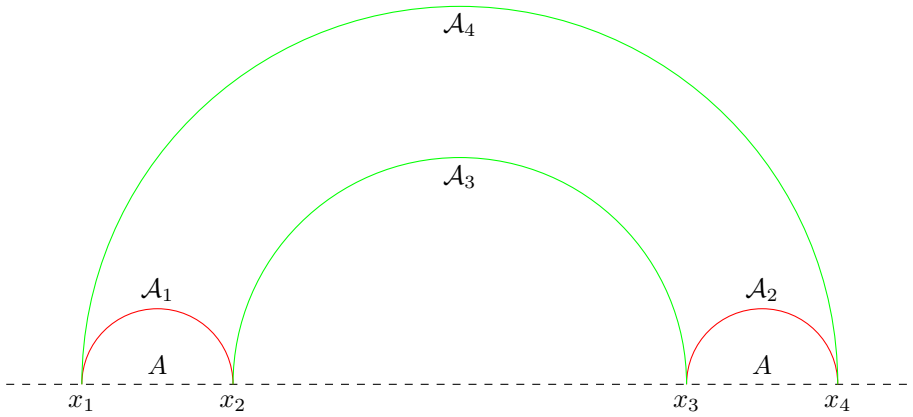

Figure 4.4: Here we display the extremal surfaces for two intervals. The first candidate HRT surface is the union of the two smaller arcs (marked in red and labeled $\mathcal{A}_1$ and $\mathcal{A}_2$). The second candidate is the union of the two larger arcs (marked in green and labeled $\mathcal{A}_3$ and $\mathcal{A}_4$).

close together. Then we have

$$S(\mathfrak{t}) = 2s_{\text{eq}} \times \begin{cases} 2\mathfrak{t}, & \mathfrak{t} < \frac{R}{2}, \\ \mathfrak{t} + \frac{R}{2}, & \frac{R}{2} < \mathfrak{t} < \frac{L_1+L_2-R}{2}, \\ \frac{L_1+L_2}{2}, & \mathfrak{t} > \frac{L_1+L_2-R}{2}. \end{cases} \tag{4.9}$$

In the other two cases, $L_1 < R < L_2$ and $L_1 < L_2 < R$, we have

$$S(\mathfrak{t}) = 2s_{\text{eq}} \times \begin{cases} \mathfrak{t}, & \mathfrak{t} < \frac{L_1}{2}, \\ \mathfrak{t} + \frac{L_1}{2}, & \frac{L_1}{2} < \mathfrak{t} < \frac{L_2}{2}, \\ \frac{L_1+L_2}{2}, & \mathfrak{t} > \frac{L_2}{2}. \end{cases} \tag{4.10}$$

A plot of the case $L_1 = L_2 < R$ is in Fig. (4.1). Unlike the quasiparticle model, the holographic calculation gives a non-decreasing answer for the entropy. It is easy to see why this is the case. For an arbitrary boundary region, each of the candidate HRT surfaces is the union of a collection of extremal surfaces anchored on boundary intervals. But each surface anchored on a boundary interval has a non-decreasing area. Therefore each candidate HRT surface has a non-decreasing area, and so the true HRT surface has a non-decreasing area (even though the identity of the true surface may change as a function of time).

4.3 Large-c CFT Calculation

Vacuum State Entanglement

In this section, we review the standard machinery for calculating the entanglement entropy of disjoint intervals in a (1+1)-dimensional CFT. The idea is to use the replica trick [96, 106, 107] to write the entanglement entropy as a limit of correlation functions of twist operators. The symmetries of the CFT are used to evaluate those correlation functions, which lets us find the entropy. In this section, the correlation functions will be vacuum correlation functions, and we will review how the large-c, sparse spectrum assumption reproduces the holographic answer in these cases. In the following section, we will consider the time-dependent situation of a global quench, where the relevant correlation functions are those of a BCFT.

We calculate the entanglement entropy of a region A using the replica trick, which realizes the entropy as a limit of traces of powers of the density matrix:

$$S = \lim_{n\to 1} \frac{1}{1-n} \log \mathrm{Tr}\rho_A^n \tag{4.11}$$

A standard way to compute $\mathrm{Tr}\rho_A^n$ is via a path integral on an n-sheeted cover of the original surface, with branch points located at the endpoints of A. This means that the sheets of the cover are sewn together along A, which is the path integral representation of the matrix multiplication that defines ρ_A^n. Alternatively, $\mathrm{Tr}\rho_A^n$ can be computed as a certain correlation function in the theory CFT^n, consisting of n copies of the original CFT. The twist operator $\mathcal{T}_n(x)$ is defined in the CFT^n theory as the operator which implements the boundary conditions of the n-sheeted cover: monodromy around the twist operator shifts a local operator $\mathcal{O}_k(x)$ in the kth copy of the CFT to the same operator $\mathcal{O}_{k+1}(x)$ in the k+1st copy of the CFT. When the region A consists of a union of intervals, $\mathrm{Tr}\rho_A^n$ can be computed (up to a constant of proportionality) as the correlation function of twist operators inserted at the endpoints of the intervals. The twist operator $\mathcal{T}_n$ is inserted at all of the left endpoints, and the anti-twist operator $\mathcal{T}_{-n}$ (which sends $\mathcal{O}_k \to \mathcal{O}_{k-1}$) is inserted at the right endpoints. To actually evaluate these correlation functions, we make use of the fact that twist operators are primary with scaling dimension

$$\Delta_n = \frac{c}{12n}(n^2-1), \tag{4.12}$$

where c is the central charge of the CFT.

As an illustration, consider the region A consisting of two intervals, $[x_1, x_2]$ and $[x_3, x_4]$, with $x_i < x_{i+1}$. Then $\mathrm{Tr}\rho_A^n$ can be computed as a four-point function of twist operators. Defining the cross-ratio η as

$$\eta = \frac{(x_2-x_1)(x_4-x_3)}{(x_3-x_1)(x_4-x_2)}, \tag{4.13}$$

noting that $\eta \in [0,1]$, and the new coordinate w,

$$w(z) = \frac{(z-x_1)(x_4-x_3)}{(x_3-x_1)(x_4-z)}, \tag{4.14}$$

we can write the required four-point function as

$$\langle \mathcal{T}_n(x_1)\mathcal{T}_{-n}(x_2)\mathcal{T}_n(x_3)\mathcal{T}_{-n}(x_4)\rangle = \left|\frac{\eta}{(x_2-x_1)(x_4-x_3)}\right|^{2\Delta_n} \langle \mathcal{T}_n(0)\mathcal{T}_{-n}(\eta)\mathcal{T}_n(1)\mathcal{T}_{-n}(\infty)\rangle \tag{4.15}$$

$$= \left|\frac{1-\eta}{(x_3-x_2)(x_4-x_1)}\right|^{2\Delta_n} \langle \mathcal{T}_n(0)\mathcal{T}_{-n}(\eta)\mathcal{T}_n(1)\mathcal{T}_{-n}(\infty)\rangle\,, \tag{4.16}$$

where the correlation function appearing on the right-hand side is defined via the limit

$$\langle \mathcal{T}_n(0)\mathcal{T}_{-n}(\eta)\mathcal{T}_n(1)\mathcal{T}_{-n}(\infty)\rangle \equiv \lim_{w\to\infty} |w|^{2\Delta_n} \langle \mathcal{T}_n(0)\mathcal{T}_{-n}(\eta)\mathcal{T}_n(1)\mathcal{T}_{-n}(w)\rangle\,. \tag{4.17}$$

A general four-point function can be evaluated using the conformal block decomposition:

$$\langle \mathcal{O}_1(0)\mathcal{O}_2(\eta)\mathcal{O}_3(1)\mathcal{O}_4(\infty)\rangle = \sum_p C_{12}^p C_{34}^p \mathcal{F}(c,h_p,\{h_i\},\eta)\mathcal{F}(c,\overline{h}_p,\{\overline{h}_i\},\overline{\eta}). \tag{4.18}$$

The sum is over all primary operators in the theory, with h_p ($\overline{h}_p$) being the (anti-) holomorphic scaling dimension of the primary operator. This sum is sometimes called the s-channel decomposition, but there is also a t-channel decomposition which features the coefficients $C_{23}^p C_{14}^p$ instead. Evaluating this sum requires an expression for the conformal blocks $\mathcal{F}$, which there are efficient algorithms for computing, as well as knowledge of the coefficients C_{ij}^p, which depend on the theory in question. We are only interested in correlations of twist operators, so we can set all of the h_i equal to the same value $h_i = \overline{h}_i = h = \Delta_n/2$. For small η, the Taylor series of the conformal block gives $\mathcal{F} = \eta^{h_p-2h}(1+O(\eta))$. So at small η, the dominant term in the sum comes from $h_p = 0$, which is the identity block [108]. This is the disconnected part of the four-point function: keeping this term alone reduces it to a product of two two-point functions:

$$\begin{aligned}\langle \mathcal{T}_n(x_1)\mathcal{T}_{-n}(x_2)\mathcal{T}_n(x_3)\mathcal{T}_{-n}(x_4)\rangle &\approx \left|\frac{1}{(x_2-x_1)(x_4-x_3)}\right|^{2\Delta_n} \\ &= \langle \mathcal{T}_n(x_1)\mathcal{T}_{-n}(x_2)\rangle \langle \mathcal{T}_n(x_3)\mathcal{T}_{-n}(x_4)\rangle\,.\end{aligned} \tag{4.19}$$

This is a manifestation of the cluster decomposition principle. A nontrivial fact about large-c CFTs with a sparse spectrum is that this is the dominant contribution even for *finite* values of η, all the way to $\eta = 1/2$ [108]. This can be proved by looking at a large-c expansion of the conformal blocks, where it is seem explicitly that the identity block makes the largest contribution. Here the assumption of a sparse spectrum means that the number of operators with scaling dimensions less that $O(c)$ should not scale with c.

For $\eta \approx 1$, the contribution of the identity block in the t-channel decomposition says

$$\begin{aligned}\langle \mathcal{T}_n(x_1)\mathcal{T}_{-n}(x_2)\mathcal{T}_n(x_3)\mathcal{T}_{-n}(x_4)\rangle &\approx \left|\frac{1}{(x_3-x_2)(x_4-x_1)}\right|^{2\Delta_n} \\ &= \langle \mathcal{T}_n(x_3)\mathcal{T}_{-n}(x_2)\rangle \langle \mathcal{T}_n(x_4)\mathcal{T}_{-n}(x_1)\rangle\,.\end{aligned} \tag{4.20}$$

Again, at large-c with a sparse spectrum this formula is expected to hold down to $\eta = 1/2$. In the $c \to \infty$ limit there is a sharp phase transition between the s-channel and t-channel results at $\eta = 1/2$. Finite-c corrections should smooth this transition, but consideration of those effects is beyond the scope of this work. Taking the appropriate limit as $n \to 1$, these results show that the vacuum entanglement entropy of a pair of intervals at large-c is given by

$$S = \min\Big(\frac{c}{3}\log\frac{(x_2-x_1)(x_4-x_3)}{\epsilon^2},\ \frac{c}{3}\log\frac{(x_4-x_1)(x_3-x_2)}{\epsilon^2}\Big), \tag{4.21}$$

where ϵ is the UV cutoff scale. This matches the holographic answer [26].

When there are N intervals, we must compute a $2N$-point function of twist operators. There are many possible decomposition channels, and the dramatic simplification at large-c with a sparse spectrum is that there is always some channel in which the identity block provides the dominant contribution. In this channel, the $2N$-point function decomposes as a product of N two-point functions. Taking the $n \to 1$ limit to extract the entanglement entropy, this precisely reproduces the Ryu-Takayanagi formula for arbitrary numbers of intervals [108, 109].

Global Quench

Following the setup of [96, 110, 111], the global quench is effectively modeled as a BCFT calculation. The correlation functions we need can be computed at large-c with a sparse spectrum using the techniques of [108]. The leading-order holographic result is obtained by assuming that the only primary operator of scaling dimension less than $O(c)$ is the identity, which contributes an amount of $O(c)$ to the entanglement entropy. This will also be the dominant contribution when the spectrum is sparse since other primary operators will contribute at $O(1)$ to the entropy. If the number of operators scales with c, then clearly this will compete with the identity contribution and the holographic result does not apply.

We wish to compute the four-point function of the twist operators after a quantum quench, where we take the state to be $|\Psi(\mathfrak{t})\rangle = U(\mathfrak{t})\,|\Psi\rangle$. We are interested in times well after the local equilibration time, and so it turns out to be useful to model the local equilibration by an initially Euclidean evolution over a small imaginary time τ_0, which can be thought of as a regulator for the calculation. Introducing the coordinate $z = x + i\tau$, the path integral preparing the ket state at $\mathfrak{t} = \tau = 0$ is then a path integral over the strip $\mathrm{Im}z \in [-\tau_0, 0)$, with a boundary wavefunction at $z = -i\tau_0$, while the bra state can be obtained by integrating over the strip $\mathrm{Im}z \in (0, \tau_0]$. To find the correlation functions at real times $\mathfrak{t} \gg \tau_0$, we would continue to path-integrate over a real-time contour before inserting our operators, as in the Schwinger-Keldysh formalism. Alternatively, we can compute correlation functions in the strip $\mathrm{Im}z \in [-\tau_0, \tau_0]$ for arbitrary values of the imaginary time τ and then afterward analytically continue the answers to real time.

For a collection of N intervals, we need to compute a $2N$-point function of twist operators

in the strip $\mathrm{Im} z \in [-\tau_0, \tau_0]$:

$$\mathrm{Tr}\,\rho^n = \langle \mathcal{T}_n(x_1 + i\tau)\mathcal{T}_{-n}(x_2 + i\tau)\cdots\mathcal{T}_n(x_{2N-1} + i\tau)\mathcal{T}_{-n}(x_{2N} + i\tau)\rangle_{\text{strip}}\,, \tag{4.22}$$

for arbitrary values of the imaginary time $\tau \in [-\tau_0, \tau_0]$. We will take τ to be a real number initially, and then analytically continue $\tau \to i\mathfrak{t}$ in the final answer to extract the real-time post-quench correlation functions.

We can conformally transform the strip to the upper half plane by setting

$$w(z) = \exp\left[\frac{\pi}{2\tau_0}(z + i\tau_0)\right]. \tag{4.23}$$

Then the lines $z = \mp i\tau_0$ map to the positive and negative real w axes, respectively. The $z = i\tau$ line maps to $\arg w = \pi/2 + \tau/2\tau_0$. We can write the correlation function as

$$\mathrm{Tr}\,\rho_A^n = \left|\left(\frac{\pi}{2\tau_0}\right)^{2N} e^{\frac{\pi}{2\tau_0}\sum x_i}\right|^{\Delta_n} \langle \mathcal{T}_n(w_1)\,\mathcal{T}_{-n}(w_2)\cdots\mathcal{T}_n(w_{2N-1})\,\mathcal{T}_{-n}(w_{2N})\rangle_{\text{UHP}}\,, \tag{4.24}$$

where the w_i are the images the x_i.

The upper half plane correlation functions should be computed in the context of BCFT, which tells us that each primary operator in the upper half plane can be thought of as the product of a holomorphic operator at its location times another holomorphic operator at the conjugate location (reflected over the real axis) [112, 113]. Then the $2N$-point function in the upper half-plane can be computed as a $4N$-point function in the full plane, which is just a vacuum correlation function. It is useful to parametrize the four-point function in terms of $\binom{2N}{2}$ real parameters η_{ij}, which are invariant cross-ratios characterizing the separation of w_i and w_j,

$$\eta_{ij} \equiv 1 - \frac{w_{i\bar{i}}w_{j\bar{j}}}{w_{i\bar{j}}w_{j\bar{i}}} = \frac{w_{ij}w_{\bar{j}\bar{i}}}{w_{i\bar{j}}w_{j\bar{i}}}, \tag{4.25}$$

where we have used the notation $w_{ij} = w_i - w_j$ and $w_{i\bar{j}} = w_i - \overline{w_j}$. Note that $\eta_{ij} \in [0, 1]$. Also, the UHP $2N$-point function we started with should only depend on $4N - 3$ real degrees of freedom (after making use of the part of the conformal symmetry which maps the real axis to itself), so the η_{ij} parameters are not all independent. They are still a useful parametrization, however. When $\eta_{ij} \approx 1$, the operators at w_i and w_j are much closer to their respective image points than to each other. Likewise, at $\eta_{ij} \approx 0$ the operators at w_i and w_j are closer to each other than to their respective images. This behavior helps determine efficient OPE expansion channels, as we will see below.

The time-dependence of the correlation function is reflected in the time-dependence of the η_{ij} cross-ratios, which in the $\tau_0 \to 0$ limit are given by

$$\eta_{ij}(\mathfrak{t}) = 1 - \frac{2\cosh^2(\pi\mathfrak{t}/2\tau_0)}{\cosh(\pi|x_i - x_j|/2\tau_0) + \cosh(\pi\mathfrak{t}/\tau_0)} \approx \frac{1}{1 + \exp\left[\frac{\pi}{\tau_0}\left(\mathfrak{t} - \frac{|x_i - x_j|}{2}\right)\right]}. \tag{4.26}$$

We see that there are sharp transitions between $\eta_{ij} \approx 1$ and $\eta_{ij} \approx 0$, which occur at half the light-crossing time, $|x_i - x_j|/2$.

At early times (meaning for times less than the length scales defining the intervals, but still much greater than the local equilibrium scale τ_0), all of the η_{ij} are approximately equal to one. Then the upper half-plane $2N$-point function approximately factorizes into $2N$ full-plane two-point functions: this is the cluster decomposition limit where each operator in the upper half plane is paired with its image point in the lower half plane. Then we find

$$\operatorname{Tr} \rho^n = \left| \frac{\pi}{2\tau_0} e^{-\pi \mathrm{t}/2\tau_0} \right|^{2N\Delta_n}. \tag{4.27}$$

This leads to a linear growth of the entanglement entropy at a rate which is N times as fast as it would have been for a single interval (in agreement with the quasiparticle picture).

At very late times, all of the η_{ij} parameters are very small. One can check that this corresponds to a different cluster decomposition limit: now adjacent operators in the upper half-plane are paired with each other, and their image points are paired with each other. So again we find a product of $2N$ full-plane two-point functions. One can check that in this limit the thermal entropy formula $S = s_{\mathrm{eq}} V_A$ is produced.

At intermediate times, when some of the η_{ij} are small and others are approximately equal to one, we need to be more careful. This is where the real difference between holographic and weakly coupled CFTs lies. To simplify the notation, we will restrict ourselves to $N = 1$ and $N = 2$, though similar arguments hold for all N.

At $N = 1$ there are no real surprises, but it is useful to go through it to illustrate some of the key points. There is only a single interval and a single cross-ratio η, and the two-point function in the upper half-plane can be written as a four-point function in the full plane, which we analyzed above. The conformal block decomposition of the four-point function implies that we can write the UHP two-point function as

$$\langle \mathcal{T}_n(w_1)\, \mathcal{T}_{-n}(w_2) \rangle_{\mathrm{UHP}} = \frac{1}{|w_{1\bar{1}} w_{2\bar{2}} \eta|^{2\Delta_n}} F_n(\eta). \tag{4.28}$$

Even though $F_n(\eta)$ may be a very complicated function, the cluster decomposition limits tell us that $F_n \to 1$ both when $\eta \to 0$ and $\eta \to 1$, since the prefactor alone reproduces both of those limits. This makes the global quench computation easy to perform when $\tau_0 \to 0$ (i.e., at times and distances much greater than the equilibration scale), since η makes a rapid transition from zero to one in that case. Then for arbitrary CFTs, the factor $F_n(\eta)$ is completely inconsequential and can be dropped; the result agrees with both the quasiparticle model and the holographic calculation. However, we would like to point out that a stronger statement can be made about large-c CFTs with a sparse spectrum. In the limit $c \to \infty$, we have an exact formula for $F_n(\eta)$ that comes from demanding that the full-plane four-point function always factorize in either the s-channel or t-channel:

$$F_n(\eta) = \begin{cases} \eta^{\Delta_n}, & \eta > 1/2, \\ (1-\eta)^{\Delta_n}, & \eta < 1/2. \end{cases} \tag{4.29}$$

Although this formula did not make a difference for a single interval, we will now see how things change with multiple intervals.

With two intervals, $N = 2$, the relevant correlation function is a four-point function in the upper half-plane. Following [114], we will parametrize the four-point function as

$$\langle \mathcal{T}_n(w_1)\,\mathcal{T}_{-n}(w_2)\,\mathcal{T}_n(w_3)\,\mathcal{T}_{-n}(w_4)\rangle_{\text{UHP}} = \frac{1}{\prod_i |w_i - \bar{w}_i|^{\Delta_n}} \left(\frac{\eta_{13}\eta_{24}}{\eta_{12}\eta_{23}\eta_{14}\eta_{34}}\right)^{\Delta_n} F_n(\{\eta_{ij}\}). \tag{4.30}$$

The function F_n (different from above, but with the same name) is in principle very complicated, but since we only care about $\eta_{ij} \approx 1$ or $\eta_{ij} \approx 0$, only the values of F_n at those points are necessary to find the entanglement entropy. So as time passes and the η_{ij} transition from one to zero, F_n effectively becomes a piecewise constant function of time. This translates into an additive term in the entropy, which is usually argued to be subleading in the $\tau_0 \to 0$ limit. However, this reasoning does not apply if the leading constant term in F_n is zero during any given phase. Then we have to consider terms which are proportional to some of the nearly-vanishing η_{ij}, which are exponentially small and in particular time-dependent. This is what happens for theories with a holographic dual. At large-c and with a sparse spectrum, the eight-point function in the full plane, which is equal to the four-point function we wish to compute in the upper half-plane, always factorizes in some channel into a product of two-point functions [108]. By comparing this result to Eq. (4.30), we find that the effective F_n factors are proportional to the η_{ij} whenever the quasiparticle model (i.e., the prefactor in Eq. (4.30)) says that the entropy should decrease. In particular, the resulting time dependence of F_n precisely cancels out the time dependence of the prefactor, meaning that the entropy remains saturated at its thermal value and does not decrease.

4.4 Entanglement Tsunami

It would be desirable to have a picture of propagating interacting quasiparticles to replace the free-streaming quasiparticle picture that seems to work well for free theories. Such a picture should reproduce the linear growth rate evident at early times, but avoid decreases in entropy. We have not been able to derive such a picture in terms of particles, but a simple heuristic which gives the correct answer is the "entanglement tsunami" of [101, 102], which we will elaborate on here. We will begin with a discussion that applies to one or two disjoint intervals, where the holographic entropy can be reproduced exactly, and then explain how to extend the idea to arbitrary numbers of disjoint intervals where we only have an upper bound on the entropy.

One or Two Intervals

Our picture of the entanglement tsunami is as a wave which begins at each of the endpoints of A at $\mathfrak{t} = 0$ and flows outward in both directions (see Fig. (4.5)). This wave is not

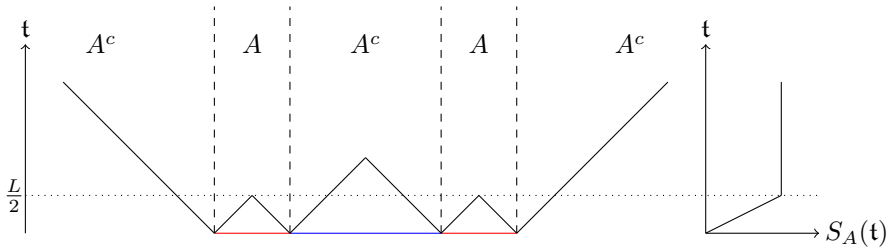

Figure 4.5: The quench for two intervals of length L separated by a distance R when $L > R$. On the left, we show the entanglement tsunami wavefront as a function of time (jagged black line.) The region A is marked as red. The intervals between the disconnected components of A are marked as blue. On the right, we show the entanglement entropy as a function of time.

a physical wave representing the propagation of particles or energy: it is merely a tool for understanding the entanglement. In particular, note that the quenched state is homogeneous, while the wave begins at particular locations picked out by the region A we have chosen. At any time $\mathfrak{t} > 0$, the wave divides the space into two regions: one which has already been overtaken by the wave, and one which has yet to be overtaken by the wave. We will call the former region the "entangled" region, and the latter region the "unentangled" region. This picture is reminiscent of a vacuum decay, where at $\mathfrak{t} = 0$ we have tunneling events at each of the endpoints of A and the entanglement tsunami wavefront is like a bubble wall which converts the metastable vacuum (the unentangled region) into the true vacuum (the entangled region). (Though we should emphasize once more that there is no physical sense in which the entanglement tsunami is changing the vacuum; it just has the same cartoon picture.) If A has more than one endpoint, i.e., it is not just a half-line, then eventually the entanglement tsunami wavefronts starting from adjacent endpoints will collide. For all times after the collision, the entire interval between those two endpoints will be part of the entangled region.

We still have to give a rule for computing the entanglement entropy of the region A given this tsunami picture. Let the entangled region at time $\mathfrak{t}$ be denoted by $E(\mathfrak{t})$. When A consists of just one or two intervals, then its entanglement entropy is

$$S(\mathfrak{t}) = s_{\text{eq}} \times \min\Big(\text{Vol}(E(\mathfrak{t}) \cap A), \text{Vol}(E(\mathfrak{t}) \cap A^c)\Big). \tag{4.31}$$

It is not hard to see that this rule agrees with the holographic prescription for entanglement entropy: for one interval it is trivial, and for two intervals the two options essentially coincide with the two possible HRT surfaces. Also, note that the entropy is symmetric with respect to A and A^c, which is as it should be for a globally pure state.

Although we have emphasized that the entanglement tsunami does not represent the propagation of a physical excitation, there is a suggestive interpretation in which we do imagine a collection of excited particles living in $E(\mathfrak{t})$. Suppose that a finite density of

qubits populates the region $E(\mathfrak{t})$ and that those qubits are in a typical pure state. Then the entanglement entropy of the qubits in $E(\mathfrak{t}) \cap A$ will follow the Page rule, meaning that their entanglement entropy will be proportional to either the number of qubits in $E(\mathfrak{t}) \cap A$ or $E(\mathfrak{t}) \cap A^c$, whichever is smaller [115]. This is precisely the entanglement tsunami prescription.

Multiple Intervals

When A consists of more than two intervals, there does not appear to be a simple rule like Eq. (4.31) which correctly reproduces the holographic answer. One can attempt the following simple and natural generalization, which involves a refinement of our notion of the entangled region $E(\mathfrak{t})$. Instead of a single region, the entangled region is naturally the union of disjoint intervals:

$$E(\mathfrak{t}) = \bigcup_i E_i(\mathfrak{t}), \tag{4.32}$$

where each $E_i(\mathfrak{t})$ is an interval representing a single connected component of $E(\mathfrak{t})$. The number of $E_i(\mathfrak{t})$ regions changes with time. For N intervals, $E(\mathfrak{t})$ has $N+1$ connected components at early times (each being a small neighborhood around an endpoint of an interval) and only a single connected component at late times. A collision of entanglement tsunami wavefronts indicates that two of the $E_i(\mathfrak{t})$ are merging, and thereafter will be treated as a single unit. We illustrate this behavior in Fig. (4.6).

With this refinement of the entangled region, we have the following upper bound on the holographic entanglement entropy[1]:

$$S(\mathfrak{t}) \leq s_{\text{eq}} \sum_i \min\Big(\text{Vol}(E_i(\mathfrak{t}) \cap A), \text{Vol}(E_i(\mathfrak{t}) \cap A^c)\Big). \tag{4.33}$$

In other words, we have a separate minimization problem for each connected component of the entangled region, and at the end, we add them all up. This rule is numerically the same as Eq. (4.31) for one or two intervals, and so there is equality. For more than two intervals, Eq. (4.33) corresponds to the area of one of the candidate HRT surfaces, though not necessarily the minimal one. Therefore it represents only an upper bound on the entropy. (See [116] for a discussion on such an upper bound beyond the context of holography.) We also note that Eq. (4.33) is manifestly symmetric with respect to A and A^c, even though each minimization subproblem is free to choose to use region A or A^c independently for its contribution to the entropy.

There is also still a suggestive qubit picture for the right-hand side of Eq. (4.33). Now instead of one collection of qubits in $E(\mathfrak{t})$, there is an independent collection of qubits in each of the $E_i(\mathfrak{t})$, and the total qubit state is a product state over the connected components. We can imagine that the qubits are somehow being emitted at the endpoints of the intervals, and when two chains of qubits come into contact (i.e., when two wavefronts merge), they

[1]We would like to thank Mark Mezei for providing us with an example of three disjoint intervals where equality fails.

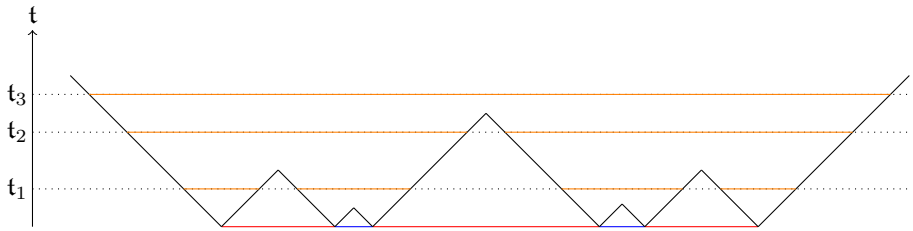

Figure 4.6: Entanglement tsunami for many intervals. The region A is marked as red. The intervals between the disconnected components of A are marked as blue. Note that at time $\mathfrak{t}_1$, $E(\mathfrak{t})$ consists of four disconnected components (orange solid lines) separated by the entanglement tsunami wavefront (jagged black line). But at time $\mathfrak{t}_2$, the first pair and second pair have merged, leaving two disconnected regions. At time $\mathfrak{t}_3$, there is only a single connected region.

undergo a very rapid mixing and end up in a typical pure state of the composite system. Even though this picture only provides an upper bound on the entropy, it could be that a similar picture is accurate for the real system.

4.5 Discussion

Summary

We have seen that for a (1+1)-dimensional CFT in the limit of large-c, with a sparse spectrum of operators, the time-dependence for the entanglement entropy of multiple intervals is not correctly captured by the quasiparticle model of [95, 96]. The correct answer, which is correctly reproduced holographically, is non-decreasing with time, whereas the quasiparticle model features crops in the entropy. A heuristic model which gives the correct time evolution is provided by the entanglement tsunami, a picture originally introduced in [101, 102] which we have developed into a rule for calculating the entanglement. There are many unanswered questions about this model, which we will now discuss.

Higher Dimensions

In higher dimensions, as in (1+1)-dimensions, the entanglement entropy for disjoint regions in the quasiparticle picture will experience periods of decrease that are not present in the holographic calculation. The entanglement tsunami picture will solve this problem since, like the holographic calculation, it does not allow for decreases in the entropy. There remains the puzzle of the velocity of the entanglement tsunami wavefront. In (1+1)-dimensions, it seems natural to say that the wavefront moves at the speed of light. But this would cause the entanglement to grow more quickly than the holographic calculation indicates. At the

same time, a wavefront made up of quasiparticles traveling in random directions moves too slowly. A field-theoretic derivation of the entanglement tsunami velocity would do much to clarify the picture.

Interacting Quasiparticles?

A natural guess for fixing up the quasiparticle picture is simply to add interactions. Instead of free-streaming, the particles would bump into each other and generate multipartite entanglement. It is not clear whether a simple picture of this type can accurately reproduce the holographic calculation, but the entanglement tsunami prescription may provide a useful starting point. In the entanglement tsunami, it appears as though there are clouds of particles being emitted by the endpoints of the region A (or, in higher dimensions, by the boundary of A), beginning at the quench time. The unphysical aspect of this model is that it is not homogeneous: the boundaries of A are not preferred locations in the state, so it doesn't make sense to say that they are the sources of particles. Instead, the state should describe a finite density of interacting particles everywhere at once. However, since we are asking about the entanglement entropy of A, there may be a sense in which the particles in a neighborhood of the boundary of A are the only ones that matter. Then the entanglement tsunami would represent a growing sphere of influence, picking out the parts of the homogenous matter distribution which determine the entanglement. We leave an exploration of this possibility to future work.

Chapter 5

Dynamics of the Area Law of Entanglement Entropy

5.1 Introduction

In recent years, the study of the time-dependence of entanglement entropy has received a considerable attention [95, 98, 99, 100, 101, 102, 117, 116, 118]. In the simplest scenario, one studies the evolution of the spatial entanglement entropy under the assumption that the system begins in the vacuum state in the asymptotic past while a relevant (i.e., positive mass dimension) coupling constant in the Hamiltonian is given a non-trivial time dependence which asymptotes to a constant value in the far future.

Although the assumption that the system starts in the vacuum state might seem to be an oversimplification, certain questions about the entanglement may still be addressed without loss of generality. For example, in quantum field theory the entropy of a region is always UV divergent [24, 25], whereas the structure of these divergences is state independent, see *e.g.,* [119]. Hence, assuming that the system resides in the vacuum state is enough to determine the pattern of divergences in *any* state. Indeed, this pattern is fixed by the entanglement of degrees of freedom near the UV cutoff scale, δ, and therefore the characteristic scale of an excited state plays no role in this regime. Furthermore, the dynamics of the divergent part of the entanglement entropy in a time-dependent setup is not trivial, since the asymptotic vacua, in general, are not identical.

Even though the time dependence of the full entanglement entropy in a generic setup is very complicated, we expect that evolution of the UV divergences is quasi-adiabatic, and therefore tractable. Our expectation rests on the locality of UV divergences when all length scales, ℓ_i, including the characteristic time scale of the change in couplings, are much longer than the UV cut off, $\ell_i \gg \delta$, *i.e.,* when the system is found in the physical regime.[1] In

[1] In principle, one could study situations when the coupling varies over time scales of order the UV cut off. However, the interpretation of these results might be questionable, and we leave this regime outside the scope of the current work.

particular, the divergent part of the entropy at time $\mathfrak{t}$ will only depend on the instantaneous value of the coupling and its time derivatives.

There is an additional outcome that stems directly from the locality of divergences. It is now a well-established fact that entanglement entropy is sensitive to the geometry of the background and shape of the entangling surface [120, 121, 122, 123, 124, 125, 126, 127, 128]. The full answer can be expressed as a sum of certain geometric structures with coefficients fixed by QFT data. Not all of these structures are necessarily local, however, those which are multiplied by divergent coefficients as $\delta \to 0$ should be local.

The ubiquitous 'area law' [24, 25] is probably the most prominent and simple example of a local geometric structure. In a static d-dimensional CFT it is proportional to $\delta^{2-d}\mathcal{A}$ since δ in this case is the only admissible scale at hand, while entropy is dimensionless and area of the surface, $\mathcal{A}$, has length dimension $d-2$. Therefore the 'area law' term is not universal in a CFT – it is sensitive to the choice of regularization scheme. However, the presence of an additional scale in a non-conformal field theory may overturn this conclusion and result in a *universal* 'area law' of entanglement, *e.g.,* a logarithmically divergent term proportional to the area multiplied by an appropriate power of some built-in scale.

In this chapter, we focus on the evolution of the 'area law' terms when a QFT undergoes a quantum quench, and calculate the time-dependence of the universal coefficients in a variety of examples. To make the field theory analysis analytically tractable, we expand the entanglement entropy to linear order in the time-dependent coupling $\lambda(\mathfrak{t})$. This is not necessary to recover the exact pattern of the universal divergences in the holographic approach since it is completely fixed by the asymptotic region of the dual geometry. Even though our focus is on the 'area law' only, we expect qualitatively similar behavior from the subleading divergences as well.

If the mass dimension of $\lambda(\mathfrak{t})$ is α, then for $\alpha = (d-2)/k$ we may have a universal term proportional to $\lambda^k(\mathfrak{t})\mathcal{A}$. Similarly, if $\alpha = (d-2-l)/k$ with l being a non-negative integer, then a term proportional to $\lambda^{k-m}(\mathfrak{t})\partial_t^l\lambda^m(\mathfrak{t})\mathcal{A}$ with $1 \leq m \leq k$ is allowed. It may happen that for a given α there is more than one choice of l and k, in which case there is a proliferation of possible universal structures. Generically, one would expect all allowed terms to appear, and with independent coefficients. Note, however, that for a given α there are only finitely many allowed terms.

In Sec. (5.2) and Sec. (5.3) we carry out explicit calculations for a set of special values of k and l in holographic and free field theories. In both cases, we observe the quasi-adiabatic behavior that we had argued for. Moreover, our holographic and free field calculations exactly match in some cases. Such an agreement between the time-dependent terms of entanglement entropy in the weakly and strongly coupled regimes resembles similar match in the static case [129, 130] and can be attributed to the universality of certain two- and three-point correlation functions in a CFT. In particular, we observe explicit match when $\alpha = 1, 2$ and $k = 2$ in various dimensions.[2] These values of α correspond to the Dirac and scalar mass

[2]In fact, there is also a trivial match when $k = 1$. The universal term, in this case, is independent of λ_0, and therefore the final answer remains intact if we set $\lambda_0 = 0$. However, if the theory is conformal at $\lambda_0 = 0$

operators, respectively. Recalling now that $\alpha = (d-2-l)/k$ results in the following cases explicitly elaborated in the text:

- $\alpha = 1$, $d = 4$, $l = 0$. This case corresponds to a 4D massive Dirac field. Up to a numerical factor the universal entanglement entropy is given by $\sim \lambda^2(\mathfrak{t})\mathcal{A}$, where $\lambda(\mathfrak{t})$ is the time-dependent mass of the Dirac field.

- $\alpha = 2$, $d = 6$, $l = 0$. This case of a 6D massive scalar field is analogous to the previous case, *i.e.,* the entanglement entropy is given by $\sim \lambda^2(\mathfrak{t})\mathcal{A}$, except that $\lambda(\mathfrak{t})$ is mass squared this time.

- $\alpha = 1$, $d = 6$, $l = 2$. In six dimensions, there is a universal term involving two time derivatives of the Dirac mass $\sim \lambda(\mathfrak{t})\ddot{\lambda}(\mathfrak{t})\mathcal{A}$. We calculate the numerical coefficient for the first time both holographically and in the free field theory, and find exact agreement.

- $\alpha = 2$, $d = 8$, $l = 2$. The behavior of the universal term for the massive scalar field in eight dimensions $\sim \lambda(\mathfrak{t})\ddot{\lambda}(\mathfrak{t})\mathcal{A}$ resembles the massive Dirac field in six dimensions, and again we calculate the precise numerical coefficient holographically and in free field theory, finding agreement.

The remainder of this chapter is organized as follows. In Sec. (5.2) we build on the holographic proposal [26, 27] to compute the time-dependent universal entanglement entropy for holographic field theories. Since we are only interested in divergent terms, the gravity calculation is localized in the asymptotic region of the dual geometry; this feature allows us to calculate the universal coefficients exactly even though the geometry is only determined perturbatively. We calculate the coefficients of the terms for which agreement with the free fields is expected, as well as for the terms where agreement is not anticipated. In the latter case, the answer on the field theory side depends on more than just the universal correlation functions of the underlying CFT.

In Sec. (5.3) we derive a general expression for the time-dependent first order correction to the 'area law', and show that for a generic QFT it can be expressed in terms of the spectral function defining the two-point correlation function of the trace of the energy-momentum tensor. We use these formulas to calculate the universal 'area law' for massive free fields with time-dependent masses. We end with conclusions in Sec. (5.4), and a number of Appendices detailing some of the more technical aspects of the calculation.

---

such terms must vanish independently of the values of α and l for the same reason as in the static case [131], see Sec. (5.3).

5.2 Holographic Calculation

Setup

We consider a CFT in d spacetime dimensions on the boundary, dual to Einstein gravity in the $d+1$-dimensional bulk. The computation of the entanglement entropy of some boundary region, B, can be done using HRT prescription [26, 27]. The prescription tells us to find the codimension-2 surface in the bulk of the extremal area, Σ_B, subject to the condition that B and Σ_B are homologous. If there are multiple extremal surfaces, we must choose the one with the minimum area. We will call this minimal extremal surface the HRT surface from now on. The entanglement entropy of B and the area of the HRT surface are related by

$$S = \frac{\text{Area}(\Sigma_B)}{4G_{d+1}}\,. \tag{5.1}$$

Beginning with the vacuum state of the CFT, we turn on a relevant operator $\mathcal{O}$ of dimension $\Delta < d$ at $\mathfrak{t} = 0$ by giving it a nonzero, time-dependent, spatially homogeneous coupling $\lambda(\mathfrak{t})$. It will be useful to express our results in terms of the mass dimension of the coupling, $\alpha \equiv d - \Delta$. The operator $\mathcal{O}$ is dual to a scalar field Φ in the bulk of mass $m^2 = \Delta(\Delta - d)$ [132, 133]. A nonzero coupling $\lambda(\mathfrak{t})$ corresponds to nontrivial boundary conditions for Φ. Through the Einstein-scalar field equations, this will change the bulk metric and therefore affect the calculation of the HRT surface and its area.

The Einstein-scalar equations are given by the variation of the bulk action [119]

$$I(g_{\lambda\nu}, \Phi) = \frac{1}{16\pi G_{d+1}} \int d^{d+1}x\, \sqrt{-g}\, \left\{ R - \frac{1}{2} g^{\lambda\nu} \partial_\lambda \Phi \partial_\nu \Phi - V(\Phi) \right\}, \tag{5.2}$$

$$V(\Phi) = -\,d(d-1) + \frac{1}{2} m^2 \Phi^2 + \frac{\kappa}{6}\Phi^3 + \frac{\omega}{24}\Phi^4 + O(\Phi^5)\,, \tag{5.3}$$

where we have set $L_{AdS} = 1$. We have chosen to normalize the bulk scalar action so that there is an overall factor of $1/16\pi G_{d+1}$ in front; this amounts to a normalization condition on the operator $\mathcal{O}$. In particular, with this normalization, we can read off Newton's constant from the two-point function of $\mathcal{O}$ [134]:

$$\langle \mathcal{O}(x)\mathcal{O}(y)\rangle = \frac{2\Delta - d}{8\pi G_{d+1}} \frac{\Gamma(\Delta)}{\Gamma(\Delta - d/2)} \frac{1}{\pi^{d/2}|x-y|^{2\Delta}}\,. \tag{5.4}$$

This will allow us to make contact with the free field calculations in Sec. (5.3).[3] The bulk interaction parameters κ, ω, etc., are similarly determined by the three, four, and higher-point functions of $\mathcal{O}$. The most interesting terms in the entanglement entropy are the ones

[3] Alternatively, we could have left the normalization unspecified at the cost of introducing another parameter η which multiplies the bulk scalar field action. The normalization we have chosen is convenient because it simplifies the Einstein-scalar equations of motion.

which depend only on the two-point function, since these may be the same across theories once the normalization has been fixed using Eq. (5.4). Thus we should pay special attention below to those terms which depend only on G_{d+1}.

The coupled Einstein-scalar equations are

$$R_{\mu\nu} = \frac{1}{2}\partial_\mu\Phi\partial_\nu\Phi + \frac{1}{d-1}g_{\mu\nu}V(\Phi)\,, \tag{5.5}$$

$$\frac{1}{\sqrt{-g}}\partial_\mu\Big(\sqrt{-g}g^{\mu\nu}\partial_\nu\Phi\Big) - \frac{\delta}{\delta\phi}V(\Phi) = 0\,. \tag{5.6}$$

Following [94], we choose our bulk 'radial' coordinate z to be orthogonal to all of the boundary coordinates. This corresponds to the gauge fixing

$$g_{zt} = g_{zi} = 0\,, \tag{5.7}$$

where x^i for $i = 1, ..., d-1$ are the spatial coordinates of the boundary, and t is the time coordinate in the bulk. We also rescale the bulk coordinate to fix $g_{zz} = \frac{1}{z^2}$.

Since our quench is homogenous and isotropic, the bulk geometry must be homogenous and isotropic as well. Then we can write the bulk metric as

$$ds^2 = \frac{1}{z^2}\Big(dz^2 - f(t,z)dt^2 + h(t,z)\sum_{i=1}^{d-1}dx_i^2\Big)\,, \tag{5.8}$$

with the boundary conditions that $f(t, z=0) = h(t, z=0) = 1$, and $f(t<0, z) = h(t<0, z) = 1$.

With this choice of metric, Eq. (5.5) and Eq. (5.6) take the following form[4]:

$$0 = \frac{d-1}{4}\frac{\dot{h}}{h}\frac{h'}{h} + \frac{d-1}{4}\frac{\dot{h}}{h}\frac{f'}{f} - \frac{d-1}{2}\frac{\dot{h}'}{h} - \frac{1}{2}\dot{\Phi}\Phi'\,, \tag{5.9}$$

$$\begin{aligned} 0 = {} & \frac{d-1}{4}\Big(\frac{\dot{h}}{h}\Big)^2 - \frac{d}{2}\frac{f'}{z} + \frac{d-1}{4}\frac{\dot{f}}{f}\frac{\dot{h}}{h} - \frac{1}{4}\frac{f'^2}{f} + \frac{d}{z^2}f - \frac{d-1}{2}\frac{f}{z}\frac{h'}{h} \\ & - \frac{d-1}{2}\frac{\ddot{h}}{h} + \frac{d-1}{4}\frac{f'h'}{h} + \frac{1}{2}f'' - \frac{1}{2}\dot{\Phi}^2 + \frac{1}{d-1}\frac{f}{z^2}V(\Phi)\,, \end{aligned} \tag{5.10}$$

$$\begin{aligned} 0 = {} & z^2\Phi'' - \frac{z^2}{f}\ddot{\Phi} - (d-1)z\Phi' + \frac{z^2}{2}\dot{\Phi}\frac{\dot{f}}{f} + \frac{z^2}{2}\Phi'\frac{f'}{f} + (d-1)\frac{z^2}{2}\Phi'\frac{h'}{h} \\ & - (d-1)\frac{z^2}{2}\frac{\dot{\Phi}}{f}\frac{\dot{h}}{h} - \frac{\delta}{\delta\phi}V(\Phi)\,, \end{aligned} \tag{5.11}$$

where prime and dot denote the derivative with respect to z and t respectively.

[4]These equations are the zt-component Eq. (5.9) and tt-component Eq. (5.10) of the Einstein equation, and the scalar field equation of motion Eq. (5.11). We will not need the remaining equations in our analysis.

The UV divergences in the entanglement entropy arise from the divergences of the area functional of the HRT surface, Σ_B, near the asymptotic boundary ($z = 0$). To compute these divergences, we need to find the area functional, or the induced metric on Σ_B, near $z = 0$. In [119], the authors studied the solutions of Eqs. (5.9)-(5.11) as a power series in z. They have shown that the solutions can be written as the sum of two separate power series. One of them is independent of the state of the boundary theory, whereas the other series solution carries information about the state of the boundary theory. They also showed that the latter solution does not contribute to the divergences in the entanglement entropy, which implies that the divergences in the entanglement entropy are state-independent (as expected).

Having learned that the state-dependent power series solution does not contribute to the divergences, we will only be writing the state-independent solution in the following analysis.[5] In [119], all the powers of z that arise in the asymptotic solution have been identified. Using their result, we make the following ansatz for the metric and the scalar field:

$$h(z,t) = 1 + \sum_{m=2}\sum_{n=0} z^{m\alpha+n}\, h_{m,n}(t)\,, \tag{5.12}$$

$$f(z,t) = 1 + \sum_{m=2}\sum_{n=0} z^{m\alpha+n}\, f_{m,n}(t)\,, \tag{5.13}$$

$$\Phi(z,t) = z^{\alpha} \sum_{m=0}\sum_{n=0} z^{m\alpha+n}\, \phi_{m,n}(t)\,, \tag{5.14}$$

where $\phi_{0,0}(t)$ is equal to the time-dependent coupling, $\lambda(t)$. That is,

$$\phi_{0,0}(t) = \lambda(t)\,. \tag{5.15}$$

HRT Surface

In this chapter, we will only consider terms which are independent of the curvature of the entangling surface. Then it will be enough to consider the entanglements of a half-space in the field theory, which means the entangling surface is a flat plane. That is, the region B in the boundary is given by

$$B: \qquad x_1 > 0, \qquad t = \mathfrak{t}\,. \tag{5.16}$$

The natural coordinates on the codimension-2 HRT surface in the bulk are $\{z, x^i\}$ for $i = 2, ..., d-1$, with t and x_1 left as functions determining the position of the surface in the bulk. The HRT surface must be invariant under translation in x^i direction, for $i = 2, ..., d-1$. This means $t = t(z)$ and $x_1 = x_1(z)$ are functions of z alone. The state is also translation-invariant in the x_1 direction, and so we can fix $x_1(z) = 0$. To summarize, the HRT surface, Σ_B, is

$$\Sigma_B: \qquad x_1 = x_1(z) = 0\,, \qquad t = t(z)\,, \tag{5.17}$$

[5] This is not to say that the state-dependent terms are unimportant for the non-divergent parts of the entropy or that they are actually equal to zero in the solutions we consider, but only that we do not need to keep track of them in our analysis.

with the boundary condition, $t(z=0)=\mathfrak{t}$, the time at which we are computing the entropy.

The area functional of the HRT surface is given by

$$\text{Area}(\Sigma_B) = \ 2\mathcal{A}\ \int_\delta^\infty dz\ \frac{h^{\frac{d-2}{2}}(z,t(z))}{z^{d-1}}\ \sqrt{1-f(z,t(z))(t'(z))^2}\,, \tag{5.18}$$

where $\mathcal{A}$ is the area of the entangling surface in the boundary, and prime denotes the derivative with respect to z. Also note that we have introduced a cut-off surface near the boundary at $z=\delta$.

Applying the variational principle to the above functional gives us an equation for $t(z)$. As mentioned above, we are only interested in the asymptotic behavior of the solution near $z=0$. As we will show in Appendix (D.1), the lowest nontrivial power of z that appears in the solution of $t(z)$ is $z^{2+2\alpha}$. That is, at the lowest order, the solution of the stationary surface is

$$t(z) = \ \mathfrak{t} + z^{2+2\alpha}\ t_{2+2\alpha} + \dots\,, \tag{5.19}$$

where $t_{2+2\alpha}$ is a constant.

By expanding the integrand of Eq. (5.18) in z, we see that we can see that $t_{2+2\alpha}$ in Eq. (5.19) enters as the coefficient of $z^{4\alpha+3-d}$. This will not affect the divergent terms in the entropy as long as

$$\alpha > \frac{d-4}{4}\,. \tag{5.20}$$

In the following, we will perform explicit calculations for $\alpha=1,2$ in $d=4,5,6$, and for $\alpha=2$ in $d=8$. These values of α corresponds to the mass term of a Dirac fermion and scalar boson, respectively. For these values of α and d, the above inequality is true. This allows us to forget about the details of the HRT surface, and simply set $t(z)=\mathfrak{t}$ in Eq. (5.18). With this simplification, Eq. (5.18) becomes

$$\text{Area}(\Sigma_B) = \ 2\mathcal{A}\ \int_\delta^\infty dz\ \frac{h^{\frac{d-2}{2}}(z,\mathfrak{t})}{z^{d-1}}\,. \tag{5.21}$$

The entanglement entropy of the boundary region B is then given by

$$S(\mathfrak{t}) = \frac{\mathcal{A}}{2G_{d+1}}\ \int_\delta^\infty dz\ \frac{h^{\frac{d-2}{2}}(z,\mathfrak{t})}{z^{d-1}}\,, \tag{5.22}$$

where we can give G_{d+1} a field-theory definition by relating it to the two-point function of the operator $\mathcal{O}$ as in Eq. (5.4), reproduced here:

$$\langle\mathcal{O}(x)\mathcal{O}(y)\rangle = \ \frac{2\Delta-d}{8\pi G_{d+1}}\ \frac{\Gamma(\Delta)}{\Gamma(\Delta-d/2)}\ \frac{1}{\pi^{d/2}|x-y|^{2\Delta}}\,. \tag{5.23}$$

Scalar Mass Operator: $\alpha = 2$

In this subsection, we specialize to the case where $\alpha = 2$. In the free field case, this corresponds to a time-dependent mass:

$$\mathcal{O}(x) = \phi^2(x)\,, \tag{5.24}$$

$$\lambda(\mathfrak{t}) = \frac{1}{2}m^2(\mathfrak{t})\,. \tag{5.25}$$

The entanglement entropy is given by Eq. (5.22). The ansatz for $h(z,t)$ given in Eq. (5.12) becomes

$$h(z,t) = \ 1 + z^4 h_{2,0}(t) + O(z^6)\,. \tag{5.26}$$

By counting powers of z in the integral Eq. (5.22), we deduce that there is no time-dependent universal log-divergence in the entanglement entropy for $d = 4$ and $d = 5$. This result is consistent with the time-independent holographic calculations [119]. Now we turn to $d = 6$ and $d = 8$. To facilitate comparison to the free field case (wherever applicable), we will use Eq. (5.4) and the result [129]

$$\langle \phi^2(x)\phi^2(y)\rangle_{\text{boundary}} = \ \frac{2}{(d-2)^2\Omega_d^2}\ \frac{1}{|x-y|^{2(d-2)}}\,, \tag{5.27}$$

which says that the effective value of Newton's constant is

$$G_{d+1} = \frac{(d-2)^2(d-4)^2\pi^{d/2-1}}{16(d-1)}\frac{\Gamma(d)}{(\Gamma(d/2))^3}\,. \tag{5.28}$$

$d = 6$

Using Eq. (5.22), we get

$$S(\mathfrak{t}) = \ \frac{\mathcal{A}}{2G_7}\ \int_\delta^\infty dz\ \frac{h^2(z,\mathfrak{t})}{z^5}\,. \tag{5.29}$$

After inserting Eq. (5.26) in the above expression, and extracting the log-divergence, we get

$$S_{\log}(\mathfrak{t}) = \ -\frac{\mathcal{A}}{G_7}\ h_{2,0}(\mathfrak{t})\ \log\delta\,. \tag{5.30}$$

Using Eq. (D.7), we get

$$h_{2,0}(t) = \ -\frac{1}{20}\phi^2_{0,0}(t) = -\frac{1}{20}\lambda^2(t)\,, \tag{5.31}$$

and hence

$$S_{\log}(\mathfrak{t}) = \frac{\mathcal{A}}{20G_7}\lambda^2(\mathfrak{t})\log\delta\,. \tag{5.32}$$

This is an example of a result which depends only on Newton's constant and not any of the other parameters in $V(\Phi)$. Then it depends only on the two-point function of $\mathcal{O}$, through Eq. (5.4). Using Eq. (5.28), we get $G_7 = 12\pi^2$. Then the holographic result, extrapolated to the free scalar, is

$$S_{\log}(\mathfrak{t}) = \frac{\mathcal{A}}{240\pi^2}\lambda^2(\mathfrak{t})\log\delta = \frac{\mathcal{A}}{960\pi^2}m^4(\mathfrak{t})\log\delta\,. \tag{5.33}$$

If $m^2(t)$ is constant, this agrees with the well-known answer for the static case [119]. We will see below in Sec. (5.3) that we have full agreement also in the time-dependent case.

$d = 8$

Using Eq. (5.22), we get

$$S(\mathfrak{t}) = \frac{\mathcal{A}}{2G_9}\int_\delta^\infty dz\,\frac{h^3(z,\mathfrak{t})}{z^7}\,. \tag{5.34}$$

After inserting Eq. (5.26) in the above expression, and extracting the log-divergence, we get

$$S_{\log}(\mathfrak{t}) = -\frac{3\mathcal{A}}{2G_9}\Big(h_{2,2}(\mathfrak{t}) + h_{3,0}(\mathfrak{t})\Big)\log\delta\,. \tag{5.35}$$

Using Eq. (D.10) and using Eq. (5.15), we get

$$h_{2,2}(t) + h_{3,0}(t) = \frac{\kappa}{126}\lambda^3(t) + \frac{1}{168}\dot\lambda^2(t) + \frac{1}{84}\lambda(t)\ddot\lambda(t)\,, \tag{5.36}$$

and hence

$$S_{\log}(\mathfrak{t}) = -\frac{\mathcal{A}}{2G_9}\Big(\frac{\kappa}{42}\lambda^3(\mathfrak{t}) + \frac{1}{56}\dot\lambda^2(\mathfrak{t}) + \frac{1}{28}\lambda(\mathfrak{t})\ddot\lambda(\mathfrak{t})\Big)\log\delta\,, \tag{5.37}$$

where $G_9 = 120\pi^3$ is given by Eq. (5.28). Note that the coefficent of the $\lambda^3(t)$ term is proportional to κ and hence it's not expected to be universal for all unperturbed CFTs.

Fermionic Mass Operator: $\alpha = 1$

In this subsection, we turn to the case $\alpha = 1$. This corresponds in the free field limit to a Dirac mass for a fermion:

$$\mathcal{O}(x) = \bar\psi(x)\psi(x)\,, \tag{5.38}$$

$$\lambda(\mathfrak{t}) = m(\mathfrak{t})\,. \tag{5.39}$$

The ansatz for $h(z,t)$ given in Eq. (5.12) for $\alpha = 1$ is

$$h(z,t) = 1 + z^2h_{2,0}(t) + z^3h_{3,0}(t) + z^4\Big(h_{2,2}(t) + h_{4,0}(t)\Big) + O(z^5)\,. \tag{5.40}$$

By a power counting argument, we find that there is a log divergence for all $d > 3$. The absence of the log term in $d = 3$ is consistent with the known result [119, 131] that the

change in the entanglement entropy to first order in a perturbation away from a CFT is zero: the coefficient of the log term, if present, would have been proportional to m.

To determine the effective value of G_{d+1} using Eq. (5.4), we will use the following two point function of $\mathcal{O}_\psi(x) = \bar{\psi}(x)\psi(x)$ with itself [129]:

$$\langle \mathcal{O}_\psi(x)\mathcal{O}_\psi(0)\rangle = \frac{2^{\lfloor d/2\rfloor}}{\Omega_d^2}\frac{1}{x^{2(d-1)}}\,. \tag{5.41}$$

$d = 4$

The log divergence in Eq. (5.22) in $d = 4$ is equal to

$$S_{\log}(\mathfrak{t}) = -\frac{\mathcal{A}}{2G_5}\, h_{2,0}(\mathfrak{t})\, \log\delta\,, \tag{5.42}$$

where $h_{2,0}(t)$ is given in Eq. (D.12):

$$h_{2,0}(t) = -\frac{1}{12}\phi_{0,0}^2(t) = -\frac{1}{12}\lambda^2(t)\,. \tag{5.43}$$

Using Eq. (5.4) and Eq. (5.41), we get $G_5 = \frac{\pi}{2}$. Then we have

$$S_{\log}(\mathfrak{t}) = \frac{\mathcal{A}}{12\pi}\lambda^2(\mathfrak{t})\log\delta\,. \tag{5.44}$$

$d = 5$

In this case, the log divergence in the entanglement entropy is equal to

$$S_{\log}(\mathfrak{t}) = -\frac{3\mathcal{A}}{4G_6}\, h_{3,0}(\mathfrak{t})\log\delta\,. \tag{5.45}$$

We copy the result for $h_{3,0}(t)$ from Eq. (D.15):

$$h_{3,0}(t) = \frac{\kappa}{36}\,\phi_{0,0}^3(t)\,. \tag{5.46}$$

Using Eq. (5.4) and Eq. (5.41), we get $G_6 = 8$. Therefore, the entanglement entropy becomes

$$S_{\log}(\mathfrak{t}) = -\frac{\mathcal{A}}{384}\kappa\phi_{0,0}^3(\mathfrak{t})\log\delta = -\frac{\mathcal{A}}{384}\kappa\lambda^3(\mathfrak{t})\log\delta\,. \tag{5.47}$$

In this case the answer depends on the bulk interaction strength κ, and hence is not expected to be universal across all theories.

$d = 6$

In this case, the entanglement entropy in Eq. (5.22) simplifies to

$$S(\mathfrak{t}) = \frac{\mathcal{A}}{2G_7} \int_\delta^\infty dz \, \frac{h^2(z,\mathfrak{t})}{z^5} \,. \tag{5.48}$$

By expanding Eq. (5.40) in the above expression and extracting the log term, we get

$$S_{\log}(\mathfrak{t}) = -\frac{\mathcal{A}}{2G_7} \Big(h^2_{2,0}(\mathfrak{t}) + 2h_{2,2}(\mathfrak{t}) + 2h_{4,0}(\mathfrak{t}) \Big) \, \log \delta \,. \tag{5.49}$$

Using Eq. (D.19), we get

$$h^2_{2,0}(t) + 2h_{2,2}(t) + 2h_{4,0}(t) = \frac{(117 - 65\kappa^2 + 45\omega)}{7200} \, \phi^4_{0,0}(t) + \frac{1}{80} \, \partial_t^2 \Big(\phi^2_{0,0}(t) \Big) \,. \tag{5.50}$$

Using Eq. (5.4) and Eq. (5.41), we get $G_7 = \frac{3}{2}\pi^2$. Combining these results gives us the log term divergence which not only depends on the instantaneous value of the coupling, but also on the instantaneous values of its derivatives. Notice that the derivative term does not depend on the higher-point interactions. Putting together the above results gives

$$S_{\partial^2,\log}(\mathfrak{t}) = -\frac{\mathcal{A}}{240\pi^2} \partial^2_{\mathfrak{t}} \Big(\lambda^2(\mathfrak{t}) \Big) \log \delta \,. \tag{5.51}$$

5.3 Field Theory Calculation

In this section, we use the Hamiltonian formalism to find the time evolution of the log term in the entanglement entropy for a general field theory to first order in perturbation theory. We will identify the linear term in the time-dependent entropy with a certain correlation function in the original theory. Using the free scalar field as a guiding example, we will go on to evaluate the divergent parts of this correlation function in terms of the spectral function $c^{(0)}(\mu)$ of the theory, defined in terms of the two-point function of the trace of the energy-momentum tensor [135]. Finally, we use this general prescription to calculate the answer for a free Dirac field.

Entropy Perturbation as a Correlation Function

The time-dependent Hamiltonian of our theory is

$$H(\mathfrak{t}) = H_0 + \lambda(\mathfrak{t}) \mathcal{O} \,, \tag{5.52}$$

where H_0 is the Hamiltonian of the unperturbed theory, and $\lambda(\mathfrak{t} \leq 0) = 0$.

We start with the system in the vacuum state, $|0\rangle$, of the unperturbed Hamiltonian. The global state at any time $\mathfrak{t} > 0$ is given by the time-dependent density matrix, $\hat{\rho}(\mathfrak{t}) =$

$|\chi(\mathfrak{t})\rangle\langle\chi(\mathfrak{t})|$, where $|\chi(\mathfrak{t})\rangle$ solves the Schrödinger equation generated by $H(\mathfrak{t})$ with initial condition $|\chi(\mathfrak{t}=0)\rangle = |0\rangle$. The time-dependent reduced density matrix of some spatial region B is given by the tracing over the Hilbert space of complementary region, $\bar{B}$. That is

$$\rho(\mathfrak{t}) = \mathrm{Tr}_{\bar{B}}\ |\chi(\mathfrak{t})\rangle\langle\chi(\mathfrak{t})| \ . \tag{5.53}$$

We define the time-dependent modular Hamiltonian $K(\mathfrak{t})$ of region B as

$$\rho(\mathfrak{t}) \equiv\ e^{-K(\mathfrak{t})}\,, \tag{5.54}$$

where $K(\mathfrak{t})$ has only support in the region B. In other words, this operator acts as the identity operator on the Hilbert space on the region $\bar{B}$.

The entanglement entropy of B can be written using the modular Hamiltonian:

$$\begin{aligned} S(\mathfrak{t}) =&\ -\mathrm{T}r_B\ \rho(\mathfrak{t})\log\rho(\mathfrak{t})\,, && (5.55)\\ =&\ \mathrm{T}r_B\Big(K(\mathfrak{t})\mathrm{T}r_{\bar{B}}\,|\chi(\mathfrak{t})\rangle\langle\chi(\mathfrak{t})|\Big)\,, && (5.56)\\ =&\ \mathrm{T}r_{B\cup\bar{B}}\Big(K(\mathfrak{t})\,|\chi(\mathfrak{t})\rangle\langle\chi(\mathfrak{t})|\Big)\,, && (5.57)\\ =&\ \langle\chi(\mathfrak{t})|\,K(\mathfrak{t})\,|\chi(\mathfrak{t})\rangle\ . && (5.58) \end{aligned}$$

To extract the term linear in $\lambda(\mathfrak{t})$, we define the state in the interaction picture. That is

$$|\tilde{\chi}(\mathfrak{t})\rangle \equiv e^{iH_0\mathfrak{t}}\,|\chi(\mathfrak{t})\rangle\ , \tag{5.59}$$

where the interaction picture state solves the equation

$$i\partial_{\mathfrak{t}}\,|\tilde{\chi}(\mathfrak{t})\rangle = \lambda(\mathfrak{t})\tilde{\mathcal{O}}(\mathfrak{t})\,|\tilde{\chi}(\mathfrak{t})\rangle\ , \tag{5.60}$$

where $\tilde{\mathcal{O}}(\mathfrak{t}) = e^{iH_0\mathfrak{t}}\mathcal{O}e^{-iH_0\mathfrak{t}}$. We can solve the above equation perturbatively

$$|\tilde{\chi}(\mathfrak{t})\rangle = |0\rangle + \big|\tilde{\chi}^{(1)}(\mathfrak{t})\big\rangle + \frac{1}{2}\big|\tilde{\chi}^{(2)}(\mathfrak{t})\big\rangle + \dots\ , \tag{5.61}$$

where the first order correction is

$$\big|\tilde{\chi}^{(1)}(\mathfrak{t})\big\rangle = -i\int_0^{\mathfrak{t}} d\mathfrak{t}'\ \lambda(\mathfrak{t}')\tilde{\mathcal{O}}(\mathfrak{t}')\,|0\rangle\ . \tag{5.62}$$

We expand the modular Hamiltonian in the same fashion

$$K(\mathfrak{t}) = K_0 + K^{(1)}(\mathfrak{t}) + \frac{1}{2}K^{(2)}(\mathfrak{t}) + \cdots\,, \tag{5.63}$$

where K_0 is the modular Hamiltonian of the vacuum state of the CFT, and hence is time-independent, and $K^{(n)}$ involves n powers of λ.

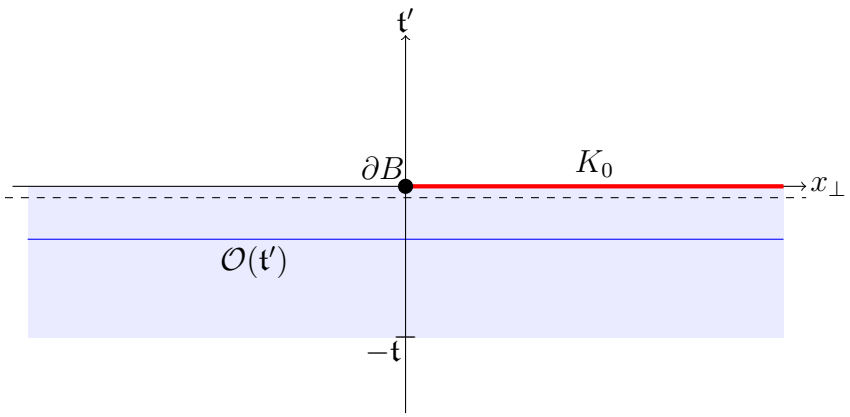

Figure 5.1: Two dimensional cross-section of our setup illustrating equation Eq. (5.67). The entangling surface, ∂B, is at $\mathfrak{t}' = 0$ and $x_\perp = 0$ (marked as the black dot). The modular Hamiltonian of the unperturbed state lives entirely in the region B at $\mathfrak{t}' = 0$, indicated by the red line. We first compute the correlation function of K_0 with the relevant operator, $\mathcal{O}$, inserted at the blue line, and then integrate over the shaded region. The dashed line at $\mathfrak{t}' = -\delta$ serves as the UV cutoff.

Combining these expansions we get the first order change in the entanglement entropy:

$$S^{(1)}(\mathfrak{t}) = \left\langle \tilde{\chi}^{(1)}(\mathfrak{t}) \right| e^{iH_0\mathfrak{t}} K_0 \left|0\right\rangle + \left\langle 0\right| K_0 e^{-iH_0\mathfrak{t}} \left|\tilde{\chi}^{(1)}(\mathfrak{t})\right\rangle + \left\langle 0\right| K^{(1)}(\mathfrak{t}) \left|0\right\rangle \,. \tag{5.64}$$

The normalization of the reduced density matrix provides a constraint on the modular Hamiltonian:

$$\mathrm{T}r_B\, e^{-K(\mathfrak{t})} = 1\,. \tag{5.65}$$

Expanding this constraint to leading order yields

$$\left\langle 0\right| K^{(1)} \left|0\right\rangle = 0\,, \tag{5.66}$$

which simplifies Eq. (5.64) to

$$S^{(1)}(\mathfrak{t}) = 2\mathrm{R}e\left[\left\langle 0\right| K_0 e^{-iH_0\mathfrak{t}} \left|\tilde{\chi}^{(1)}(\mathfrak{t})\right\rangle\right] = -2\int_{-\mathfrak{t}}^{0} d\mathfrak{t}'\lambda(\mathfrak{t}'+\mathfrak{t})\ \mathrm{R}e\left[i\left\langle 0\right| K_0 \tilde{\mathcal{O}}(\mathfrak{t}')\left|0\right\rangle\right]\,. \tag{5.67}$$

This is one of our main results. The content of this formula is summarized in Fig. (5.1).

The formula (5.67) is applicable for any spatial region B. However, the vacuum modular Hamiltonian K_0 is not known for a general region. We will therefore again restrict ourselves to the case where an entangling surface is an infinite plane so that the region B is a half-space. In that case, the modular Hamiltonian of the vacuum state is well known [136, 137, 138, 139]

$$K_0 = \ 2\pi \int d\mathbf{x}_\parallel \int_0^\infty dx_\perp\ x_\perp T_{00}(\mathfrak{t}=0, x_\perp, \mathbf{x}_\parallel)\,. \tag{5.68}$$

Here we have adopted the following notation for spatial vectors, $\mathbf{v}$. We write $\mathbf{v} = (v_\perp, \mathbf{v}_\parallel)$, where $v_\perp$ is the component of $\mathbf{v}$ in the direction orthogonal to the entangling surface and $\mathbf{v}_\parallel$ is the projection of $\mathbf{v}$ parallel to the entangling surface.

Putting this together, we see that the first-order change in the entropy is related to the commutator of the energy density and the perturbation:

$$S^{(1)}(\mathfrak{t}) = -2\pi i \int_{-\mathfrak{t}}^{0} d\mathfrak{t}' \int d\mathbf{x}_\parallel \int_0^\infty dx_\perp \; x_\perp \lambda(\mathfrak{t}'+\mathfrak{t}) \left\langle 0 \right| \Big[T_{00}(0, x_\perp, \mathbf{x}_\parallel), \tilde{\mathcal{O}}(\mathfrak{t}') \Big] \left| 0 \right\rangle \,. \tag{5.69}$$

Notice that the interaction picture operator $\tilde{\mathcal{O}}(\mathfrak{t})$ is identical to the Heisenberg operator $\mathcal{O}(\mathfrak{t})$ in the original $\lambda(\mathfrak{t}) = 0$ theory, i.e., when the total Hamiltonian is equal to H_0. In the following, $\mathcal{O}$ itself will be the integral of a local operator, so we effectively reduce the problem to a commutator of local operators (or equivalently the imaginary part of a two-point function) in the original theory.

Example: Free Scalar Field

In the static perturbation theory, the first order change in the entanglement entropy after perturbing a CFT by a relevant operator vanishes [131]. It follows from Eq. (5.69) that similar conclusion holds in the time-dependent case. To resolve this difficulty, we will start with the free scalar with non-zero mass, m, and then introduce a time-dependent perturbation to the mass, $m^2(\mathfrak{t}) = m^2 + 2\lambda(\mathfrak{t})$.[6] The action of our theory is[7]

$$I[\phi(\mathfrak{t}, \mathbf{x})] = \int d\mathfrak{t} d\mathbf{x} \, \Big(\frac{1}{2} (\partial \phi(\mathfrak{t}, \mathbf{x}))^2 - \frac{1}{2} m^2 \phi^2(\mathfrak{t}, \mathbf{x}) - \lambda(\mathfrak{t}) \phi^2(\mathfrak{t}, \mathbf{x}) \Big) \,, \tag{5.70}$$

where $\lambda(\mathfrak{t} \leq 0) = 0$. The perturbing operator is $\mathcal{O}(\mathfrak{t}') = \int d\mathbf{x}' \, \phi^2(\mathfrak{t}', \mathbf{x}')$, where the time dependence of these operators is governed by the free Hamiltonian with $\lambda = 0$. From (5.69) we see that the entropy is determined by correlation functions of T_{00} and ϕ^2. The energy-momentum tensor of the free scalar field is given by

$$T_{\mu\nu} = \partial_\mu \phi \partial_\nu \phi - \frac{1}{2} \eta_{\mu\nu} \Big((\partial\phi)^2 - m^2 \phi^2 \Big) + \xi \Big(\eta_{\mu\nu} \partial^2 - \partial_\mu \partial_\nu \Big) \phi^2 \,, \tag{5.71}$$

where the last term is a possible improvement term. The energy-momentum tensor is traceless if it is massless and $\xi = \xi_c \equiv \frac{d-2}{4(d-1)}$, in which case the scalar field is said to be conformally coupled. The other noteworthy case is the minimally coupled scalar, where $\xi = 0$. The required correlation functions are easily computed using Wick's theorem:

$$\left\langle 0 \right| T_{00}(x) \phi^2(x') \left| 0 \right\rangle = (\partial_\mathfrak{t} G)^2 + (\nabla G)^2 + m^2 G^2 - 2\xi \nabla^2 G^2 \,, \tag{5.72}$$

where

$$G(x - x') = \left\langle 0 \right| \phi(x) \phi(x') \left| 0 \right\rangle = \int \frac{d\mathbf{p}}{(2\pi)^{d-1}} \frac{1}{2E_\mathbf{p}} e^{-ip\cdot(x-x')} \tag{5.73}$$

[6] The factor of two is so our definition of λ remains consistent with the previous section.

[7] We use mostly minus signature.

is the (unordered Lorentzian) two-point function of the scalar field. The expectation value of the commutator $[T_{00}(x), \phi(x')^2]$ is simply twice the imaginary part of the correlation function, up to a factor of i. Before taking the imaginary part, we first perform the required integrations, the details of which we leave to Appendix (E). From Eq. (E.5) we find

$$\int_{-\mathfrak{t}}^{0} d\mathfrak{t}' \int d\mathbf{x}' \int d\mathbf{x}_{\parallel} \int_0^{\infty} dx_{\perp}\; x_{\perp} \lambda(\mathfrak{t}'+\mathfrak{t}) \langle 0| T_{00}(0, x_{\perp}, \mathbf{x}_{\parallel}) \phi^2(\mathfrak{t}', \mathbf{x}') |0\rangle \tag{5.74}$$

$$= \mathcal{A} \int_0^{\mathfrak{t}} d\mathfrak{t}'\, \lambda(\mathfrak{t}') \int \frac{d\mathbf{p}}{(2\pi)^{d-1}} \left(\frac{1 - p_{\perp}^2/E^2 - 4\xi}{8E^2} \right) e^{2iE(\mathfrak{t}'-\mathfrak{t})} \,. \tag{5.75}$$

Using this result in Eq. (5.69) yields

$$S^{(1)}_{\rm scalar}(\mathfrak{t}) = \frac{\Omega_{d-1}}{4(2\pi)^{d-2}}\, \mathcal{A} \int_0^{\mathfrak{t}} d\mathfrak{t}' \lambda(\mathfrak{t}') \int_0^{\infty} dp\, \left(4(\xi_c - \xi)\, \frac{p^{d-2}}{E^2} \;+\; \frac{m^2}{d-1}\, \frac{p^{d-2}}{E^4} \right) \sin\big(2E(\mathfrak{t}'-\mathfrak{t})\big)\,, \tag{5.76}$$

where $\Omega_d = \frac{2\pi^{d/2}}{\Gamma(d/2)}$.

To isolate UV divergences in the above expression, we expand the integrand around $x \equiv E/m \gg 1$

$$\begin{aligned} S^{(1)}_{\rm scalar}(\mathfrak{t}) \;&=\; \frac{\Omega_{d-1}}{4(2\pi)^{d-2}(d-1)} m^{d-3} \mathcal{A} \sum_{n=0}^{\infty} \frac{(-1)^n \Gamma\left(\frac{d-1}{2}\right)}{\Gamma\left(\frac{d-1-2n}{2}\right) \Gamma(n+1)} \int_0^{\mathfrak{t}} d\mathfrak{t}' \lambda(\mathfrak{t}') \\ &\times\; \int_1^{\infty} dx\, x^{d-6-2n} \Big(4(\xi_c - \xi)(d-1)x^2 + 1 \Big) \sin\big(2(\mathfrak{t}'-\mathfrak{t}) m\, x\big)\,. \end{aligned} \tag{5.77}$$

Next, we note that for any given d, the integral over x in the above expression results in a UV-divergent $S^{(1)}$ if and only if $d - 4 - 2n \geq 0$. There are only a finite number of such terms, and therefore we regularize them by assuming that n is sufficiently large, carry out the integral over x and treat the special values of n by analytic continuation.

The final result depends on the parity of d. For odd d there are no divergences, and $S^{(1)}$ is finite.[8] On the other hand, for even d we obtain

$$\begin{aligned} S^{(1)}_{\rm scalar}(\mathfrak{t}) \;&=\; \frac{\Omega_{d-1}}{4(2\pi)^{d-2}(d-1)} m^{d-3} \mathcal{A} \sum_{0 \leq n \leq \frac{d-4}{2}} \frac{(-1)^{\frac{d}{2}} \Gamma\left(\frac{d-1}{2}\right)}{\Gamma\left(\frac{d-1-2n}{2}\right) \Gamma(n+1)} \int_0^{\mathfrak{t}} d\mathfrak{t}' \lambda(\mathfrak{t}') \\ &\times\; \left(\frac{4(\xi_c - \xi)(d-1)\Gamma(d-2n-3)}{\big(2(\mathfrak{t}'-\mathfrak{t})m\big)^{d-2n-3}} - \frac{\Gamma(d-2n-5)}{\big(2(\mathfrak{t}'-\mathfrak{t})m\big)^{d-2n-5}} \right) + \text{finite terms}\,. \end{aligned} \tag{5.78}$$

[8] The non-universal divergences vanish for our choice of regularization scheme.

Introducing a UV cut off surface $\mathfrak{t}' = \mathfrak{t} - \delta$ to ensures that the integral over $\mathfrak{t}'$ is finite, and expanding $\lambda(\mathfrak{t}')$ in the vicinity of the cutoff yields

$$\begin{aligned} S^{(1)}_{\rm scalar}(\mathfrak{t}) &= \frac{(-1)^{\frac{d}{2}}}{(16\pi)^{\frac{d-3}{2}}\Gamma\left(\frac{d-1}{2}\right)}\mathcal{A}\left((\xi_c-\xi)\lambda^{(d-4)}(\mathfrak{t}) - \sum_{0\le n\le\frac{d-6}{2}} \frac{(4m^2)^n\Gamma\left(\frac{d-1}{2}\right)}{\Gamma\left(\frac{d-1}{2}-n\right)\Gamma(n+1)}\right. \\ &\times \left. m^2\,\lambda^{(d-2n-6)}(\mathfrak{t})\Big(\frac{2(d-2n-3)}{n+1}(\xi-\xi_c)+\frac{1}{d-1}\Big)\right)\log\delta + \text{ finite terms} \end{aligned} \tag{5.79}$$

There are two points to make about this result: (i) It gives us the expected adiabatic expansion of the time-dependence of the divergent terms in the entanglement entropy, wherein accord with local nature of the divergences only the instantaneous value of the coupling and its derivatives matter. (ii) Only even numbers of derivatives appear in the divergent terms, which is consistent with the holographic result.

As an initial check of our calculations, let us consider a static mass perturbation, i.e. $\lambda(\mathfrak{t}) = \lambda$. In this case only $n = (d-6)/2$ term in Eq. (5.79) survives, and we get

$$S^{(1)}_{\rm scalar} = (1-6\xi)\,\frac{(-1)^{\frac{d}{2}}\mathcal{A}}{3(4\pi)^{\frac{d-2}{2}}\Gamma\left(\frac{d-2}{2}\right)}\; m^{d-4}\lambda\;\log\delta + \text{ finite terms}\,. \tag{5.80}$$

For $\xi = 0$ this formula matches the well-known first-order expansion of the static result [140, 141, 142], while for $\xi \neq 0$ it agrees with [143, 144, 145] .

For the time-dependent $\lambda(\mathfrak{t})$ in $d = \{4, 6, 8\}$, the explicit form of the first order correction is

$$S^{(1)}_{\rm scalar}(\mathfrak{t})\Big|_{d=4} = (\xi_c-\xi)\frac{\mathcal{A}}{2\pi}\;\lambda(\mathfrak{t})\log\delta + \text{ finite terms}\,. \tag{5.81}$$

$$S^{(1)}_{\rm scalar}(\mathfrak{t})\Big|_{d=6} = \frac{-\mathcal{A}}{48\pi^2}\Big((\xi_c-\xi)\ddot{\lambda}(\mathfrak{t}) + \left(6(\xi_c-\xi)-\frac{1}{5}\right)m^2\lambda(\mathfrak{t})\Big)\log\delta + \text{ finite terms}\,.$$

$$\begin{aligned} S^{(1)}_{\rm scalar}(\mathfrak{t})\Big|_{d=8} &= \frac{\mathcal{A}}{1920\pi^3}\Big((\xi_c-\xi)\lambda^{(4)}(\mathfrak{t}) + \left(10(\xi_c-\xi)-\frac{1}{7}\right)m^2\ddot{\lambda}(\mathfrak{t}) \\ &\qquad +10\left(3(\xi_c-\xi)-\frac{1}{7}\right)m^4\lambda(\mathfrak{t})\Big)\log\delta + \text{ finite terms}\,. \end{aligned}$$

Setting $\xi = \xi_c$ we find that terms proportional to $m^2\lambda$ and $m^2\ddot{\lambda}$ in $d = 6$ and $d = 8$ respectively agree with their holographic counterparts.[9] Furthermore, linear terms in $\lambda(t)$ and its derivatives vanish in all dimensions which is also in full agreement with holography. Such a match between the calculations for the free field theory and strongly coupled $\mathcal{N} = 4$ SYM might seem surprising at first sight. However, as we argue in the next section, similarly to the time-independent case [119, 146], this match can be attributed to the universality of $\langle T_{\mu\nu}O\rangle$, $\langle OO\rangle$ and $\langle T_{\mu\nu}OO\rangle$ in a conformal field theory [129, 130]. We note that tuning ξ to a conformal value ξ_c was important to ensure tracelessness of the stress tensor in a CFT.

[9] To see matching recall that $m^2(\mathfrak{t}) = m^2 + 2\lambda(\mathfrak{t})$.

Spectral Representation

The scalar field theory example of the previous section suggests that the time-dependent universal terms of EE can be easily identified if we rewrite Eq. (5.69) as an integral over energy states. The main goal of this section is to perform such spectral analysis for an interacting QFT which is driven by the action with only one operator, $\mathcal{O}(x)$, of scaling dimension $\Delta < d$. The corresponding relevant coupling will be denoted by λ. We assume that λ is equal to some fixed value plus a time-dependent perturbation: $\lambda(\mathfrak{t}) = \lambda_0 + \delta\lambda(\mathfrak{t})$.

We start by noting that our main result Eq. (5.67) (or equivalently, Eq. (5.69) in the case of a planar entangling surface) can be written as follows

$$S^{(1)}(\mathfrak{t}) = -2\int_{-\mathfrak{t}}^{0} d\mathfrak{t}'\lambda(\mathfrak{t}'+\mathfrak{t})\,\mathrm{Re}\left[i\langle 0|K_{\lambda_0}\mathcal{O}(\mathfrak{t}')|0\rangle_{\lambda_0}\right] \ . \tag{5.82}$$

where $\langle ...\rangle_{\lambda_0}$ denotes the correlator in the unperturbed theory with coupling λ_0.

Recalling now that by definition K_{λ_0} is sitting at the $\mathfrak{t} = 0$ slice, we deduce that the above correlator can be easily obtained from its Euclidean counterpart by analytic continuation. One simply evaluates the Euclidean correlator $\langle K_{\lambda_0}\mathcal{O}(\mathfrak{t}'_{\rm E})\rangle_{\lambda_0}$ and then substitutes Euclidean time, $\mathfrak{t}'_{\rm E}$, with $i(\mathfrak{t}' + i\epsilon)$.

Moreover, if we implement conformal perturbation theory and expand this correlator around $\lambda_0 = 0$, we will get [129]

$$\langle 0|K_{\lambda_0}\mathcal{O}|0\rangle_{\lambda_0} = -\lambda_0\Big(\langle K_0\mathcal{O}\mathcal{O}\rangle_0 - \langle\mathcal{O}\mathcal{O}\rangle_0\Big) + O(\lambda_0^2)\,. \tag{5.83}$$

where we have used the fact that the correlator $\langle K_0\mathcal{O}\rangle_0$ vanishes for the CFT [10]. This observation implies that the result for $S^{(1)}(\mathfrak{t})$ to linear order in λ_0 will be independent of the underlying CFT.[11] This follows from the universality of conformal correlators $\langle OO\rangle$ and $\langle T_{\mu\nu}OO\rangle$ [147, 148]. Thus we conclude that all terms of $S^{(1)}(\mathfrak{t})$ which are proportional to $\lambda_0\,\delta\lambda(\mathfrak{t})$ (or $\lambda_0\,\partial_{\mathfrak{t}}^2\delta\lambda(\mathfrak{t})$ and so on) are identical for *any* perturbed CFT. In particular, this explains the perfect matching, mentioned in the previous section, between certain terms in the holographic and free field theory calculations. This can be seen in the following way: Note that the terms proportional to $\lambda_0\,\delta\lambda(\mathfrak{t})$ in $S^{(1)}(\mathfrak{t})$ complete into terms which are quadratic in $\lambda(\mathfrak{t})$ or its derivatives in the full time-dependent entropy, $S(\mathfrak{t})$. Recall from the Sec. (5.2) that the terms that are quadratic in $\lambda(\mathfrak{t})$ or its derivatives (*eg.* $\lambda^2(\mathfrak{t})$ or $\lambda(\mathfrak{t})\ddot{\lambda}(\mathfrak{t})$) in the holographic entanglement entropy only multiply the effective Newton constant, G_{d+1}, whereas $\lambda^3(\mathfrak{t})$ contributions also multiply κ and $\lambda^4(\mathfrak{t})$ also multiply ω, where κ and ω are coupling constants in Eq. (5.2). Since the effective Newton constant is determined by the boundary two-point function according to Eq. (5.4), the coefficients of terms quadratic in $\lambda(\mathfrak{t})$ or its derivatives in the holographic calculation are therefore universal. See [129, 130] where this universality was observed in a static setup.

[10] This just means that the first order change in the entanglement entropy after perturbing a CFT by a relevant operator vanishes. [131]

[11] In fact, this conclusion also holds in the presence of multiple relevant couplings in the theory.

By assumption, there is only one relevant coupling, g, in the action. Hence, it can be shown that [149, 150, 143]

$$\langle\, \mathcal{O}(\mathfrak{t}'_{\rm E}, x_\perp, \mathbf{x}_\parallel)\, K_0 \,\rangle = \frac{\Omega_d}{g\,(d-\Delta+\beta)2^{d-1}(d-1)(d+1)\Gamma(d)} \int_0^\infty d\mu\, \mu^2\, c^{(0)}(\mu)\, K_0\big(\mu\, \sqrt{\mathfrak{t}_{\rm E}^2 + x_\perp^2}\big)\ , \tag{5.84}$$

where $c^{(0)}(\mu)$ is the spectral function defined by the 2-point function of the energy-momentum trace [135], K_0 on the right-hand side is the modified Bessel function of the second kind[12], β is the anomalous dimension of g and $\Omega_d = 2\pi^{d/2}/\Gamma(d/2)$.

Like in the free scalar case we first integrate this correlator over $x_\parallel$ and $x_\perp$,

$$\int d^{d-2}x_\parallel \int dx_\perp \langle\, \mathcal{O}(x)\, K_0 \,\rangle = \frac{\pi\, \Omega_d\, \mathcal{A}}{g\,(d-\Delta+\beta)2^{d-1}(d-1)(d+1)\Gamma(d)} \int_0^\infty d\mu\ \mu\, c^{(0)}(\mu)\, e^{-|\mathfrak{t}_{\rm E}|\mu}\ . \tag{5.85}$$

Next, we analytically continue this result back to Lorentzian signature $\mathfrak{t}_{\rm E} \to i(\mathfrak{t}' + i\epsilon)$, substitute it into Eq. (5.82) and get the following spectral representation of the general formula Eq. (5.69)

$$S^{(1)}(\mathfrak{t}) = \frac{2\pi\, \Omega_d\, \mathcal{A}}{g\,(d-\Delta+\beta)2^{d-1}(d-1)(d+1)\Gamma(d)} \int_0^\infty d\mu\ \mu\, c^{(0)}(\mu)\, \Lambda(\mathfrak{t},\mu)\ , \tag{5.86}$$

where we have absorbed the time-dependence in the function $\Lambda(\mathfrak{t},\mu)$ defined as

$$\Lambda(\mathfrak{t},\mu) = \int_{-\mathfrak{t}}^0 d\mathfrak{t}' \lambda(\mathfrak{t}'+\mathfrak{t})\, \sin(\mathfrak{t}'\mu)\ . \tag{5.87}$$

The divergences of Eq. (5.86) depend on the $\mu \to \infty$ behavior of $c^{(0)}(\mu)$. Expanding $c^{(0)}(\mu)$ near $\mu = \infty$ results in a finite number of terms of the form μ^s for $s > 0$, and upon substituting these terms into Eq. (5.86) we find integrals of the form

$$\int_0^\infty d\mu \int_{-\mathfrak{t}}^0 d\mathfrak{t}'\ \mu^{s+1} \lambda(\mathfrak{t}'+\mathfrak{t})\, \sin(\mathfrak{t}'\mu)\,. \tag{5.88}$$

Note that the oscillatory nature of the integrand means that integrating over μ alone is not enough to give a divergence: integrating over μ would only produce a factor $\propto |\mathfrak{t}'|^{-s-2}$, but the subsequent integral over $\mathfrak{t}'$ could have a divergence near $\mathfrak{t}' = 0$, depending on the behavior of $\lambda(\mathfrak{t}+\mathfrak{t}')$.

[12] On the left-hand side, as in all other equations, K_0 is the unperturbed modular Hamiltonian.

To isolate the divergent terms, we begin by integrating Eq. (5.87) by parts with respect to $\mathfrak{t}'$ a total of $2N+1$ times. This results in the identity

$$\begin{aligned}\int_{-\mathfrak{t}}^{0} dt'\ \lambda(\mathfrak{t}'+\mathfrak{t})\,\sin(\mathfrak{t}'\mu) = &-\frac{\lambda(\mathfrak{t})}{\mu}+\frac{\lambda^{(2)}(\mathfrak{t})}{\mu^3}+\cdots-(-1)^N\frac{\lambda^{(2N)}(\mathfrak{t})}{\mu^{2N+1}}\\ &+\sin(\mu\mathfrak{t})\left(\frac{\lambda^{(1)}(0)}{\mu^2}-\frac{\lambda^{(3)}(0)}{\mu^4}+\cdots-(-1)^N\frac{\lambda^{(2N-1)}(0)}{\mu^{2N}}\right)\\ &+\cos(\mu\mathfrak{t})\left(\frac{\lambda(0)}{\mu}-\frac{\lambda^{(2)}(0)}{\mu^3}+\cdots+(-1)^N\frac{\lambda^{(2N)}(0)}{\mu^{2N+1}}\right)\\ &-(-1)^N\int_{-\mathfrak{t}}^{0} dt'\ \mu^{-2N-1}\lambda^{(2N+1)}(\mathfrak{t}'+\mathfrak{t})\,\sin(\mathfrak{t}'\mu)\,. \end{aligned} \tag{5.89}$$

If $2N > s+1$, then the last line produces no UV divergences upon substitution back into Eq. (5.88). The oscillatory terms in the middle two lines likewise produce no divergences in Eq. (5.88). All that remains is the first line. There we see clearly that a logarithmic divergence is produced if and only if s is an odd integer, with the coefficient of the divergence proportional to $\lambda^{(s+1)}(\mathfrak{t})$. The non-universal coefficients can also be determined this way.

Thus we learn that the quasi-adiabatic expansion holds for the divergences in the entanglement entropy in a general interacting theory to this order in perturbations, and that the coefficients are entirely determined by the large-μ behavior of the spectral function $c^{(0)}(\mu)$.

Example: Free Dirac Field

Let us implement Eq. (5.86) in the case of free massive Dirac field with a time-dependent mass deformation. In this case $\Delta = d-1$, $\beta = 0$, and the spectral function is given by [135]

$$c^{(0)}_{\rm Dirac}(\mu) = 2^{[d/2]}\,\frac{2(d+1)(d-1)}{\Omega_d^2}\,m^2\,\mu^{d-5}\left(1-\frac{4m^2}{\mu^2}\right)^{(d-1)/2}\Theta(\mu-2m)\ . \tag{5.90}$$

Or equivalently,

$$c^{(0)}_{\rm Dirac}(\mu) = 2^{[d/2]}\,\frac{2(d+1)(d-1)}{\Omega_d^2}\,m^2\,\mu^{d-5}\Theta(\mu-2m)\sum_{n=0}^{\infty}\frac{(-1)^n\Gamma\left(\frac{d+1}{2}\right)}{\Gamma\left(\frac{d+1-2n}{2}\right)\Gamma(n+1)}\left(\frac{2m}{\mu}\right)^{2n}\ . \tag{5.91}$$

This representation is useful for analyzing the UV divergences, which are built from the modes satisfying $\mu/(2m) \gg 1$.

Thus, for the free Dirac fermion we get

$$\begin{aligned} S^{(1)}_{\rm Dirac}(\mathfrak{t}) &= \frac{2^{[d/2]}\pi}{\Omega_d\Gamma(d)}\,m^{d-2}\mathcal{A}\sum_{n=0}^{\infty}\frac{(-1)^n\Gamma\left(\frac{d+1}{2}\right)}{\Gamma\left(\frac{d+1-2n}{2}\right)\Gamma(n+1)}\int_{-\mathfrak{t}}^{0} d\mathfrak{t}'\lambda(\mathfrak{t}'+\mathfrak{t})\\ &\times\ \int_1^{\infty} dx\,x^{d-4-2n}\sin\left(2m\mathfrak{t}'x\right)\ , \end{aligned} \tag{5.92}$$

where we introduced a dimensionless integration variable $x = \mu/(2m)$. From the above expression, it is obvious that only terms satisfying $d-4-2n \geq 0$ result in UV divergences, whereas for $d-4-2n < 0$ integrals over $\mathfrak{t}'$ and x are finite.

In fact, the universal divergences can be readily isolated. We assume that n is sufficiently large and carry out integral over x. Small values of n are treated by analytic continuation. Hence,

$$\begin{aligned} S^{(1)}_{\rm Dirac}(\mathfrak{t}) &= \frac{2^{[d/2]}\pi}{\Omega_d \Gamma(d)}\, m^{d-2}\mathcal{A} \sum_{0\leq n\leq \frac{d-4}{2}} \frac{(-1)^n \Gamma\left(\frac{d+1}{2}\right)\Gamma(d-3-2n)\cos\left((d-2n)\frac{\pi}{2}\right)}{\Gamma\left(\frac{d+1-2n}{2}\right)\Gamma(n+1)} \\ &\times \int_{-\mathfrak{t}}^{-\delta} d\mathfrak{t}' \frac{\lambda(\mathfrak{t}'+\mathfrak{t})}{(2m\mathfrak{t}')^{d-2n-3}} \;+\; \text{finite terms}\,. \end{aligned} \tag{5.93}$$

In particular, there are no universal divergences for odd d,[13] while for even d the above formula reads

$$S^{(1)}_{\rm Dirac}(\mathfrak{t}) = \frac{2^{\frac{6-d}{2}}\pi}{\Omega_d\Gamma(d)}\,\mathcal{A} \sum_{0\leq n\leq \frac{d-4}{2}} \frac{4^n(-1)^{\frac{d}{2}}\Gamma\left(\frac{d+1}{2}\right) m^{2n+1}}{\Gamma\left(\frac{d+1}{2}-n\right)\Gamma(n+1)}\,\lambda^{(d-2n-4)}(\mathfrak{t})\,\log\delta + \text{ finite terms}\,. \tag{5.94}$$

For a static perturbation $\lambda(\mathfrak{t}) = \lambda$, only $n = (d-4)/2$ contributes

$$S^{(1)}_{\rm Dirac} = \frac{(-1)^{\frac{d}{2}}}{3(2\pi)^{\frac{d-2}{2}}\Gamma\left(\frac{d-2}{2}\right)}\, m^{d-3}\lambda\,\mathcal{A}\log\delta + \text{ finite terms}\,. \tag{5.95}$$

This result is in full agreement with known calculations in the literature [140, 141, 142]. For the time-dependent case, we find

$$S^{(1)}_{\rm Dirac}(\mathfrak{t})\Big|_{d=4} = \frac{\mathcal{A}\,m\,\lambda(\mathfrak{t})}{6\pi}\,\log\delta + \text{ finite terms}\,, \tag{5.96}$$

$$S^{(1)}_{\rm Dirac}(\mathfrak{t})\Big|_{d=6} = -\frac{\mathcal{A}\,m}{120\pi^2}\Big(\ddot{\lambda}(\mathfrak{t}) + 10\,m^2\lambda(\mathfrak{t})\Big)\log\delta + \text{ finite terms}\,. \tag{5.97}$$

Note that if we take the holographic result in $d=4$, Eq. (5.44), and set $m(\mathfrak{t}) = m + \lambda(\mathfrak{t})$, then we find agreement with Eq. (5.96). Similarly, the double derivative term in $d=6$ in Eq. (5.51) matches with that in Eq. (5.97). The precise match between the calculations for the free field theory and strongly coupled holographic CFT has to do with the universality of certain correlators that we discussed in the previous section, see also [129, 130].

5.4 Conclusions

In this chapter, we studied the evolution of the 'area law' of the spatial entanglement when the relevant coupling of the field theory undergoes a quantum quench. Our main results,

[13] Recall that non-universal divergences vanish within our choice of regularization scheme.

Eq. (5.67) and Eq. (5.69), for the time-dependent first order correction to the area law were derived under the assumption that the relevant coupling satisfies $\delta\lambda(\mathfrak{t})/\lambda_0 \ll 1$, where λ_0 is the unperturbed value and $\delta\lambda(\mathfrak{t})$ is a time-dependent perturbation which vanishes in the past and asymptotes to a constant value in the future.

We argued that if λ_0 is the only relevant parameter in the system, then further simplification takes place and the final expression Eq. (5.86) for the time-dependent correction to the area law can be expressed in terms of the spectral function, $c^{(0)}(\mu)$, which is defined in terms of the two-point correlation function of the trace of the energy-momentum tensor in the theory.

As an application of these general formulas, we scrutinized the time dependence of the area law in a generic QFT. In particular, we illustrated that 'area law' divergences reveal a quasi-adiabatic behavior, *i.e.,* they are local and depend on the instantaneous value of the relevant coupling and finitely many derivatives. We showed that this qualitative behavior is in full agreement with the holographic prediction based on the HRT proposal [27].

We also carried out explicit calculations of the universal terms in the case of free fields perturbed by a time-dependent mass and found quantitative agreement with the HRT predictions of the coefficient of $\lambda^2(\mathfrak{t})$ in the entanglement entropy.[14] From the point of view of the holographic calculation, we observed in Sec. (5.2) that the coefficients of the terms which are quadratic in $\lambda(\mathfrak{t})$ or its derivatives (*eg.* $\lambda^2(\mathfrak{t})$ or $\lambda(\mathfrak{t})\ddot{\lambda}(\mathfrak{t})$) in the entanglement entropy only multiply the effective Newton's constant, which is fixed by the boundary two-point functions. Since CFT two-point functions have a universal form, this ensures that coefficients of these terms are independent of the exact nature of the unperturbed CFT. From the purely field-theoretic point of view, we observed in equation Eq. (5.83) that the coefficient of $\lambda_0\,\delta\lambda(\mathfrak{t})$ in $S^{(1)}(\mathfrak{t})$ is fixed by the universal CFT correlation functions $\langle T_{\mu\nu}\mathcal{O}\mathcal{O}\rangle$ and $\langle\mathcal{O}\mathcal{O}\rangle$. As the term proportional to $\lambda_0\delta\lambda(\mathfrak{t})$ in $S^{(1)}(\mathfrak{t})$ completes into the terms quadratic in $\lambda(\mathfrak{t})$ and its derivative, this explains the matching of the coefficients of these quadratic terms between free field theory and holographic calculations.

It would be interesting to extend our analysis to the next-to-leading order correction in $\delta\lambda(\mathfrak{t})/\lambda_0 \ll 1$. Such an extension might shed light on the fundamentals of the linear growth of entanglement entropy sufficiently far from the instant of quench [95, 98, 99, 100, 101, 102, 117, 116, 118], and help to uncover the underlying reason for the universality of this behaviour. To make a step in this direction, it is necessary to establish a consistent perturbative expansion for the modular Hamiltonian. In fact, this problem is interesting by itself since it has many valuable practical applications beyond the analysis of the time-dependent program studied in this work, and we plan to address it in the future.

[14] For a similar match in the static case see [129, 130].

Part III

Computational Complexity and Holography

Chapter 6

Evolution of Complexity Following a Global Quench

6.1 Introduction

The quantum complexity of a state is defined as the minimum number of gates required to prepare this state starting from some reference state [36, 37]. The complexity was introduced in the context of AdS-CFT correspondence to describe the growth of the interior of a two-sided black hole from the CFT perspective. More precisely, it was proposed that the growth of the interior of the black hole is dual to the growth of the complexity of the dual CFT state [36].

These ideas were made more precise in [39, 40], where it was conjectured that the complexity $\mathcal{C}(\mathfrak{t})$ of the boundary state at time $\mathfrak{t}$ is proportional to the value of the on-shell gravitational action $\mathcal{A}(\mathfrak{t})$ of a certain bulk region. This bulk region is the domain of dependence of a Cauchy slice anchored on the boundary at time $\mathfrak{t}$ (see Fig. (6.1) for an example). This conjecture is known as *complexity equals action* (CA) conjecture and the bulk region is called the Wheeler-DeWitt (WDW) patch. The CA conjecture asserts that

$$\mathcal{C}(\mathfrak{t}) = \frac{\mathcal{A}(\mathfrak{t})}{\pi}\,. \tag{6.1}$$

A universal bound, known as Lloyd's bound [42], conjectures that the energy in the system bounds the rate of computation by the system. Inspired by this, [39, 40] conjectured an analogous bound on the rate of the growth of the complexity. The bound states

$$\frac{d}{d\mathfrak{t}}\mathcal{C}(\mathfrak{t}) \leq \frac{2}{\pi}\,E\,, \tag{6.2}$$

where E is the average energy of the state at time $\mathfrak{t}$. The original works [39, 40] performed various calculations to test this conjecture. These works used CA conjecture, Eq. (6.1), to find the rate of complexification at late times for isolated two-sided black hole and for

two-sided black hole perturbed by shock waves [151]. Since then, the CA conjecture has been studied in detail. It was shown in [152] that the rate of complexification for two-sided black hole satisfies the bound of Eq. (6.2) at late times if the matter fields only appear outside the killing horizon. The bound is also saturated for BTZ black holes in minimally massive gravity model [153]. The complexity of entangling two CFTs was computed in [154] by calculating the difference between the complexity of a thermo-field double state and the complexity of a product state of vacua of two CFTs. Recently, the late time analysis of [39, 40] was extended in [155, 156], where the full time-dependence of the rate of complexification for a two-sided black hole was calculated. It was shown in these papers that the conjectured bound of Eq. (6.2) is violated at earlier times. Similar violations were also observed for the dual of the non-commutative gauge theories in [157]. A generalization of Eq. (6.1) for the reduced state of some subsystem of the CFT was proposed in [158]. The CA conjecture has also sparked interests to study quantum complexity for quantum field theories without making a connection to holography [159, 160, 161, 162].

Even though the CA conjecture, Eq. (6.1), and the bound of the rate of complexification, Eq. (6.2), are not consistent in general, our goal in this chapter is to check their consistency for a quenched quantum system. The study of global quenches has gained considerable attention in recent years as a tool to understand how a closed quantum system equilibrates. The idea behind quantum quenches is to excite the system out of equilibrium and let it evolve under unitary time evolution. The global quenches have been extensively studied using both field-theoretic methods and holography [95, 96, 97, 163, 98, 99, 103, 105, 100, 101, 102, 104, 164, 118, 165, 166, 167, 168, 169, 170, 171]. Previous works on this topic focus on studying the time evolution of the correlation functions, Wilson loops, and entanglement entropy of subregions. Since the complexity does not stop growing even after the system has achieved equilibrium, we do not expect to get new insights about the system's approach to equilibrium. Nevertheless, we expect quantum quenches to provide a non-trivial test of the bound in Eq. (6.2).

Our approach in this chapter is to use AdS-CFT correspondence to study the quantum quench of the CFT. This allows us to use the CA conjecture, Eq. (6.1), to calculate the complexity of the boundary state. Recall that the time evolution of the quenched CFT state and its approach to thermalization can be described by a black hole formed by a collapse in the bulk [97, 98, 103, 105, 100, 102, 104, 164, 118]. The Penrose diagram for this spacetime is shown in Fig. (6.1), where the WDW patch corresponding to boundary state at time $\mathfrak{t}$ is shown as the shaded region. We describe in detail the quench protocol and the bulk geometry in Sec. (6.2).

We carry out the main calculations of this chapter in Sec. (6.3). Here, we summarize the results of our calculation. For two-dimensional CFTs, we find the full time-dependence of the complexity of the quenched state (see Eq. (6.55)). For CFTs in higher spacetime dimensions, we derive an analytical expression for the rate of complexification as a function of time. Our expression for the rate of complexification is in terms of the position of the codimension-2 plane where the null boundary of the WDW patch intersects the infalling shell. This plane is labeled P in Fig. (6.1) and Fig. (6.2). We find that the fact that the

plane P never crosses the event horizon is equivalent to the bound of Eq. (6.2). This provides a non-trivial consistency check of the CA conjecture, Eq. (6.1), and the conjectured bound, Eq. (6.2), for a quenched quantum system. We further find, using numerical analysis, that the growth of complexity of the quenched state saturates this bound when the system has approached local equilibrium.

We end with a summary and some possible extensions of our work in Sec. (6.4).

6.2 Setup

We consider a CFT with a holographic dual in a d-dimensional flat spacetime. We start with the vacuum state of this CFT and at time $\mathfrak{t} = 0$ globally *quench* the system by suddenly injecting energy with finite density everywhere in the system. We can achieve this by turning on a global source for a small amount of time. We assume that the quench is homogeneous and isotropic to preserve the symmetries of the system. The state of the system after the quench is no longer an eigenstate of the Hamiltonian of our CFT. Hence, it evolves with time until it equilibrates.

The global quench and the approach to thermalization of the quenched state have a simpler description in the bulk side of the AdS-CFT correspondence. The quench in the CFT corresponds to introducing a planar 'shell' of matter near the boundary of the AdS spacetime. This shell then collapses to form a black hole in the bulk, which represents the equilibrium state in the boundary CFT. We follow [97, 98, 103, 105, 100, 102, 104, 164, 118] and model the global quench by a $(d+1)$-dimensional planar AdS-Vaidya metric [1],

$$ds^2 = \frac{1}{z^2}\Big(- f(v,z)\, dv^2 - 2dvdz + d\mathbf{x}_{d-1}^2 \Big)\,, \tag{6.3}$$

where

$$f(v,z) = \begin{cases} 1 & \text{for } v < 0\,, \\ 1 - \dfrac{z^d}{z_h^d} & \text{for } v > 0\,, \end{cases} \tag{6.4}$$

and $z = z_h$ is the position of the event horizon. This metric describes the AdS-Schwarzschild black hole for $v > 0$ and the vacuum AdS for $v < 0$. The Penrose diagram of this spacetime is shown in Fig. (6.1).

The parameter z_h can be interpreted as the *local equilibrium scale* after which time the system achieves local equilibrium [102]. The temperature and energy of the equilibrium state in the boundary are same as those of the black hole formed in the bulk and are given in terms of z_h as

$$T_d = \frac{d}{4\pi\, z_h}\,, \qquad\qquad E_d = \frac{d-1}{16\pi G}\,\frac{L_{d-1}}{z_h^d}\,, \tag{6.5}$$

[1] We set $\ell_{AdS} = 1$.

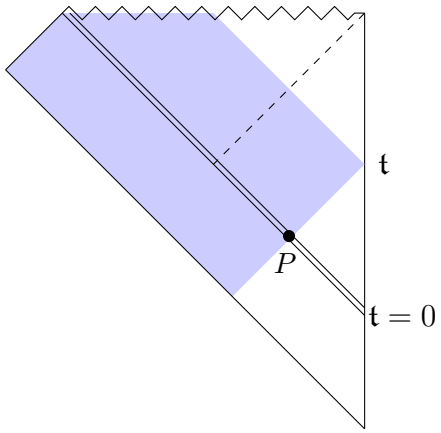

Figure 6.1: The Penrose diagram of the time-dependent geometry as a result of a collapse of a null shell (shown as a double line). The dashed line is the event horizon, and the shaded region denotes the WDW patch corresponding to boundary time $\mathfrak{t}$. The intersection of the past null boundary of the WDW patch and the collapsing null shell is denoted by a black dot and is labeled by P.

where we have defined

$$L_{d-1} \equiv \int d^{d-1}x \,, \tag{6.6}$$

as the volume of our boundary system.

Our goal is to compute the complexity of the boundary state after the global quench as a function of time. According to the CA conjecture, Eq. (6.1), this complexity of the boundary state at time $\mathfrak{t}$ is related to the action of the WDW patch corresponding to the boundary time $\mathfrak{t}$. This patch is shown as the shaded region in Fig. (6.1). Note that the on-shell action of a null dust vanishes [172, 173]. Moreover, since the stress-energy tensor only has a T_{vv} component, the trace of the Einstein's equations implies that the Ricci scalar is non-singular at $v = 0$. This allows us to use the additive property of the gravitational action [174], and split our WDW patch into two parts. One that lies entirely inside the infalling null shell ($v > 0$) and the other that lies outside the null shell ($v < 0$). That is,

$$\mathcal{A} = \mathcal{A}_{(v>0)} + \mathcal{A}_{(v<0)} \,, \tag{6.7}$$

where $\mathcal{A}_{(v>0)}$ and $\mathcal{A}_{(v<0)}$ are the gravitational actions of the shaded regions in the left and right columns of Fig. (6.2) respectively. As a result, instead of working with the time-dependent metric of Eq. (6.3), we can simply do our calculations in stationary AdS-Schwarzschild and vacuum AdS spacetimes. We carry out these calculations in the next section.

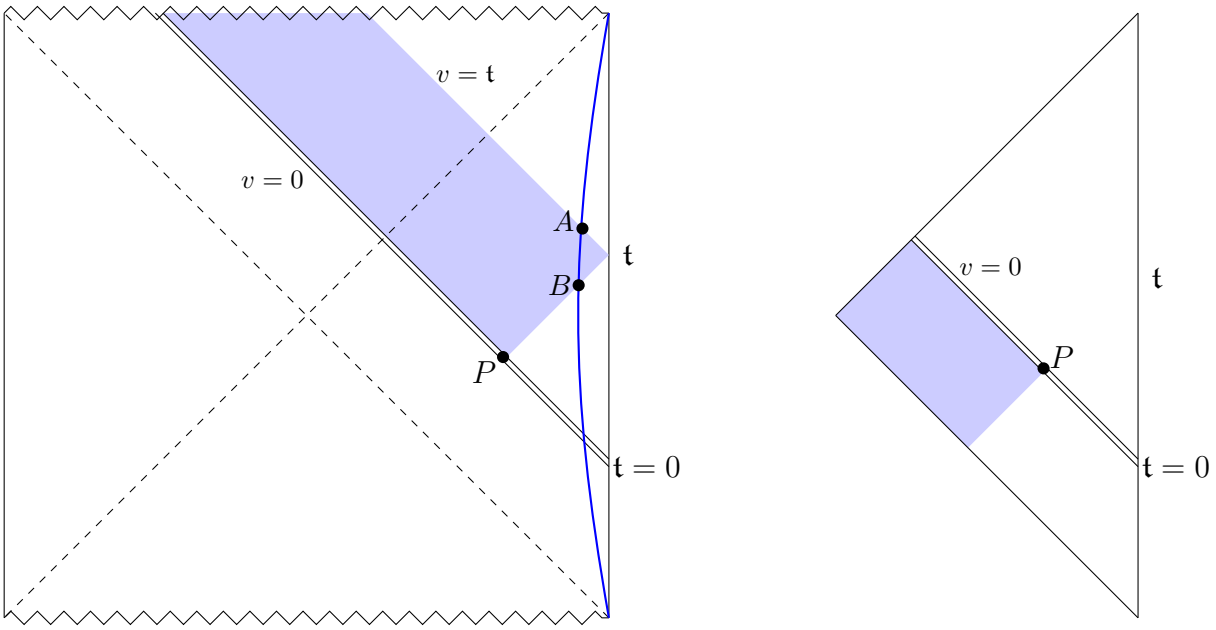

Figure 6.2: The Penrose diagrams for AdS-Schwarzschild black hole (left) and vacuum AdS (right). The shaded region on the left/right corresponds to the part of the WDW inside/outside the collapsing null shell in Fig. (6.1). We have also included a cut-off surface at $z = \delta$ (shown as a blue line) in the Penrose diagram of AdS-Schwarzschild. The intersections of the WDW patch with the cut-off surface are labeled A and B, whereas the intersection of the past null boundary of the WDW patch and the collapsing null shell is denoted by a black dot and is labeled P.

6.3 Calculations

In this section, we perform the main calculations of this chapter. In Sec. (6.3), we consider the part of the WDW patch that lies inside the infalling shell (left column of Fig. (6.2)) and we calculate its action, $\mathcal{A}_{(v>0)}$. We then calculate the action $\mathcal{A}_{(v<0)}$ of the part of the WDW patch that lies outside the infalling shell (right column of Fig. (6.2)). We combine the results of these calculations in Sec. (6.3) and show that the rate of complexification, determined using the CA conjecture, Eq. (6.1), satisfies the bound of Eq. (6.2).

Calculation of $\mathcal{A}_{(v>0)}$

The shaded region inside the collapsing shell has one spacelike, one timelike, and three null boundaries. The spacelike boundary is the singularity ($z = \infty$). The timelike boundary is the cut-off surface ($z = \delta$) that we have introduced to regulate the UV divergence in the gravitational action. Two of the null boundaries are $v = 0$ and $v = \mathfrak{t}$, while the third null

boundary is the plane joining points B and P in Fig. (6.2). Let's assume that this null boundary is described by $z_1(v;\mathfrak{t})$. The function $z_1(v;\mathfrak{t})$ then satisfies the integral equation

$$\frac{1}{2}(\mathfrak{t}-v) = \int_0^{z_1(v;\mathfrak{t})} dz\, \frac{1}{f(z)}\,, \tag{6.8}$$

where $f(z) = f(v>0,z)$ in Eq. (6.4). The coordinates of the points A, B, and P are

$$A: \quad v_A = \mathfrak{t}\,, \qquad z_A = \delta\,, \tag{6.9}$$

$$B: \quad v_B = \mathfrak{t} - 2\delta\,, \qquad z_B = \delta\,, \tag{6.10}$$

$$P: \quad v_A = 0\,, \qquad z_P(\mathfrak{t}) = z_1(0,\mathfrak{t})\,. \tag{6.11}$$

In the case of $d=2$, the Eq. (6.8) can be exactly solved and the solution is given by

$$z_1(v;\mathfrak{t}) = z_h \tanh\left(\frac{\mathfrak{t}-v}{2z_h}\right), \qquad \text{for } d=2\,. \tag{6.12}$$

However, the closed form solution of Eq. (6.8) is not available for $d \geq 3$.

We now focus our attention to compute the gravitational action $\mathcal{A}_{(v>0)}$ of the shaded region in the left column of Fig. (6.2). The bulk contribution to the gravitational action is given by the Einstein-Hilbert term. Since the Ricci scalar of the AdS-Schwarzschild black hole is constant, the bulk contribution to $\mathcal{A}_{(v>0)}$ is proportional to the volume $\mathcal{V}_{(v>0)}$ of the shaded region in the left column of Fig. (6.2). That is,

$$\mathcal{A}^{\text{bulk}}_{(v>0)} = \frac{1}{16\pi G}\Big(R - 2\Lambda\Big)\,\mathcal{V}_{(v>0)}\,, \tag{6.13}$$

where R is the Ricci scalar and Λ is the cosmological constant. The volume of the shaded region is given by

$$\begin{aligned}
\mathcal{V}_{(v>0)} &= \int d^{d-1}x \int_0^{\mathfrak{t}-2\delta} dv \int_{z_1(v;\mathfrak{t})}^{\infty} dz\, \frac{1}{z^{d+1}} \\
&\quad + \int d^{d-1}x \int_{\mathfrak{t}-2\delta}^{\mathfrak{t}} dv \int_{\delta}^{\infty} dz\, \frac{1}{z^{d+1}}\,, \\
&= \frac{L_{d-1}}{d}\,\frac{2}{\delta^{d-1}} + \frac{L_{d-1}}{d}\int_0^{\mathfrak{t}-2\delta} dv\, \frac{1}{z_1^d(v;\mathfrak{t})}\,,
\end{aligned} \tag{6.14}$$

where we have used Eq. (6.6).

In the case of $d=2$, we can use Eq. (6.12) to get

$$\mathcal{V}^{(d=2)}_{(v>0)} = \frac{2L_1}{\delta} + \frac{L_1}{2z_h^2}\,\mathfrak{t} - \frac{L_1}{z_h \tanh\left(\frac{\mathfrak{t}}{2z_h}\right)}\,. \tag{6.15}$$

Since we do not have a closed form formula of $z_1(v;\mathfrak{t})$ for $d \geq 3$, we cannot perform the integrals in Eq. (6.14). Regardless, we can still calculate the contribution of the Einstein-Hilbert term to the rate of complexification. To do this, we take the time derivative of the volume in Eq. (6.14). We get

$$\frac{d}{d\mathfrak{t}}\mathcal{V}_{(v>0)} = \frac{L_{d-1}}{d}\frac{1}{z_P^d(\mathfrak{t})}\,. \tag{6.16}$$

In deriving this result, we have used the following property of the derivatives of $z_1(v;\mathfrak{t})$

$$\frac{d}{d\mathfrak{t}}z_1(v;\mathfrak{t}) = -\frac{d}{dv}z_1(v;\mathfrak{t})\,. \tag{6.17}$$

Our approach in this and the next subsection is to write all the contributions to the gravitational action in terms of $z_P(\mathfrak{t})$. We then analyze these results in Sec. (6.3) where we numerically solve for $z_P(\mathfrak{t})$ for $d \geq 3$.

Recall that the cosmological constant is equal to $\Lambda = -\frac{1}{2}d(d-1)$. The vacuum Einstein's equations then imply $R = -d(d+1)$. We combine Eq. (6.13) and Eq. (6.15) to get

$$\mathcal{A}^{\text{bulk}}_{(v>0)} = \frac{L_1}{8\pi G}\left(\frac{2}{z_h\tanh\left(\frac{\mathfrak{t}}{2z_h}\right)} - \frac{1}{z_h^2}\,\mathfrak{t} - \frac{4}{\delta}\right), \qquad \text{for } d=2\,, \tag{6.18}$$

and we combine Eq. (6.13) and Eq. (6.16) to get

$$\frac{d}{d\mathfrak{t}}\mathcal{A}^{\text{bulk}}_{(v>0)} = -\frac{L_{d-1}}{16\pi G}\frac{2}{z_P^d(\mathfrak{t})}\,. \tag{6.19}$$

We now consider the boundary contributions to $\mathcal{A}_{(v>0)}$. There are two contributions to the action from a null boundary. The first contribution is proportional to the surface integral of the 'surface gravity' κ of the null generator k^a of the null surface (see for *e.g.* [174]). The second contribution is a counterterm which ensures that the action is independent of a choice of the parameterization of the null surface [174, 175]. The 'surface gravity' κ of the null generator k^a is defined as

$$k^a\nabla_a k^b = \kappa\, k^b\,. \tag{6.20}$$

Let's denote the generator of the null boundaries $v = 0$ and $v = \mathfrak{t}$ by k^a_{in} and that of the null boundary between points B and P in Fig. (6.2) by k^a_{out}. We choose the following normalization of the null generators

$$k^a_{\text{in}} = -z^2\left(\partial_z\right)^a, \tag{6.21}$$

$$k^a_{\text{out}} = \frac{2z^2}{f(z)}\left(\partial_v\right)^a - z^2\left(\partial_z\right)^a. \tag{6.22}$$

The advantage of this particular normalization of the null generators is that the surface gravity of both of these null generators vanishes. Therefore, we only have to focus on the

counterterms. The contributions from the counterterms is [174]

$$\mathcal{A}^{\rm null}_{(v>0)} = \frac{1}{8\pi G}\int d^{d-1}x\int_{\delta}^{\infty}\frac{dz}{z^2}\sqrt{q}\,\theta_{\rm in}\log\theta_{\rm in} - \frac{1}{8\pi G}\int d^{d-1}x\int_{z_P(\mathfrak{t})}^{\infty}\frac{dz}{z^2}\sqrt{q}\,\theta_{\rm in}\log\theta_{\rm in} + \frac{1}{8\pi G}\int d^{d-1}x\int_{\delta}^{z_P(\mathfrak{t})}\frac{dz}{z^2}\sqrt{q}\,\theta_{\rm out}\log\theta_{\rm out}\,, \tag{6.23}$$

where $\sqrt{q} = z^{1-d}$ is the determinant of the induced metric of the codimension-2 cross-sections of the null hypersurface, and $\theta_{\rm in}$ ($\theta_{\rm out}$) is the null expansion of $k^a_{\rm in}$ ($k^a_{\rm out}$). Using Eqs. (6.21)-(6.22), we find

$$\theta_{\rm in} = \theta_{\rm out} = (d-1)\,z\,. \tag{6.24}$$

With this result, Eq. (6.23) becomes

$$\mathcal{A}^{\rm null}_{(v>0)} = \frac{L_{d-1}}{4\pi G}\frac{1}{d-1}\frac{1}{\delta^{d-1}}\Big(1+(d-1)\log\big[(d-1)\delta\big]\Big) - \frac{L_{d-1}}{4\pi G}\frac{1}{d-1}\frac{1}{z_P^{d-1}(\mathfrak{t})}\Big(1+(d-1)\log\big[(d-1)z_P(\mathfrak{t})\big]\Big)\,. \tag{6.25}$$

Next, we consider the cut-off boundary ($z=\delta$) that we have introduced to regulate the UV divergences. The contribution of this timelike boundary to the gravitational action is given by the Gibbons-Hawking-York (GHY) term. The normal vector to the cut-off boundary is

$$s^a = \delta\big(\partial_v\big)^a - \delta\big(\partial_z\big)^a\,. \tag{6.26}$$

The GHY term for the cut-off surface is

$$\mathcal{A}^{(z=\delta)}_{(v>0)} = \frac{1}{8\pi G}\int d^{d-1}x\int_{\mathfrak{t}-2\delta}^{\mathfrak{t}} dv\,\sqrt{|\gamma|}\,\gamma^{ab}\nabla_a s_b\,, \tag{6.27}$$

where $\gamma^{ab}\equiv g^{ab}-s^a s^b$ is the inverse induced metric on the cut-off surface. Solving this surface integral yields

$$\mathcal{A}^{(z=\delta)}_{(v>0)} = \frac{L_{d-1}}{8\pi G}\frac{2d}{\delta^{d-1}}\,. \tag{6.28}$$

The last boundary that we have to consider is the spacelike spacetime singularity ($z=\infty$). The contribution of this boundary is also given by GHY term. To compute this term, we first consider the spacelike surface at $z=z_\infty \gg z_h$ and then take the limit $z_\infty\to\infty$. The future-directed vector normal to the $z=z_\infty$ surface is

$$n^a = -\frac{z_h^{d/2}}{z_\infty^{d/2-1}}\big(\partial_v\big)^a - \frac{z_\infty^{d/2+1}}{z_h^{d/2}}\big(\partial_z\big)^a\,. \tag{6.29}$$

The GHY term is then given by

$$\mathcal{A}^{(z=\infty)}_{(v>0)} = \lim_{z_\infty\to\infty} -\frac{1}{8\pi G}\int d^{d-1}x\int_0^{\mathfrak{t}} dv\,\sqrt{|\widetilde{\gamma}|}\,\widetilde{\gamma}^{ab}\nabla_a n_b\,, \tag{6.30}$$

where $\widetilde{\gamma}^{ab} \equiv g^{ab} + n^a n^b$ is the inverse induced metric on the $z = z_\infty$ surface. The negative sign in Eq. (6.30) is due to the fact that the shaded region is to the past of the $z = z_\infty$ boundary. (See [174] for a summary of the rules to assign the sign to each of the terms in the gravitational action.) Solving the integrals in Eq. (6.30) yields

$$\mathcal{A}^{(z=\infty)}_{(v>0)} = \frac{L_{d-1}}{16\pi G}\,\frac{d}{z_h^d}\,\mathfrak{t}\,. \tag{6.31}$$

Lastly, we consider the contributions of the corner terms to $\mathcal{A}_{(v>0)}$. The corners where null boundaries $v = 0$ and $v = \mathfrak{t}$ intersect the singularity do not contribute because the volume density of the codimension-2 corners falls as z^{1-d}. The total contribution to $\mathcal{A}_{(v>0)}$ from the corners is [174]

$$\mathcal{A}^{\text{corner}}_{(v>0)} = -\frac{1}{8\pi G}\int_A d^{d-1}x\,\sqrt{q}\,a_A - \frac{1}{8\pi G}\int_B d^{d-1}x\,\sqrt{q}\,a_B + \frac{1}{8\pi G}\int_P d^{d-1}x\,\sqrt{q}\,a_P\,, \tag{6.32}$$

where $\sqrt{q} = z^{1-d}$ is the determinant of the induced metric of the codimension-2 corners, and

$$a_A = \log|k_{\text{in}}\cdot s|\,, \tag{6.33}$$

$$a_B = \log|k_{\text{out}}\cdot s|\,, \tag{6.34}$$

$$a_P = \log\left|\frac{k_{\text{in}}\cdot k_{\text{out}}}{2}\right|\,. \tag{6.35}$$

Using Eqs. (6.9)-(6.11) and Eq. (6.21)-(6.26), we get

$$\mathcal{A}^{\text{corner}}_{(v>0)} = -\frac{L_{d-1}}{8\pi G}\,\frac{2}{\delta^{d-1}}\,\log\delta + \frac{L_{d-1}}{8\pi G}\,\frac{1}{z_P^{d-1}(\mathfrak{t})}\left(2\log z_P(\mathfrak{t}) - \log f\big(z_P(\mathfrak{t})\big)\right). \tag{6.36}$$

The total gravitational action of the shaded region on the left side of Fig. (6.2) is given by the sum of the contributions from the bulk, surfaces, and corners. For $d = 2$, we use the expression of $z_P(\mathfrak{t})$ from Eq. (6.12) to get

$$\mathcal{A}^{(d=2)}_{(v>0)} = \frac{L_1}{4\pi G}\,\frac{1}{\delta} + 4\,E_2\,z_h\,\coth\left(\frac{\mathfrak{t}}{2z_h}\right)\log\left(\cosh\left(\frac{\mathfrak{t}}{2z_h}\right)\right), \tag{6.37}$$

where we have used Eq. (6.5). We also compute the time derivative of $\mathcal{A}_{(v>0)}$ for general dimensions. Using the differential equation for $z_P(\mathfrak{t})$

$$\frac{d}{d\mathfrak{t}}z_P(\mathfrak{t}) = \frac{1}{2}\,f\big(z_P(\mathfrak{t})\big)\,, \tag{6.38}$$

we get

$$\frac{d}{d\mathfrak{t}}\mathcal{A}_{(v>0)} = 2\,E_d\left\{1 + \left(\frac{z_h^d}{z_P^d(\mathfrak{t})} - 1\right)\left(\log\Big(d-1\Big) + \frac{1}{2}\log\Big(f\big(z_P(\mathfrak{t})\big)\Big)\right)\right\}, \tag{6.39}$$

where we have once again used Eq. (6.5).

This finishes our discussion of the gravitational action of the shaded region on the left column of Fig. (6.2). Next, we repeat the analysis of this subsection for the shaded region on the right column of Fig. (6.2).

Calculation of $\mathcal{A}_{(v<0)}$

We now consider the shaded region on the right side of Fig. (6.2). This shaded region has three boundaries. One of these is the Poincaré horizon ($z = \infty$), the other is the infalling null shell ($v = 0$), and the third is the null boundary that connects plane P with the past Poincaré horizon. This third boundary is described by the equation

$$z = z_P(\mathfrak{t}) - \frac{v}{2}\,. \tag{6.40}$$

The bulk contribution to $\mathcal{A}_{(v<0)}$ is given by the Einstein-Hilbert term. This term is proportional to the volume of the shaded region on the right side of Fig. (6.2). That is,

$$\mathcal{A}^{\text{bulk}}_{(v<0)} = \frac{1}{16\pi G}\Big(R - 2\Lambda\Big)\,\mathcal{V}_{(v<0)}\,, \tag{6.41}$$

where the volume is

$$\begin{aligned}\mathcal{V}_{(v<0)} &= \int d^{d-1}x \int_{-\infty}^{0} dv \int_{z_P(\mathfrak{t})-\frac{v}{2}}^{\infty} dz\,\frac{1}{z^{d+1}}\,,\\ &= \frac{L_{d-1}}{d(d-1)}\,\frac{2}{z_P^{d-1}(\mathfrak{t})}\,.\end{aligned} \tag{6.42}$$

Using $R - 2\Lambda = -2d$, we get

$$\mathcal{A}^{\text{bulk}}_{(v<0)} = -\frac{L_{d-1}}{4\pi G(d-1)}\,\frac{1}{z_P^{d-1}(\mathfrak{t})}\,. \tag{6.43}$$

We now consider the boundary contributions to $\mathcal{A}_{(v<0)}$. Note that the Poincaré horizon ($z = \infty$) does not contribute to $\mathcal{A}_{(v<0)}$ [154]. For the null boundary at $v = 0$, we use the following normalization of the null generator

$$\bar{k}^a_{\text{in}} = -z^2\left(\partial_z\right)^a\,, \tag{6.44}$$

and for the other null boundary, we use the following normalization of the null generator

$$\bar{k}^a_{\text{out}} = 2\,z^2\left(\partial_v\right)^a - z^2\left(\partial_z\right)^a\,. \tag{6.45}$$

As was the case in Sec. (6.3), the surface gravity of these null generators vanish. Therefore, we only have to focus on the null counter terms [174, 175]. The contributions from the counterterms is [174]

$$\mathcal{A}^{\text{null}}_{(v<0)} = \frac{1}{8\pi G}\int d^{d-1}x \int_{z_P(\mathfrak{t})}^{\infty}\frac{dz}{z^2}\,\sqrt{q}\,\bar{\theta}_{\text{in}}\log\bar{\theta}_{\text{in}} + \frac{1}{8\pi G}\int d^{d-1}x \int_{z_P(\mathfrak{t})}^{\infty}\frac{dz}{z^2}\,\sqrt{q}\,\bar{\theta}_{\text{out}}\log\bar{\theta}_{\text{out}}\,, \tag{6.46}$$

where $\bar{\theta}_{\rm in}$ and $\bar{\theta}_{\rm out}$ are the null expansion of $\bar{k}^a_{\rm in}$ and $\bar{k}^a_{\rm out}$ respectively. Using $\bar{\theta}_{\rm in} = \bar{\theta}_{\rm out} = (d-1)z$, we simplify Eq. (6.46) as

$$\mathcal{A}^{\rm null}_{(v<0)} = \frac{L_{d-1}}{4\pi G}\,\frac{1}{d-1}\frac{1}{z_P^{d-1}(\mathfrak{t})}\left(1+(d-1)\log\left[(d-1)z_P(\mathfrak{t})\right]\right). \tag{6.47}$$

Now let's consider the corner terms. The corners at the intersection of the Poincaré horizon with the null boundaries do not contribute because the volume density of the codimension-2 surfaces falls off as z^{1-d}. Therefore, the only corner contribution comes from the corner P and is given by [174]

$$\mathcal{A}^{\rm corner}_{(v<0)} = -\frac{1}{8\pi G}\int_P d^{d-1}x\,\sqrt{q}\,\bar{a}_P\,, \tag{6.48}$$

where $\sqrt{q}$ is the volume density of the codimension-2 corner, and

$$\bar{a}_P = \log\left|\frac{\bar{k}_{\rm in}\cdot\bar{k}_{\rm out}}{2}\right|. \tag{6.49}$$

With this, we get

$$\mathcal{A}^{\rm corner}_{(v<0)} = -\frac{L_{d-1}}{4\pi G}\,\frac{1}{z_P^{d-1}(\mathfrak{t})}\,\log\left(z_P(\mathfrak{t})\right). \tag{6.50}$$

After calculating all the contributions to the gravitational action of the shaded region on the right side of Fig. (6.2), we add them to get

$$\mathcal{A}_{(v<0)} = \frac{L_{d-1}}{4\pi G}\,\log\Big(d-1\Big)\,\frac{1}{z_P^{d-1}(\mathfrak{t})}\,. \tag{6.51}$$

In the case of $d=2$, the above result vanishes. That is

$$\mathcal{A}^{\rm (d=2)}_{(v<0)} = 0\,. \tag{6.52}$$

To find the contribution to the rate of complexification from the shaded region on the right side of Fig. (6.2), we take the time derivative of Eq. (6.51)

$$\frac{d}{d\mathfrak{t}}\mathcal{A}_{(v<0)} = -2\,E_d\,\left(\frac{z_h^d}{z_P^d(\mathfrak{t})}-1\right)\,\log\Big(d-1\Big)\,, \tag{6.53}$$

where we have once again used Eq. (6.38).

In the next subsection, we combine the results of this and the previous subsections to find the total action of the WDW patch and hence, the complexity of the boundary state.

Calculation of the Total Action

The total gravitational action of the WDW patch is given by Eq. (6.7). In the case of $d = 2$, we add Eq. (6.37) and Eq. (6.52) to get

$$\mathcal{A}^{(\mathrm{d=2})} = \frac{L_1}{4\pi G}\frac{1}{\delta} + 4\,E_2\;z_h\,\coth\left(\frac{\mathfrak{t}}{2z_h}\right)\log\left(\cosh\left(\frac{\mathfrak{t}}{2z_h}\right)\right). \tag{6.54}$$

The CA conjecture, Eq. (6.1), then implies that the complexity of the perturbed state at time $\mathfrak{t}$ is given by

$$\mathcal{C}^{(\mathrm{d=2})}(\mathfrak{t}) = \frac{L_1}{4\pi^2 G}\frac{1}{\delta} + \frac{4}{\pi}\,E_2\;z_h\,\coth\left(\frac{\mathfrak{t}}{2z_h}\right)\log\left(\cosh\left(\frac{\mathfrak{t}}{2z_h}\right)\right). \tag{6.55}$$

The analytical expression for the time-dependence of the complexity in $d = 2$ is one of the main results of this chapter. For $d \geq 3$, we do not have the analytical result for the time-dependence of the complexity. The reason for this is that we do not have the closed form solution of Eq. (6.8). In spite of that, we can still study the time evolution of the complexity in $d \geq 3$ by studying its rate of growth. We add Eq. (6.39) and Eq. (6.53) and use CA conjecture to get

$$\frac{d}{d\mathfrak{t}}\mathcal{C}(\mathfrak{t}) = \frac{2}{\pi}\,E_d\left\{1 + \frac{1}{2}\left(\frac{z_h^d}{z_P^d(\mathfrak{t})} - 1\right)\log\Big(f\big(z_P(\mathfrak{t})\big)\Big)\right\}, \tag{6.56}$$

We use this expression to study the bound on the rate of complexification. As is evident from Fig. (6.1) and from the left side of Fig. (6.2), the plane P never crosses the event horizon (*i.e.* $z_P(\mathfrak{t}) \leq z_h$). This means that the second term inside the parenthesis on the right side of Eq. (6.56) can never be positive. This gives us the following bound

$$\frac{d}{d\mathfrak{t}}\mathcal{C}(\mathfrak{t}) \leq \frac{2}{\pi}\,E_d\,, \tag{6.57}$$

which is in agreement with the bound of Eq. (6.2). Furthermore, note that the plane P approaches the event horizon (*i.e.* $z_p(\mathfrak{t}) \to z_h$) at late times ($\mathfrak{t} \gg z_h$). This means that the above inequality eventually saturates. This analytical consistency check of the CA conjecture and the conjectured bound on the rate of complexification is another main result of this chapter.

Another interesting question that one may ask is how long does it take for the rate of growth of complexity to approach its maximum possible value. To answer this question, we need to find how long does it take for the plane P to reach the event horizon. Recall that the function $z_P(\mathfrak{t})$ satisfies the differential equation, Eq. (6.38), with the boundary condition $z_P(\mathfrak{t} = 0) = 0$ (see Eq. (6.8)). We numerically solve this differential equation for $d = \{3, 4, 5, 6\}$. The plots of $z_P(\mathfrak{t})$ as a function of time are shown in Fig. (6.3). It is clear

from these plots that the plane P approaches the event horizon when $\mathfrak{t} \sim z_h$. This time scale is same as the inverse temperature of the CFT state (see Eq. (6.5)) or the local equilibrium scale. This result, together with Eq. (6.56), implies that the rate of complexification attains its maximum value soon after the system has achieved local equilibrium.

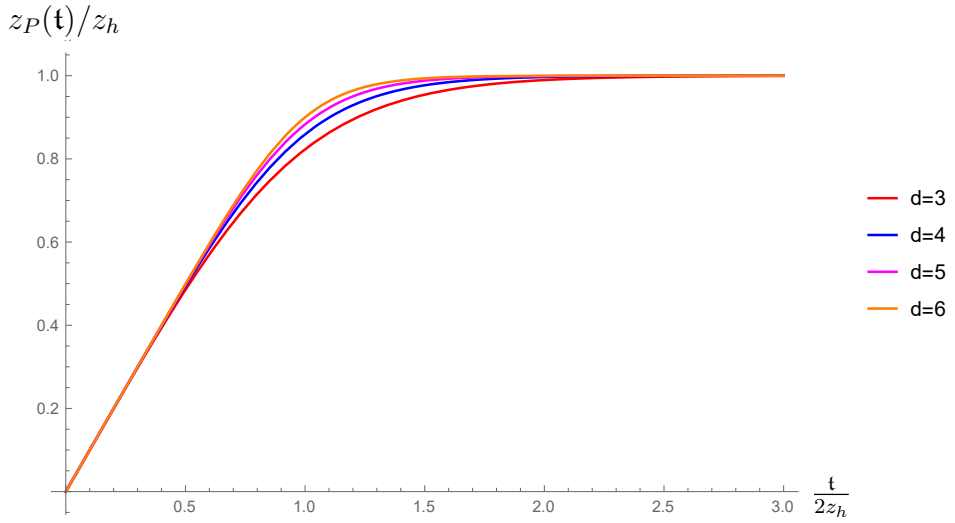

Figure 6.3: The plots showing the position of the plane P as a function of time for $d = \{3, 4, 5, 6\}$. It is evident from these plots that $z_P(\mathfrak{t}) \to z_h$ when $\mathfrak{t} \sim z_h$.

6.4 Discussion

In this chapter, we have excited the vacuum state of a d-dimensional CFT by a global quench and studied the growth of the complexity of the resultant time-dependent state. We quenched the system by injecting homogeneous and isotropic energy globally in the system. In the gravity side of the AdS-CFT correspondence, this quench is described as an infalling null shell which collapses to form a black hole [97, 98, 103, 105, 100, 102, 104, 164, 118]. We used the CA conjecture, Eq. (6.1), to study the growth of the complexity of the boundary state.

For $d = 2$, we derived an expression of the time-dependence of the complexity. This expression is given in Eq. (6.55). For $d \geq 2$, we derived the rate of growth of complexity in terms of single time-dependent function, $z_P(\mathfrak{t})$. This is given in Eq. (6.56). The function $z_P(\mathfrak{t})$ is the position of the codimension-2 plane where the WDW patch corresponding to boundary state at time $\mathfrak{t}$ intersects the infalling null shell. One can deduce from Fig. (6.1) and Fig. (6.2) that the plane P never crosses the event horizon. That is, $z_P(\mathfrak{t}) \leq z_h$. With this inequality, our general expression for the rate of complexification reduces to the conjectured

bound of Eq. (6.2). Furthermore, we found the time-dependence of $z_P(\mathfrak{t})$ by numerically solving Eq. (6.38). The plots for $z_P(\mathfrak{t})$ for $d = \{3, 4, 5, 6\}$ are shown in Fig. (6.3). This numerical analysis allowed us to deduce that the quenched state saturates the bound on the rate of complexification soon after the system has achieved local equilibrium.

There are few possible directions in which the present work can be extended. One possible direction is explored in the next chapter. Here, we now propose another possible extension of our work: The complexity equals action was generalized in [158] for reduced states of some subsystem of the CFT. This proposal relates the complexity of the reduced state of some boundary subregion A with the on-shell action of the bulk region defined as the intersection of the entanglement wedge of A and the WDW patch of a boundary slice that includes region A. One may consider repeating the analysis of this chapter for the time-dependence of the complexity of some fixed boundary region. However, it is known [163, 101, 102] that there can be discontinuities in the position of the HRT surface [27], and consequently in the entanglement wedge, when the time $\mathfrak{t}$ is of the order of the size of the boundary subregion. This is due to the presence of more than one boundary anchored extremal surfaces. This jump in the HRT surface of the subregion can result in the discontinuity of the complexity of the reduced state of the subregion. It will be interesting to investigate if this really happens, and if it does, then how it is compatible with the bound on the rate of complexification.

Chapter 7

Divergences in the Rate of Complexification

7.1 Introduction

The complexity of a quantum state is defined as the minimum number of gates that map a reference state to that quantum state [36, 37]. It was conjectured in [36] that the growth of the complexity of a boundary CFT state as a function of time is holographically dual to the *stretching* of the interior of a black hole in the bulk. To make this connection more concrete, various holographic definitions for the complexity have been put forward. One such proposal, known as the *complexity equals action* (CA) conjecture, relates the holographic complexity with the on-shell gravitational action of a certain bulk region [39, 40]. This region, called the Wheeler-DeWitt (WDW) patch, is defined as the domain of dependence of a bulk Cauchy surface. More precisely, this conjecture states that the complexity of a CFT state at time $\mathfrak{t}$ is related to the on-shell action of the WDW patch corresponding to time $\mathfrak{t}$, $\mathcal{A}(\mathfrak{t})$, as [39, 40]

$$\mathcal{C}_A(\mathfrak{t}) = \frac{\mathcal{A}(\mathfrak{t})}{\pi}\,. \tag{7.1}$$

Another such proposal relates the complexity with the volume of an extremal Cauchy surface [38, 176]. In particular, it is conjectured that the complexity of a CFT state at time $\mathfrak{t}$ is related to the volume of an extremal Cauchy surface anchored on the boundary at time $\mathfrak{t}$, $V_{\text{ext}}(\mathfrak{t})$, according to [38]

$$\mathcal{C}_V(\mathfrak{t}) \equiv \frac{V_{\text{ext}}(\mathfrak{t})}{G\ell_{\text{AdS}}}\,. \tag{7.2}$$

This proposal is called the *complexity equals volume* (CV) conjecture.

The earliest checks [39, 40] for these conjectures were the observations that the rate of growth of these holographic complexities at late times is consistent with a universal bound by Lloyd. The Lloyd bound conjectures that the rate of complexification is bounded from

above by the energy of the system [42]. That is,

$$\frac{d}{d\mathfrak{t}}\mathcal{C}(\mathfrak{t}) \leq \frac{2}{\pi}E\,, \tag{7.3}$$

where E is the instantaneous average energy of the system. The consistency of the holographic conjectures for complexity, Eqs. (7.1)-(7.2), with the Lloyd conjecture, Eq. (7.3), has been verified in various contexts, *e.g.*, see [152, 153, 177]. However, some cases have been identified where the CA conjecture and the Lloyd bound are not compatible with each other [155, 156, 157]. Moreover, it has been argued that the holographic gates for which the CA conjecture is true do not satisfy the assumptions of the Lloyd bound [178]. In particular, these holographic gates are infinitesimal unitary transformations whereas the Lloyd bound is applicable for quantum gates that map a state into an orthogonal state [178]. Therefore, there is no reason to expect that the holographic complexity conjectures satisfy the Lloyd bound.

In this chapter, our goal is to present another example where the growth of the complexity computed using either the CA or the CV conjecture does not respect the Lloyd bound. More precisely, we consider starting from the vacuum state of a $(3+1)$-dimensional CFT and perturb the Hamiltonian at $\mathfrak{t}=0$ by a relevant operator with a time-dependent coupling. The Hamiltonian is given by

$$H(\mathfrak{t}) = H_{\rm CFT} + \lambda(\mathfrak{t})\,\mathcal{O}\,, \tag{7.4}$$

where $\lambda(\mathfrak{t}\leq 0)=0$. For simplicity, we only consider the case where the conformal dimension of the relevant operator is $\Delta=3$. The subsequent state evolves according to the perturbed Hamiltonian. We claim that the complexity of the evolved state has time-dependent UV divergences. As a result, the rate of complexification is UV divergent. The instantaneous energy, on the other hand, is UV finite. Therefore, it does not even make sense to compare the rate of complexification with the instantaneous energy of the state as required by the Lloyd bound. For this reason, we consider this example to be a more violent violation of the Lloyd bound than those discussed in [155, 156, 157].

This time-dependent perturbation of a CFT is described using the AdS-CFT correspondence by the introduction of a (tachyonic) scalar field in the bulk [133, 134, 179]. The conformal dimension Δ of the relevant operator fixes the mass whereas the coupling 'constant' $\lambda(\mathfrak{t})$ fixes the boundary condition for this scalar field. The scalar field back-reacts on the bulk spacetime and changes the bulk geometry. Since the boundary condition for the scalar field is time-dependent, the bulk geometry is also time-dependent. Consequently, the on-shell action of the WDW patch and the volume of a Cauchy slice evolve as a function of time.

The bulk geometry is determined by solving the Einstein-Klein-Gordon equations in the bulk. Finding the full solution of these equations is not an easy task. Luckily, the UV divergences in the on-shell action of the WDW patch and in the volume of a Cauchy slice only depend on the asymptotic geometry near the boundary [158, 175]. This means that it is sufficient to solve the bulk equations perturbatively in the radial coordinate. This method

was also used in [119] to investigate the UV divergences in the entanglement entropy. We perform this perturbative analysis in Sec. (7.2).

We calculate the divergences in the rate of complexification in Sec. (7.3) and in Sec. (7.4). In Sec. (7.3), we find the divergences in the time-derivative of the action of the WDW patch. This allows us to use the CA conjecture to find the divergences in the rate of complexification. In Sec. (7.4), we find the Cauchy slice with maximum volume anchored on the boundary at time $\mathfrak{t}$ and extract the divergences from its volume. Combining this result with the CV conjecture yields the divergences in the rate of complexification. We find that the structure of the divergences in the complexity is the same as that identified in [158, 175] but the coefficients of these divergences depend on the instantaneous value of the coupling 'constant', $\lambda(\mathfrak{t})$.

The instantaneous energy of the boundary state is the expectation value of the Hamiltonian in Eq. (7.4). Like any other correlation function, the energy is a UV finite quantity once the renormalization procedure is performed. The response of the one-point function of the boundary stress-tensor to the time-dependent perturbation is studied using the AdS-CFT correspondence in [180, 181]. This requires variation of the on-shell renormalized action of the bulk theory with respect to the metric of the boundary. For our purposes in this chapter, the details of the time-dependence of the energy are not significant. All we need to know for the violation of the Lloyd bound is the fact that the energy is a UV finite quantity.

7.2 Holographic Setup

In this chapter, we consider starting with a CFT (with a holographic dual) and deforming it by a relevant operator with a time-dependent coupling. The Hamiltonian of the perturbed theory is given in Eq. (7.4). The time-dependent perturbation of a CFT is studied extensively using the AdS-CFT correspondence in [180, 181, 182]. According to the AdS-CFT correspondence, a relevant operator on the boundary is dual to a (tachyonic) scalar field in the bulk [133, 134, 179]. This means that perturbing the boundary CFT by a relevant operator can be described by a scalar field in the bulk. The mass of this scalar field is fixed by the conformal dimension Δ of the relevant operator according to[1] [133, 134, 179]

$$m^2 = \Delta\,(\Delta - 4)\ . \tag{7.5}$$

For simplicity, we only focus on the relevant operator with conformal dimension $\Delta = 3$ in this chapter. In this case, we have $m^2 = -3$.

This scalar field couples with the metric in the bulk, and the bulk theory is governed by

[1] We set $\ell_{\rm AdS} = 1$.

the action [119, 180, 181, 182]

$$\mathcal{A}[\Phi, g] = \frac{1}{16\pi G}\int_{\mathcal{M}} d^5x\,\sqrt{-g}\Big(R + 12 - \frac{1}{2}(\partial\Phi)^2 - V(\Phi)\Big) + \frac{1}{8\pi G}\int_{\partial\mathcal{M}} d^4x\,\sqrt{-\gamma}\,K\,, \tag{7.6}$$

where

$$V(\Phi) = -\frac{3}{2}\Phi^2 + \sum_n \frac{1}{n!}\kappa_n\Phi^n\,. \tag{7.7}$$

The *Newton's constant* that appears in the overall factor of the action in Eq. (7.6) can be fixed by demanding that the boundary two-point function of $\mathcal{O}$ matches the holographic two-point function. That is, we can read off G from [133, 134, 179]

$$\langle\mathcal{O}(x)\mathcal{O}(y)\rangle = \frac{1}{2\pi^3 G}\,\frac{1}{|x-y|^6}\,. \tag{7.8}$$

Similarly, the coupling constants κ_n in Eq. (7.7) can be determined by comparing the boundary n-point functions with the holographic n-point functions. The term in the second line of Eq. (7.6) is the standard Gibbons-Hawking-York (GHY) boundary term without which the gravitational action does not have a well-defined variation [183]. No such boundary term is required for the scalar field with the Dirichlet boundary conditions [184].

The on-shell value of the action in Eq. (7.6) has UV divergences, which arise because the volume element diverges near the asymptotic boundary [185]. To regulate these divergences, we need to introduce a cut-off surface near the asymptotic boundary. To make a choice of the cut-off surface, we choose to work with the Fefferman-Graham coordinates in the bulk [94, 186]. The most general metric of the asymptotically local AdS spacetime in these coordinates is[2]

$$ds^2 = \frac{1}{z^2}\Big(dz^2 + G_{\mu\nu}(z,x)\,dx^\mu dx^\nu\Big)\,, \tag{7.9}$$

where $z = 0$ is the asymptotic boundary. In these coordinate system, a convenient choice of a cut-off surface is $z = \delta$.

The back-reaction of the scalar field on the bulk geometry is determined using the Einstein-Klein-Gordon equations in the bulk. The variation of the action in Eq. (7.6) with respect to the bulk metric yields

$$R_{ab} + 4\,g_{ab} - \frac{1}{2}\partial_a\Phi\,\partial_b\Phi - \frac{1}{3}\,g_{ab}\,V(\Phi) \;=\; 0\,, \tag{7.10}$$

whereas the variation of the action with respect to the bulk scalar yields

$$\frac{1}{\sqrt{-g}}\,\partial_a\Big(\sqrt{-g}\,g^{ab}\partial_b\Phi\Big) - \frac{\delta}{\delta\Phi}V(\Phi) = 0\,. \tag{7.11}$$

[2]We follow the index convention that the Greek letters $(\mu, \nu, ...)$ denote boundary coordinates and Latin letters $(a, b, ...)$ correspond to bulk coordinates.

These equations should be solved simultaneously to determine the bulk metric in Eq. (7.9). However, Eq. (7.9) is the most general metric of the asymptotically local AdS spacetime. Since the perturbation of the boundary CFT is *homogeneous* and *isotropic*, we expect the bulk metric to have translation and rotational invariance in the transverse directions. Therefore, we make the following ansatz for the bulk metric[3]

$$ds^2 = \frac{1}{z^2}\left(dz^2 - f(z,t)\,dt^2 + h(z,t)\sum_{i=1}^{3} dx_i^2\right), \tag{7.12}$$

with the boundary conditions

$$f(z=0,t) = h(z=0,t) = 1\,, \tag{7.13}$$
$$f(z,t\leq 0) = h(z,t\leq 0) = 1\,. \tag{7.14}$$

Finding the full bulk geometry and the profile of the bulk scalar field is a difficult exercise. However, as emphasized in Sec. (7.1), we are only required to solve for the bulk metric and the bulk scalar near the asymptotic boundary. This allows us to expand the metric and the scalar field as a power series in z and solve for the bulk equations perturbatively. These perturbative solutions were studied in detail in [119], where the powers of z that appear in the asymptotic solutions of the bulk metric and the scalar field were identified. Furthermore, it was shown in [119] that the power series solution for the scalar field breaks down at order z^{Δ} and that for the bulk metric breaks down at order z^d, where d is the dimensions of the boundary. Using these results, we write for $d = 4$ and $\Delta = 3$

$$f(z,t) = 1 + z^2\, f_2(t) + z^3\, f_3(t) + z^4\, F(z,t)\,, \tag{7.15}$$
$$h(z,t) = 1 + z^2\, h_2(t) + z^3\, h_3(t) + z^4\, H(z,t)\,, \tag{7.16}$$
$$\Phi(z,t) = z\,\phi_0(t) + z^2\,\phi_1(t) + z^3\,\Psi(z,t)\,, \tag{7.17}$$

with the boundary condition [133, 134, 179]

$$\phi_0(t) = \lambda(t)\,. \tag{7.18}$$

As we will see in Sec. (7.3) and in Sec. (7.4), the non-perturbative parts of the solution, that is $F(z,t)$ in Eq. (7.15), $H(z,t)$ in Eq. (7.16), and $\Psi(z,t)$ in Eq. (7.17), do not contribute to the divergences of either the action of the WDW patch or the volume of a Cauchy slice. So for our purpose, we ignore the non-perturbative part of the solutions and insert the perturbative ansatz in the bulk equations. Expanding the Klein-Gordon equation, Eq. (7.11), to leading order in z and using Eq. (7.18) yield

$$\phi_1(t) = -\frac{\kappa_3}{2}\,\phi_0^2(t) = -\frac{\kappa_3}{2}\,\lambda^2(t)\,. \tag{7.19}$$

[3]We denote bulk time coordinate by t and boundary time coordinate by $\mathfrak{t}$.

Similarly, expanding the zt-component and tt-component of the Einstein's equations, Eq. (7.10), to the leading order yields

$$f_2(t) \,=\, h_2(t) \,=\, -\frac{1}{12}\,\lambda^2(t)\,, \tag{7.20}$$

whereas expanding these equations to next to the leading order yields

$$f_3(t) \,=\, h_3(t) \,=\, \frac{2}{27}\,\kappa_3\,\lambda^3(t)\,. \tag{7.21}$$

This finishes our discussion of the time-dependent bulk geometry due to the back-reaction of the scalar field. As we will see in the next two sections, the asymptotic results in Eqs. (7.19)-(7.21) are sufficient to calculate the divergences in the rate of complexification.

7.3 Complexity using CA Conjecture

In this section, we calculate the UV divergences in the rate of complexification using the CA conjecture. That is, we extract the time-dependent UV divergences that appear in the action of the WDW patch corresponding to the boundary time $\mathfrak{t}$. Although the details of the WDW patch depend on the geometry far into the bulk, we are only concerned with the structure of the patch near the asymptotic boundary. We find the WDW patch near the asymptotic boundary in Sec. (7.3) and study its action in Sec. (7.3).

Wheeler-DeWitt Patch near the Asymptotic Boundary

The WDW patch corresponding to the boundary time $\mathfrak{t}$ is defined as the domain of dependence of a bulk Cauchy slice anchored to the boundary at time $\mathfrak{t}$. This means that near the asymptotic boundary, the WDW patch is bounded by two null hypersurfaces, $\dot{J}^{\pm}(\mathfrak{t})$. The null hypersurface $\dot{J}^{+}(\mathfrak{t})$ ($\dot{J}^{-}(\mathfrak{t})$) is the boundary of the future (past) of the time slice $\mathfrak{t}$ on the asymptotic boundary. Due to the translation invariance in the transverse directions, these codimension-1 null hypersurfaces can simply be described by

$$\dot{J}^{\pm}(\mathfrak{t}):\qquad t = t_{\pm}(z;\mathfrak{t})\,, \tag{7.22}$$

with the boundary condition $t_{\pm}(z=0;\mathfrak{t}) = \mathfrak{t}$. Using the form of the bulk metric in Eq. (7.12), we deduce that the functions $t_{\pm}(z;\mathfrak{t})$ satisfy

$$\frac{d}{dz}t_{\pm}(z;\mathfrak{t}) = \pm\frac{1}{\sqrt{f\big(z,t_{\pm}(z;\mathfrak{t})\big)}}\,. \tag{7.23}$$

The perturbative solutions of these differential equations can be determined using the series expansion of $f(z,t)$ from Eq. (7.15). Solving these equations order-by-order in z and using Eqs. (7.20)-(7.21) yields

$$t_{\pm}(z;\mathfrak{t}) = \mathfrak{t} \pm z \pm \frac{1}{72}\,z^3\lambda^2(\mathfrak{t}) + \frac{1}{96}\,z^4\left(\mp\frac{24\,\kappa_3}{27}\lambda^3(\mathfrak{t}) + \frac{d}{d\mathfrak{t}}\lambda^2(\mathfrak{t})\right) + O(z^5)\,. \tag{7.24}$$

As we discussed in Sec. (7.2), we introduce a cut-off surface near the asymptotic boundary at $z = \delta$ to regulate the UV divergences. This means that the WDW patch is also bounded by this cut-off surface. So to summarize, the WDW near the asymptotic boundary is the region bounded by the following inequalities

$$\text{WDW patch:} \qquad z \geq \delta\,, \quad \text{and} \qquad t_-(z;\mathfrak{t}) \leq t \leq t_+(z,\mathfrak{t})\,. \tag{7.25}$$

After finding the WDW patch near the asymptotic boundary, we study the action of this patch in the next subsection.

Calculation of the Action

In addition to the action of the bulk theory given in Eq. (7.6), the action of the WDW patch also has contributions from the null boundaries, $\dot{J}^{\pm}(\mathfrak{t})$, and from the corners where these null boundaries intersect the cut-off boundary, $z = \delta$ [174]. That is, the action of the WDW patch is given by the sum

$$\mathcal{A}(\mathfrak{t}) = \mathcal{A}_{\text{bulk}}(\mathfrak{t}) + \mathcal{A}_{\text{boundaries}}(\mathfrak{t}) + \mathcal{A}_{\text{corners}}(\mathfrak{t})\,, \tag{7.26}$$

where $\mathcal{A}_{\text{boundaries}}$ and $\mathcal{A}_{\text{corners}}$ include all the boundaries and all the corners respectively. In the following, we first consider all the terms in Eq. (7.26) separately and then add them together to get the total action.

The bulk contribution to the action of the region in Eq. (7.25) is given by

$$\mathcal{A}_{\text{bulk}}(\mathfrak{t}) = \frac{1}{16\pi G}\int d^3x \int_\delta dz \int_{t_-(z;\mathfrak{t})}^{t_+(z;\mathfrak{t})} dt\,\sqrt{-g}\left(R + 12 - \frac{1}{2}\left(\partial\Phi\right)^2 - V(\Phi)\right). \tag{7.27}$$

Using the trace part of the Einstein's equations, Eq. (7.10), and using the form of the metric in Eq. (7.12), we write the above expression as

$$\mathcal{A}_{\text{bulk}}(\mathfrak{t}) = \frac{L^3}{16\pi G}\int_\delta dz\,\frac{1}{z^5}\int_{t_-(z;\mathfrak{t})}^{t_+(z;\mathfrak{t})} dt\, f^{1/2}(z,t)\, h^{3/2}(z,t)\left(-8 + \frac{2}{3}V(\Phi)\right), \tag{7.28}$$

where we have also defined

$$L^3 \equiv \int d^3x\,, \tag{7.29}$$

as the volume of our boundary system. Evaluating the integrals in Eq. (7.28) is not possible without knowing an explicit form of the time-dependent coupling, $\lambda(\mathfrak{t})$. Nevertheless, we can still calculate the contribution of the bulk action to the rate of complexification. To do this, we take the time-derivative of bulk contribution in Eq. (7.28). This yields

$$\begin{aligned}\frac{d}{d\mathfrak{t}}\mathcal{A}_{\text{bulk}}(\mathfrak{t}) = \frac{L^3}{16\pi G}\int_\delta dz\,\frac{1}{z^5}\Bigg\{&\frac{dt_+(z;\mathfrak{t})}{d\mathfrak{t}}\left[f^{1/2}(z,t)h^{3/2}(z,t)\left(-8+\frac{2}{3}V(\Phi)\right)\right]\Bigg|_{t=t_+(z;\mathfrak{t})}\\ &-\frac{dt_-(z;\mathfrak{t})}{d\mathfrak{t}}\left[f^{1/2}(z,t)h^{3/2}(z,t)\left(-8+\frac{2}{3}V(\Phi)\right)\right]\Bigg|_{t=t_-(z;\mathfrak{t})}\Bigg\}.\end{aligned} \tag{7.30}$$

The integrand in the above expansion can be expanded as a power series in z using Eqs. (7.15)-(7.17) and Eq. (7.24). This allows us to extract the UV divergences in Eq. (7.30). Performing this analysis and using Eqs. (7.18)-(7.21) gives us the following time-dependent divergence in the bulk action

$$\frac{d}{d\mathfrak{t}}\mathcal{A}_{\rm bulk}(\mathfrak{t}) = \frac{L^3}{36\pi G}\,\frac{1}{\delta}\,\frac{d}{d\mathfrak{t}}\lambda^2(\mathfrak{t})\,. \tag{7.31}$$

We now consider the boundary terms in the action, Eq. (7.26). The region in Eq. (7.25) is bounded by three boundaries. One of these in the timelike cut-off surface at $z=\delta$, whereas the other two boundaries are null hypersurfaces, $\dot{J}^{\pm}(\mathfrak{t})$. We first consider the contributions from the null boundaries. This contribution is [174]

$$\begin{aligned}\mathcal{A}_{\rm null}(\mathfrak{t}) \;=\; & -\frac{1}{8\pi G}\int_{j^+(\mathfrak{t})} d^3x\, d\lambda_+\,\sqrt{q_+}\,\big(\kappa_+ + \theta_+\log\theta_+\big) \\ & +\frac{1}{8\pi G}\int_{j^-(\mathfrak{t})} d^3x\, d\lambda_-\,\sqrt{q_-}\,\big(\kappa_- + \theta_-\log\theta_-\big)\,,\end{aligned} \tag{7.32}$$

where $\lambda_\pm$ is a null parameter on $\dot{J}^{\pm}(\mathfrak{t})$ and

$$\sqrt{q_\pm} \;= \frac{1}{z^3}\,h^{3/2}\Big(z, t_\pm(z;\mathfrak{t})\Big)\,, \tag{7.33}$$

$$= \frac{1}{z^3} - \frac{1}{8}\,\lambda^2(\mathfrak{t})\,\frac{1}{z} + \left(\frac{\kappa_3}{9}\lambda^3(\mathfrak{t}) \mp \frac{1}{8}\,\frac{d}{d\mathfrak{t}}\lambda^2(\mathfrak{t})\right) + O(z)\,, \tag{7.34}$$

is the volume measure on a cross-section of $\dot{J}^{\pm}(\mathfrak{t})$. The 'surface gravity', $\kappa_\pm$, of a null generator $k^a_\pm \equiv dx^a/d\lambda_\pm$ is defined as

$$k^a_\pm \nabla_a k^b_\pm \;\equiv \kappa_\pm\, k^b_\pm\,, \tag{7.35}$$

whereas the null expansion, $\theta_\pm$, is defined as

$$\theta_\pm \;\equiv\; \frac{d}{d\lambda_\pm}\,\log\sqrt{q_\pm}\,. \tag{7.36}$$

Note that if we choose $\lambda_\pm$ to be an affine parameter, then $\kappa_\pm$ vanishes and we only have to worry about the terms with the null expansion. Therefore, we choose the null generators of $\dot{J}^{\pm}(\mathfrak{t})$ to be affine parameterized

$$k^a_\pm(\mathfrak{t}) = \; N_\pm(z;\mathfrak{t})\left(\pm z^2\big(\partial_z\big)^a + \frac{z^2}{f^{1/2}\Big(z, t_\pm(z;\mathfrak{t})\Big)}\,\big(\partial_t\big)^a\right)\,, \tag{7.37}$$

where $N_\pm(z;\mathfrak{t})$ near the asymptotic boundary is given by

$$N_\pm(z;\mathfrak{t}) = \; 1 + \frac{1}{24}z^2\lambda^2(\mathfrak{t}) - \left(\frac{\kappa_3}{27}\,\lambda^3(\mathfrak{t}) \mp \frac{1}{36}\,\frac{d}{d\mathfrak{t}}\lambda^2(\mathfrak{t})\right) z^3 + O(z^4)\,. \tag{7.38}$$

With this choice of the parameterization, the null expansions are

$$\theta_{\pm}(z;\mathfrak{t}) \,=\, \mp 3z \mp \frac{3}{8}z^3\lambda^2(\mathfrak{t}) + \left(\pm\frac{4}{9}\kappa_3\lambda^3(\mathfrak{t}) - \frac{11}{24}\,\frac{d}{d\mathfrak{t}}\lambda^2(\mathfrak{t})\right) z^4 + O(z^5)\,. \tag{7.39}$$

Using these asymptotic series expansions, we extract the following divergences in Eq. (7.32)

$$\mathcal{A}_{\rm null}(\mathfrak{t}) \,=\, \frac{L^3}{4\pi G}\left(\frac{1+3\log(3\delta)}{3\delta^3} + \frac{2-\log(3\delta)}{8\delta}\lambda^2(\mathfrak{t}) + \frac{4\kappa_3}{9}\log\delta\,\lambda^3(\mathfrak{t})\right)\,, \tag{7.40}$$

where we have also used Eq. (7.29). We take the time-derivative of this result to get

$$\frac{d}{d\mathfrak{t}}\mathcal{A}_{\rm null}(\mathfrak{t}) \,=\, \frac{L^3}{4\pi G}\left(\frac{2-\log(3\delta)}{8\delta}\,\frac{d}{d\mathfrak{t}}\lambda^2(\mathfrak{t}) + \frac{4\kappa_3}{9}\log\delta\,\frac{d}{d\mathfrak{t}}\lambda^3(\mathfrak{t})\right)\,. \tag{7.41}$$

We now focus on the timelike cut-off boundary. The action of this boundary is given by the standard GHY term

$$\mathcal{A}_{z=\delta}(\mathfrak{t}) = \,\frac{1}{8\pi G}\int d^3x \int_{t_-(\delta;\mathfrak{t})}^{t_+(\delta;\mathfrak{t})} dt\,\sqrt{-\gamma}\,\gamma^{ab}\nabla_a s_b\,, \tag{7.42}$$

where

$$s^a \,=\, -\delta(\partial_z)^a\,, \tag{7.43}$$

is the normal vector to the cut-off surface and $\gamma^{ab} \equiv g^{ab} - s^a s^b$ is the inverse induced metric on the boundary. Evaluating the integral in Eq. (7.42) is not possible. Despite that, we can still calculate its contribution to the rate of complexification. Taking the time-derivative of Eq. (7.42) yields

$$\begin{aligned}\frac{d}{d\mathfrak{t}}\mathcal{A}_{z=\delta}(\mathfrak{t}) = \,\frac{L^3}{8\pi G}\Bigg\{&\frac{dt_+(\delta;\mathfrak{t})}{d\mathfrak{t}}\Big(\sqrt{-\gamma}\,\gamma^{ab}\nabla_a s_b\Big)\Big|_{t=t_+(\delta;\mathfrak{t})}\\ &- \frac{dt_-(\delta;\mathfrak{t})}{d\mathfrak{t}}\Big(\sqrt{-\gamma}\,\gamma^{ab}\nabla_a s_b\Big)\Big|_{t=t_-(\delta;\mathfrak{t})}\Bigg\}\,,\end{aligned} \tag{7.44}$$

where we have also used Eq. (7.29). To extract the UV divergences in Eq. (7.44), we simply expand the right-hand side in the power series of δ. We get

$$\frac{d}{d\mathfrak{t}}\mathcal{A}_{z=\delta}(\mathfrak{t}) = \,-\frac{5L^3}{72\pi G}\,\frac{1}{\delta}\,\frac{d}{d\mathfrak{t}}\lambda^2(\mathfrak{t})\,. \tag{7.45}$$

Lastly, we consider the corner terms in the action, Eq. (7.26). The corners that contribute to the divergences in the action of the WDW patch are the codimension-2 surfaces where the cut-off surface intersect the null boundaries, $\dot{J}^{\pm}(\mathfrak{t})$. The action of these two corners is [174]

$$\mathcal{A}_{\rm corners}(\mathfrak{t}) = \,-\frac{1}{8\pi G}\int d^3x\,\sqrt{q_+}\,a_+(\mathfrak{t}) - \frac{1}{8\pi G}\int d^3x\,\sqrt{q_-}\,a_-(\mathfrak{t})\,, \tag{7.46}$$

where the volume element is given by

$$\sqrt{q_\pm} = \frac{1}{\delta^3}\, h^{3/2}\Big(\delta, t_\pm(\delta;\mathfrak{t})\Big)\,, \tag{7.47}$$

$$= \frac{1}{\delta^3} - \frac{1}{8}\,\lambda^2(\mathfrak{t})\,\frac{1}{\delta} + \left(\frac{\kappa_3}{9}\lambda^3(\mathfrak{t}) \mp \frac{1}{8}\,\frac{d}{d\mathfrak{t}}\lambda^2(\mathfrak{t})\right) + O(\delta)\,, \tag{7.48}$$

and [174]

$$a_\pm(\mathfrak{t}) = \log|s\cdot k_\pm|\Big|_{z=\delta\,,\, t=t_\pm(\delta;\mathfrak{t})}\,. \tag{7.49}$$

Using the null vectors from Eq. (7.37) and the normal vector from Eq. (7.43), we get

$$a_\pm(\mathfrak{t}) = \log\delta + \frac{1}{24}\,\lambda^2(\mathfrak{t})\,\delta^2 + O(\delta^3)\,. \tag{7.50}$$

We combine this result with Eq. (7.48) to simplify Eq. (7.46) as

$$\mathcal{A}_{\text{corners}}(\mathfrak{t}) = -\frac{L^3}{4\pi G}\left(\frac{\log\delta}{\delta^3} - \frac{1}{8}\,\lambda^2(\mathfrak{t})\,\frac{\log\delta}{\delta} + \frac{1}{24}\,\lambda^2(\mathfrak{t})\,\frac{1}{\delta} + \frac{\kappa_3}{9}\lambda^3(\mathfrak{t})\log\delta\right). \tag{7.51}$$

We take the time-derivative of this result to get

$$\frac{d}{d\mathfrak{t}}\mathcal{A}_{\text{corners}}(\mathfrak{t}) = \frac{L^3}{32\pi G}\,\frac{\log\delta}{\delta}\,\frac{d}{d\mathfrak{t}}\lambda^2(\mathfrak{t}) - \frac{L^3}{96\pi G}\,\frac{1}{\delta}\,\frac{d}{d\mathfrak{t}}\lambda^2(\mathfrak{t}) - \frac{L^3}{36\pi G}\,\kappa_3\log\delta\,\frac{d}{d\mathfrak{t}}\lambda^3(\mathfrak{t})\,. \tag{7.52}$$

To get the time-dependent divergences in the total action, we add the contributions from the bulk in Eq. (7.31), null boundaries in Eq. (7.41), cut-off boundary in Eq. (7.45), and corners in Eq. (7.52). We get

$$\frac{d}{d\mathfrak{t}}\mathcal{A}(\mathfrak{t}) = \frac{L^3}{96\pi G}\,\frac{1-3\log(3)}{\delta}\,\frac{d}{d\mathfrak{t}}\lambda^2(\mathfrak{t}) + \frac{L^3}{12\pi G}\,\kappa_3\log\delta\,\frac{d}{d\mathfrak{t}}\lambda^3(\mathfrak{t})\,. \tag{7.53}$$

The CA conjecture, Eq. (7.1), then implies that the UV divergence in the rate of complexification at time $\mathfrak{t}$ is

$$\frac{d}{d\mathfrak{t}}\mathcal{C}_A(\mathfrak{t}) = \frac{L^3}{96\pi^2 G}\,\frac{1-3\log(3)}{\delta}\,\frac{d}{d\mathfrak{t}}\lambda^2(\mathfrak{t}) + \frac{L^3}{12\pi^2 G}\,\kappa_3\log\delta\,\frac{d}{d\mathfrak{t}}\lambda^3(\mathfrak{t})\,. \tag{7.54}$$

This is one of the main results of this chapter. This verifies our claim from Sec. (7.1) that the rate of complexification of the state following the time-dependent perturbation of a CFT has UV divergences. As argued in Sec. (7.1), this result violates the Lloyd bound, Eq. (7.3). To see this, note that the instantaneous energy of the state is UV finite [180, 181]. Hence, it is meaningless to expect a bound between the UV divergent rate of complexification and the UV finite energy of the state.

7.4 Complexity using CV Conjecture

In this section, we use the CV conjecture to calculate the time-dependent UV divergences in the complexity of the boundary state. Our approach here is to first find an *extremal* Cauchy surface anchored on the boundary at time $\mathfrak{t}$ and then to extract the UV divergences in the volume of that surface.

Due to translation symmetry in the transverse directions, we consider a bulk Cauchy surface anchored on the boundary at time $\mathfrak{t}$ that can be described by

$$\Sigma_{\mathfrak{t}}: \qquad t = T(z;\mathfrak{t})\,, \tag{7.55}$$

with the boundary conditions $T(z=0;\mathfrak{t}) = \mathfrak{t}$. The future-directed normal vector to $\Sigma_{\mathfrak{t}}$ is

$$n^a = \mathcal{N}\left((\partial_t)^a + f\Big(z, T(z;\mathfrak{t})\Big)\, T'(z;\mathfrak{t})\,(\partial_z)^a\right), \tag{7.56}$$

where prime denotes derivative with respect to z, and the normalization factor is

$$\mathcal{N}^{-1} = \frac{1}{z}\, f^{1/2}\Big(z, T(z;\mathfrak{t})\Big)\sqrt{1 - f\Big(z, T(z;\mathfrak{t})\Big)\Big(T'(z;\mathfrak{t})\Big)^2}\,. \tag{7.57}$$

The extrinsic curvature of $\Sigma_{\mathfrak{t}}$ is defined as

$$K_{\Sigma_{\mathfrak{t}}} \equiv h^{ab}\nabla_a n_b\,, \tag{7.58}$$

where $h^{ab} \equiv g^{ab} + n^a n^b$ is the inverse induced metric on $\Sigma_{\mathfrak{t}}$. Finding an extremal bulk Cauchy surface is equivalent to demanding that the extrinsic curvature in Eq. (7.58) vanishes. This yields the following equation

$$0 = \left\{T'' + \frac{1}{2}\frac{f'}{f}T' + \frac{1}{2}\frac{\dot{f}}{f}T'^2 + \left(1 - fT'^2\right)\left(\frac{1}{2}\frac{f'}{f}T' + \frac{3}{2}\frac{h'}{h}T' + \frac{3}{2}\frac{1}{f}\frac{\dot{h}}{h} - \frac{4}{z}T'\right)\right\}\Bigg|_{t=T(z;\mathfrak{t})}, \tag{7.59}$$

where dot denotes the derivative with respect to the bulk time coordinate, t. Solving this equation for $T(z;\mathfrak{t})$ is not feasible. However, we are only interested in the profile of the extremal Cauchy surface near the asymptotic boundary. This means we only need to solve Eq. (7.59) perturbatively. Demanding a series solution for $T(z;\mathfrak{t})$ and solving Eq. (7.59) order-by-order yield

$$T_{\rm ext}(z;\mathfrak{t}) = \mathfrak{t} - \frac{1}{32}\, z^4\, \frac{d}{d\mathfrak{t}}\lambda^2(\mathfrak{t}) + O(z^5)\,. \tag{7.60}$$

After finding the extremal surface near the asymptotic boundary, we now find the divergences that appear in its volume. The volume of this extremal surface is given by

$$V_{\rm ext}(\mathfrak{t}) = \int d^3x \int_\delta dz\, \frac{1}{z^4}\, h^{3/2}\Big(z, T_{\rm ext}(z;\mathfrak{t})\Big)\sqrt{1 - f\Big(z, T_{\rm ext}(z;\mathfrak{t})\Big)\Big(T'_{\rm ext}(z;\mathfrak{t})\Big)^2}\,. \tag{7.61}$$

Since the z dependence in Eq. (7.60) appears at z^4 order, it does not contribute to the divergences in Eq. (7.61). Therefore, we simply replace $T_{\rm ext}(z;\mathfrak{t})$ with $\mathfrak{t}$ in Eq. (7.61) and get

$$V_{\rm ext}(\mathfrak{t}) = L^3 \int_\delta dz \, \frac{1}{z^4} \, h^{3/2}(z,\mathfrak{t}) \,, \tag{7.62}$$

where we have also used Eq. (7.29). Using the series expansion in Eq. (7.16) and using Eqs. (7.20)-(7.21), we find that the divergences in the volume of the extremal Cauchy surface are

$$V_{\rm ext}(\mathfrak{t}) = \frac{L^3}{3} \frac{1}{\delta^3} - \frac{L^3}{8} \frac{1}{\delta} \lambda^2(\mathfrak{t}) - \frac{L^3 \kappa_3}{9} \log\delta \, \lambda^3(\mathfrak{t}) \,. \tag{7.63}$$

The CV conjecture, Eq. (7.2), then implies that the divergences in the complexity at time $\mathfrak{t}$ are

$$C_V(\mathfrak{t}) = \frac{L^3}{3G} \frac{1}{\delta^3} - \frac{L^3}{8G} \frac{1}{\delta} \lambda^2(\mathfrak{t}) - \frac{L^3 \kappa_3}{9G} \log\delta \, \lambda^3(\mathfrak{t}) \,, \tag{7.64}$$

whereas, the divergences in the rate of complexification are

$$\frac{d}{d\mathfrak{t}} \mathcal{C}_V(\mathfrak{t}) = -\frac{L^3}{8G} \frac{1}{\delta} \frac{d}{d\mathfrak{t}} \lambda^2(\mathfrak{t}) - \frac{L^3 \kappa_3}{9G} \log\delta \, \frac{d}{d\mathfrak{t}} \lambda^3(\mathfrak{t}) \,. \tag{7.65}$$

This is another main result of this chapter. This result shows that the CV conjecture, Eq. (7.2), and the Lloyd bound, Eq. (7.3), are not consistent with each other. This follows from the fact that the energy of the state after the time-dependent perturbation is UV finite [180, 181]. This means that one of the sides of the Lloyd bound has UV divergences whereas the other side does not. Hence, the bound is not satisfied.

7.5 Discussion

Our goal in this chapter was to present a simple example where the holographic complexity computed either using the CA conjecture, Eq. (7.1), or the CV conjecture, Eq. (7.2), has time-dependent UV divergences. The example that we studied was a time-dependent deformation of a CFT Hamiltonian by a relevant operator with the assumption that the system was initially in the ground state of the unperturbed CFT. The bulk description of this perturbation involves a scalar field which back-reacts on the bulk geometry [133, 134, 179]. Due to this back-reaction, the bulk geometry becomes time-dependent. Since we were only interested in the divergences in the holographic complexity, we only had to calculate the back-reaction of the scalar field near the asymptotic boundary in Sec. (7.2). With the time-dependent geometry near the asymptotic boundary, we were able to use the CA conjecture in Sec. (7.3) to determine the time-dependent divergences in the rate of complexification. This result is given in Eq. (7.54). Similarly, we used the CV conjecture in Sec. (7.4) to find the divergences that appear in the complexity. This result is given in Eq. (7.65). We find that the structure of the divergences in Eq. (7.54) and in Eq. (7.65) is the same as the one identified in [158, 175].

The significance of our result is that it shows that neither the CA conjecture nor the CV conjecture is consistent with the Lloyd bound, Eq. (7.3). The Lloyd bound demands that the average energy of the system bounds the rate of complexification from above. However, the energy of the system following the time-dependent perturbation is a UV finite quantity. The time-dependence of the energy of the perturbed system has been studied using the AdS-CFT correspondence in [180, 181]. Since the rate of complexification according to both the CA conjecture and the CV conjecture is UV divergent, whereas the energy of the system is not, the Lloyd bound cannot be satisfied. This is the main message of this chapter. Though, note that the inconsistency of the CA conjecture and the Lloyd bound were also recently discovered in [155, 156, 157].

Appendix A

Parallel Transport of Null Vectors

Here we present a derivation of Eq. (2.63); Eq. (2.64) can be derived similarly. We start with the ansatz

$$h^b \nabla_a k_a = A k_a + B l_a + C_a \,, \tag{A.1}$$

where C_a is the projection of $h^b \nabla_b k_a$ onto the leaf. The constant A is

$$A = -l^a h^b \nabla_b k_a = \tilde{\kappa} \,, \tag{A.2}$$

where we have used Eq. (2.16). The constant B is

$$B = -k^a h^b \nabla_b k_a = 0 \,. \tag{A.3}$$

To determine C_a, we consider an arbitrary vector field, ϕ^a, tangent to the leaf, and contract it to our ansatz

$$\begin{aligned} \phi^a C_a &= \phi^a h^b \nabla_b k_a \,, & \text{(A.4)} \\ &= -k_a \mathcal{L}_h \phi^a + \phi^a \left(D_a \alpha - \alpha \Omega_a \right) \,, & \text{(A.5)} \end{aligned}$$

where we have used Eq. (2.15). A consequence of the normalization Eq. (2.5) is that for every vector field ϕ^a tangent to the leaf, $\mathcal{L}_h \phi^a$ is also tangent to the leaf [57]

$$q^a{}_b \phi^b = \phi^a \;\Rightarrow\; q^a{}_b \mathcal{L}_h \phi^b = \mathcal{L}_h \phi^a \,. \tag{A.6}$$

This with the fact that ϕ^a is arbitrary implies

$$C_a = D_a \alpha - \alpha \Omega_a \,. \tag{A.7}$$

Eq. (A.1) thus reduces to the desired result

$$h^b \nabla_b k_a = \tilde{\kappa} k_a + D_a \alpha - \alpha \Omega_a \,. \tag{A.8}$$

Appendix B

Cross-focusing Equations

Here we derive the cross-focusing equations [54, 61]

$$l^a\nabla_a\theta^{(k)} = -\,\theta^{(l)}\theta^{(k)} - \frac{1}{2}\mathcal{R} + \Omega_a\Omega^a - D_a\Omega^a - \frac{2}{\alpha}\Omega^a D_a\alpha + \frac{1}{\alpha}D^a D_a\alpha + 8\pi T_{ab}k^a l^b\,, \tag{B.1}$$

$$k^a\nabla_a\theta^{(l)} + \kappa\theta^{(l)} = -\,\theta^{(l)}\theta^{(k)} - \frac{1}{2}\mathcal{R} + \Omega_a\Omega^a + D_a\Omega^a + \frac{2}{\beta}\Omega^a D_a\beta + \frac{1}{\beta}D^a D_a\beta + 8\pi T_{ab}k^a l^b\,, \tag{B.2}$$

which will be useful in the derivation of the screen equations in Appendix (C). Note that these equations (unlike the screen equations) are highly sensitive to how we extend the null vectors, k^a and l^a, into a neighborhood of the holographic screen. We do this by demanding

$$l^b\nabla_b l^a = 0\,, \tag{B.3}$$

$$k^b\nabla_b k^a = \kappa k^a\,, \tag{B.4}$$

$$l^a k_a = -1\,. \tag{B.5}$$

With these extension, Eq. (2.63) reduces to

$$l^b\nabla_b k_a = \frac{1}{\alpha}D_a\alpha - \Omega_a\,. \tag{B.6}$$

We decompose $\nabla_a l_b$ and $\nabla_a k_b$ as

$$\nabla_a l_b = B^{(l)}_{ab} + \kappa l_a l_b - l_a\Omega_b - l_b\Omega_a - \frac{1}{\beta}l_a D_b\beta\,, \tag{B.7}$$

$$\nabla_a k_b = B^{(k)}_{ab} - \kappa l_a k_b + k_a\Omega_b + k_b\Omega_a - \frac{1}{\alpha}k_a D_b\alpha\,. \tag{B.8}$$

Now using $\theta^{(k)} = q^{ab}\nabla_a k_b$, we get

$$l^a\nabla_a\theta^{(k)} = l^a\nabla_a\left(q^{bc}\nabla_b k_c\right)\,, \tag{B.9}$$

$$= q^{bc}\nabla_b\left(l^a\nabla_a k_c\right) - q^{bc}\left(\nabla_b l^a\right)\left(\nabla_a k_c\right) + \left(l^a\nabla_a q^{bc}\right)\left(\nabla_b k_c\right) + R_{abcd}l^a q^{bc}k^d\,, \tag{B.10}$$

$$= \Omega_a\Omega^a - D_a\Omega^a - B^{(l)}_{ab}B^{ab}_{(k)} - \frac{2}{\alpha}\Omega^a D_a\alpha + \frac{1}{\alpha}D^a D_a\alpha + R_{abcd}l^a q^{bc}k^d\,. \tag{B.11}$$

With the help of the Gauss-Codazzi equation for codimension-2 spatial surfaces [187],

$$\frac{1}{2}\mathcal{R} + \theta^{(l)}\theta^{(k)} - B^{(l)}_{ab}B^{ab}_{(k)} = \frac{1}{2}R_{abcd}q^{ac}q^{bd}\,, \tag{B.12}$$

we get

$$l^a\nabla_a\theta^{(k)} = -\theta^{(l)}\theta^{(k)} - \frac{1}{2}\mathcal{R} + \Omega_a\Omega^a - D_a\Omega^a - \frac{2}{\alpha}\Omega^a D_a\alpha + \frac{1}{\alpha}D^a D_a\alpha + \frac{1}{2}R_{ab}q^{ab}\,. \tag{B.13}$$

To get Eq. (B.1), we use the Einstein equations

$$\frac{1}{2}R_{ab}q^{ab} = \left(R_{ab} - \frac{1}{2}Rg_{ab}\right)k^a l^b = 8\pi T_{ab}k^a l^b\,. \tag{B.14}$$

Eq. (B.2) can be derived in a similar fashion.

Appendix C

Derivation of Screen Equations

Here we present a derivation of the nontrivial screen equations, Eqs. (2.34)-(2.36). Eq. (2.36) was derived for the dynamical horizons in [53, 55]. The derivation made use of the Gauss Codazzi constraint equations which relate the extrinsic curvature of a hypersurface with the Ricci tensor of the background spacetime. This can only be done for a hypersurface with definite signature. Hence, this method does not obviously apply to a holographic screen. In Sec. (C.1), we will present a derivation of Eq. (2.36) in a way that makes it clear that the signature of H (and indeed, anything but the $2D$ leaf) is irrelevant. Eq. (2.34) was derived in [58]; in Sec. (C.2) , we present a simplified derivation. In Sec. (C.3), we derive Eq. (2.35), following [57].

C.1 $T_{ab}n^a k^b$ Equation

We begin by deriving Eq. (2.36). On the holographic screen, $h^a \nabla_a \theta^{(k)} = 0$. By expanding this equation, we get

$$0 = \alpha l^a \nabla_a \theta^{(k)} + \beta k^a \nabla_a \theta^{(k)} \,. \tag{C.1}$$

Replacing the first term on the right hand side with the cross-focusing Eq. (B.1), and the second term with Raychaudhuri's equation,

$$k^a \nabla_a \theta^{(k)} = \kappa \theta^{(k)} - \frac{1}{2}\theta^{(k)2} - \sigma^{(k)}_{ab}\sigma^{ab}_{(k)} - 8\pi T_{ab} k^a k^b \,, \tag{C.2}$$

we find

$$-\frac{\alpha}{2}\mathcal{R} + \alpha \Omega_a \Omega^a - \alpha D_a \Omega^a - 2\Omega^a D_a \alpha + D_a D^a \alpha = 8\pi T_{ab} n^a k^b + \beta \sigma^{(k)}_{ab}\sigma^{ab}_{(k)} \,. \tag{C.3}$$

C.2 $T_{ab}n^a h^b$ Equation

Next, we derive Eq. (2.34). By Eq. (2.3),

$$\alpha \widehat{\mathcal{L}}_h \theta^{(l)} = \alpha^2 l^a \nabla_a \theta^{(l)} + \alpha\beta k^a \nabla_a \theta^{(l)} \,. \tag{C.4}$$

We replace the second term on the right hand side with the cross-focusing Eq. (B.2) and the first term with Raychaudhuri's equation

$$l^a \nabla_a \theta^{(l)} = -\frac{1}{2}\theta^{(l)2} - \sigma^{(l)}_{ab}\sigma^{ab}_{(l)} - 8\pi T_{ab} l^a l^b \,. \tag{C.5}$$

As a result, we get

$$\begin{aligned}\alpha(\widehat{\mathcal{L}}_h + \tilde{\kappa})\theta^{(l)} = & -\alpha^2 B^{(l)}_{ab} B^{ab}_{(l)} - \frac{1}{2}\alpha\beta\mathcal{R} + \alpha\beta\Omega^a\Omega_a + \alpha\beta D_a\Omega^a \\ & + 2\alpha\Omega^a D_a\beta + \alpha D^a D_a\beta + 8\pi\alpha T_{ab} n^a l^b \,. \end{aligned} \tag{C.6}$$

We eliminate $\mathcal{R}$ from this equation by using Eq. (C.3)

$$\alpha(\widehat{\mathcal{L}}_h + \tilde{\kappa})\theta^{(l)} = D_a(2\alpha\beta\Omega^a - \beta D^a\alpha + \alpha D^a\beta) + B^{(h)}_{ab} B^{ab}_{(n)} + 8\pi T_{ab} n^a h^b \,. \tag{C.7}$$

Rearranging the terms and using Eq. (2.32) lead to Eq. (2.34).

C.3 $T_{ab}n^a q^b{}_c$ Equations

Here we closely follow the derivation by Gourgoulhon [57]. We start with the identity

$$R_{ab} n^a q^b{}_c = q_c{}^b \left(\nabla_a \nabla_b - \nabla_b \nabla_a\right) n^a \,. \tag{C.8}$$

Using $n^a = -\alpha l^a + \beta k^a$, and Eqs. (B.7)-(B.8), we get

$$\nabla_a n_b = B^{(n)}_{ab} - \kappa l_a h_b + h_a\Omega_b + h_b\Omega_a + \frac{\alpha}{\beta} l_a D_b\beta - \frac{\beta}{\alpha} k_a D_b\alpha - l_b\nabla_a\alpha + k_b\nabla_a\beta \,. \tag{C.9}$$

The first term on the right hand side of Eq. (C.8) becomes

$$\begin{aligned} q_c{}^b \nabla_a \nabla_b n^a = & \, q_c{}^b h^a \nabla_a \Omega_b + \Omega^a B^{(h)}_{ac} + \theta^{(h)}\Omega_c - \theta^{(l)} D_c\alpha + q_{cb}\nabla_a B^{ab}_{(n)} \\ & - B^{(n)}_{ca}\left(\frac{1}{\beta}D^a\beta + \frac{1}{\alpha}D^a\alpha\right) - D_c\left(l^a\nabla_a\alpha - k^a\nabla_a\beta\right) \,, \end{aligned} \tag{C.10}$$

where we have repeatedly use Eqs. (B.3)-(B.8). Similarly, the second term becomes

$$q_c{}^b \nabla_b \nabla_a n^a = D_c(\tilde{\kappa}) - \theta^{(l)} D_c\alpha - \alpha D_c\theta^{(l)} - D_c\left(l^a\nabla_a\alpha - k^a\nabla_a\beta\right) \,. \tag{C.11}$$

Combining these two results, we get

$$\begin{aligned} R_{ab} n^a q^b{}_c = & \, q_c{}^b h^a \nabla_a \Omega_b + \Omega^a B^{(h)}_{ac} + \theta^{(h)}\Omega_c - D_c\tilde{\kappa} + \alpha D_c\theta^{(l)} + q_{cb}\nabla_a B^{ab}_{(n)} \\ & - B^{(n)}_{ca}\left(\frac{1}{\beta}D^a\beta + \frac{1}{\alpha}D^a\alpha\right) \,. \end{aligned} \tag{C.12}$$

By making use of

$$D_a B_c^{(n)a} = q_c{}^b \nabla_a B_b^{(n)a} - B_c^{(n)b} \left(\frac{1}{\beta} D_b \beta + \frac{1}{\alpha} D_b \alpha \right) , \tag{C.13}$$

and

$$\widehat{\mathcal{L}}_h \Omega_c = q_c{}^b h^a \nabla_a \Omega_b + \Omega^a B_{ac}^{(h)} , \tag{C.14}$$

Eq. (C.12) reduces to

$$R_{ab} n^a q^b{}_c = \widehat{\mathcal{L}}_h \Omega_c + \theta^{(h)} \Omega_c - D_c \tilde{\kappa} + \alpha D_c \theta^{(l)} + D_a B_c^{(n)a} . \tag{C.15}$$

Finally we use Einstein's equation to obtain Eq. (2.35),

$$(\widehat{\mathcal{L}}_h + \theta^{(h)}) \Omega_c - D_c \tilde{\kappa} + \alpha D_c \theta^{(l)} = 8\pi T_{ab} n^a q_c^b - D_a B_c^{(n)a} . \tag{C.16}$$

Appendix D

Details of the Holographic Calculations in Ch. (5)

D.1 HRT Surface Calculation

In this appendix, we solve for the position of the HRT surface and verify the claim that we made in Eq. (5.19) that at the lowest order, the solution of the stationary surface is

$$t(z) = \mathfrak{t} + z^{2+2\alpha}\, t_{2+2\alpha} + \dots\,, \tag{D.1}$$

As mentioned in the Sec. (5.2), the HRT surface is given by $t = t(z)$ and $x_1 = 0$. The equation of motion for $t = t(z)$ is obtained by varying

$$A \propto \int dz \frac{h^{\frac{d-2}{2}}(z, t(z))}{z^{d-1}}\, \sqrt{1 - f(z, t(z))(t'(z))^2}\,. \tag{D.2}$$

We find

$$\begin{aligned} 0 = & -z\Big((d-2)\dot{h} + ht'(t'\dot{f} + 2f')\Big) + fh\Big(2(d-1)t' - 2zt'' + zt'^3 f'\Big) + (d-2)zfht'(t'\dot{h} - h') \\ & + f^2 t'^3\Big(-2(d-1)h + (d-2)zh'\Big)\,, \end{aligned} \tag{D.3}$$

where dot represents derivative with respect to t and prime represents derivative with respect to z.

The ansatz Eqs. (5.12)-(5.13) for the metric functions, $h(z,t)$ and $f(z,t)$, at leading order gives

$$h(z,t) = 1 + z^{2\alpha} h_{2,0}(t)\,, \tag{D.4}$$

$$f(z,t) = 1 + z^{2\alpha} f_{2,0}(t)\,. \tag{D.5}$$

Let's make the ansatz $t(z) = \mathfrak{t} + z^{\beta} t_{\beta}$. The first term of the equation of motion Eq. (D.3) is proportional to $z^{2\alpha+1}$. Out of all the other terms, the term with the smallest power of z is proportional to $z^{\beta-1}$. Thus we learn $\beta = 2 + 2\alpha$.

However, the coefficient of the $z^{\beta-1}$ term is equal to $2\beta(d-\beta)t_\beta$. Therefore, the above result is only true if $d \neq \beta$. For $d = \beta$, we would have to modify the ansatz to be $t(z) = \mathfrak{t} + z^\beta \log(z) t_\beta$. We do not consider this case in the main argument of Ch. (5), so it can be ignored.

D.2 Perturbative Solution of Einstein-Scalar Equations

In this section, we find the time-dependent coefficients $h_{m,n}(t)$, $f_{m,n}(t)$ and $\phi_{m,n}(t)$ in terms of $\phi_{0,0}(t) = \lambda(t)$ by substituting the ansatz Eqs. (5.12)-(5.14) in the Einstein-scalar equations Eqs. (5.9)-(5.11). We use this result in the holographic calculation of the entanglement entropy in Secs. (5.2)-(5.2).

- $\alpha = 2$ and $d = 6$

  This case corresponds to the holographic scalar in $d = 6$. From Eq. (5.30), we know that the universal part of the time-dependent entropy only depends on the coefficient $h_{2,0}(t)$. This can easily be found using Eq. (5.9). Expanding this equation gives us:

$$0 = \ (10\dot{h}_{2,0} + \phi_{0,0}\dot{\phi}_{0,0})z^3 + O(z^5)\,. \tag{D.6}$$

  Integrating this equation, we find

$$h_{2,0}(t) = \ -\frac{1}{20}\phi_{0,0}^2(t)\,. \tag{D.7}$$

- $\alpha = 2$ and $d = 8$

  To find the entanglement entropy for the holographic scalar in $d = 8$ using Eq. (5.35), we need to find the sum: $h_{2,2}(t) + h_{3,0}(t)$. To find this, we will substitute the ansatz Eqs. (5.12)-(5.14) into Eq. (5.9) and Eq. (5.11). Expanding Eq. (5.9) gives us

$$0 = \ (14\dot{h}_{2,0}+\phi_{0,0}\dot{\phi}_{0,0})z^3+\big(21(\dot{h}_{2,2}+\dot{h}_{3,0})+2\dot{\phi}_{0,0}(\phi_{0,2}+\phi_{2,0})+\phi_{0,0}(\dot{\phi}_{0,2}+\dot{\phi}_{2,0})\big)z^5+O(z^7)\,, \tag{D.8}$$

  and expanding Eq. (5.11) yields

$$0 = \ \big(4(\phi_{0,2}+\phi_{2,0}) + \frac{\kappa}{2}\phi_{0,0}^2 + \ddot{\phi}_{0,0}\big)z^4 + O(z^6)\,. \tag{D.9}$$

  By solving the above equations, we find

$$h_{2,2}(t) + h_{3,0}(t) = \ \frac{\kappa}{126}\phi_{0,0}^3(t) + \frac{1}{168}\dot{\phi}_{0,0}^2(t) + \frac{1}{84}\phi_{0,0}(t)\ddot{\phi}_{0,0}(t)\,. \tag{D.10}$$

- $\alpha = 1$ and $d = 4$

  This case corresponds to the fermionic mass operator in $d = 4$. The entanglement entropy in this case is given by Eq. (5.42). To find the entropy, we need to know $h_{2,0}(t)$. Expanding Eq. (5.9) yields

$$0 = \ (\dot{h}_{2,0} + \frac{1}{6}\phi_{0,0}\dot{\phi}_{0,0})z + O(z^2)\,. \tag{D.11}$$

  Integrating this equation gives

$$h_{2,0}(t) = \ -\frac{1}{12}\phi^2_{0,0}(t)\,. \tag{D.12}$$

- $\alpha = 1$ and $d = 5$

  In this case, the entanglement entropy is given by Eq. (5.45), and the entanglement entropy only depends on the coefficient $h_{3,0}(t)$. We start by expanding Eq. (5.9). This gives us

$$0 = \ (8\dot{h}_{2,0} + \phi_{0,0}\dot{\phi}_{0,0})z + (12\dot{h}_{3,0} + 2\phi_{2,0}\dot{\phi}_{0,0} + \phi_{0,0}\dot{\phi}_{2,0})z^2 + O(z^3)\,. \tag{D.13}$$

  To solve for $h_{3,0}(t)$, we first need to know $\phi_{2,0}(t)$. This can be easily found by expanding Eq. (5.11):

$$0 = \ (\phi_{2,0} + \frac{\kappa}{4}\phi^2_{0,0})z^2 + O(z^3)\,. \tag{D.14}$$

  Solving the above two equations yields

$$h_{3,0}(t_0) = \ \frac{\kappa}{36}\ \phi^3_{0,0}(t_0)\,. \tag{D.15}$$

- $\alpha = 1$ and $d = 6$

  The entanglement entropy for this case is given by Eq. (5.49). Here we need to solve for the combination $h^2_{2,0}(t) + 2h_{2,2}(t) + 2h_{4,0}(t)$. As always, we start by expanding Eq. (5.9). We get

$$\begin{aligned} 0 = \ & (10\dot{h}_{2,0} + \phi_{0,0}\dot{\phi}_{0,0})z + (15\dot{h}_{3,0} + 2\phi_{2,0}\dot{\phi}_{0,0} + \phi_{0,0}\dot{\phi}_{2,0})z^2 + \Big(20(\dot{h}_{2,2} + \dot{h}_{4,0}) \\ & -5(f_{2,0} + 3h_{3,0})\dot{h}_{2,0} + 3\dot{\phi}_{0,0}(\phi_{0,2} + \phi_{3,0}) + \phi_{0,0}(\dot{\phi}_{0,2} + \dot{\phi}_{3,0}) + 2\phi_{2,0}\dot{\phi}_{2,0}\Big)z^3 + O(z^4)\,. \end{aligned} \tag{D.16}$$

  Integrating the leading order term of this equation yields $h_{2,0}(t) = -\frac{1}{20}\phi^2_{0,0}(t)$. Furthermore, we can use the coefficient of the z^3 term to solve for the sum $h_{2,2}(t) + h_{3,0}(t)$. However, this would require us to solve for $f_{2,0}$, $\phi_{2,0}$, $\phi_{2,2}$ and $\phi_{3,0}$. All these can be found from the expansion of Eq. (5.10) and Eq. (5.11). Expanding Eq. (5.10) yields

$$0 = \ (10f_{2,0} + 10h_{2,0} + \phi^2_{0,0}) + O(z)\,, \tag{D.17}$$

which we solve to get $f_{2,0}(t) = -\frac{1}{20}\phi_{0,0}^2(t)$. Similarly, expanding the equation Eq. (5.11) yields

$$0 = \ (18\phi_{2,0}+3\kappa\phi_{0,0}^2)z^2+\Big(24(\phi_{0,2}+\phi_{3,0})+6\ddot{\phi}_{0,0}+\phi_{0,0}(-30h_{2,0}-6f_{2,0}+\omega\phi_{0,0}^2+6\kappa\phi_{2,0})\Big)z^3+O(z^4)\,. \tag{D.18}$$

After using this equation to solve for $\phi_{2,0}$ and for $\phi_{0,2}+\phi_{3,0}$, we can solve for $h_{2,0}+h_{3,0}$ using Eq. (D.16). Combining all the results, we get

$$h_{2,0}^2(t) + 2h_{2,2}(t) + 2h_{4,0}(t) = \ \frac{(117-65\kappa^2+45\omega)}{7200}\ \phi_{0,0}^4(t) + \frac{1}{80}\ \partial_t^2\Big(\phi_{0,0}^2(t)\Big)\,. \tag{D.19}$$

Appendix E

Useful Integral for Ch. (5)

In this appendix, we aim at simplifying the following integral

$$N_s(\mathfrak{t}) \equiv \int_{-\mathfrak{t}}^{0} d\mathfrak{t}' \int d\mathbf{x}' \int d\mathbf{x}_{\parallel} \int_0^{\infty} dx_{\perp}\; x_{\perp} \lambda(\mathfrak{t}'+\mathfrak{t}) \left\langle 0\right| T_{00}(0, x_{\perp}, \mathbf{x}_{\parallel}) \phi^2(\mathfrak{t}', \mathbf{x}') \left|0\right\rangle \,. \tag{E.1}$$

From Eq. (5.72) and Eq. (5.73) we have

$$\left\langle 0\right| T_{00}(x)\phi^2(x') \left|0\right\rangle = \int \frac{d\mathbf{p}_1 d\mathbf{p}_2}{(2\pi)^{2d-2}} \frac{-E_1E_2 - \mathbf{p}_1\cdot\mathbf{p}_2 + m_0^2 + 2\xi(\mathbf{p}_1+\mathbf{p}_2)^2}{4E_1E_2} e^{-i(p_1+p_2)\cdot(x-x')} \,. \tag{E.2}$$

Introducing $\mathbf{q} = \mathbf{p}_1 + \mathbf{p}_2$, $\Delta\mathfrak{t} = \mathfrak{t} - \mathfrak{t}'$, $\Delta x_{\perp} = x_{\perp} - x'_{\perp}$ and integrating Eq. (E.1) with respect to $\mathbf{x}_{\parallel}$ and $\mathbf{x}'_{\parallel}$, yields

$$\begin{aligned} N_s(\mathfrak{t}) = \mathcal{A} \int_0^{\mathfrak{t}} d\mathfrak{t}' \int dx'_{\perp} \int_0^{\infty} dx_{\perp}\; x_{\perp} \lambda(\mathfrak{t}') \\ \times \int \frac{d\mathbf{p}_1 dq_{\perp}}{(2\pi)^d} \left(\frac{-1 + p_{1\perp}^2/E_1^2 + 4\xi}{8E_1^2} q_{\perp}^2 + O(q_{\perp}^3) \right) e^{-i(E_1+E_2)\Delta\mathfrak{t} + iq_{\perp}\Delta x_{\perp}} \,. \end{aligned} \tag{E.3}$$

It is important that we perform the integrals over $x_{\perp}$ and $x'_{\perp}$ in the proper order so as to avoid an ambiguous "$0\times\infty$" result. First we integrate over $x_{\perp}$, using the identity[1]

$$\int_0^{\infty} dx_{\perp}\; x_{\perp} e^{-iq_{\perp}x_{\perp}} = \mathrm{P.V.}\frac{-1}{q_{\perp}^2} + i\pi\delta'(q_{\perp}) \,, \tag{E.4}$$

and then over $x'_{\perp}$ which results in a $2\pi\delta(q_{\perp})$. The result is

$$N_s(\mathfrak{t}) = \mathcal{A} \int_0^{\mathfrak{t}} d\mathfrak{t}' \lambda(\mathfrak{t}') \int \frac{d\mathbf{p}}{(2\pi)^{d-1}} \left(\frac{1 - p_{\perp}^2/E^2 - 4\xi}{8E^2} \right) e^{2iE(\mathfrak{t}'-\mathfrak{t})} \,. \tag{E.5}$$

[1] We ignore $\delta'(q_{\perp})$ in what follows, since it is multiplied by $q_{\perp}^n$ with $n \geq 2$. If, however, one keeps these terms, then eventually they result in the ill defined distributions of the form $q^n\delta'(q_{\perp})\delta(q_{\perp})$ which vanish within, *e.g.,* dimensional regularization.

Bibliography

[1] J. D. Bekenstein. "Black holes and the second law". In: *Nuovo Cim. Lett.* 4 (1972), pp. 737–740.

[2] S. W. Hawking. "Gravitational radiation from colliding black holes". In: *Phys. Rev. Lett.* 26 (1971), pp. 1344–1346.

[3] Jacob D. Bekenstein. "Black Holes and Entropy". In: *Phys. Rev. D* 7 (1973), p. 2333.

[4] Jacob D. Bekenstein. "Generalized second law of thermodynamics in black hole physics". In: *Phys. Rev. D* 9 (1974), p. 3292.

[5] S. W. Hawking. "Particle Creation By Black Holes". In: *Commun. Math. Phys.* 43 (1975), p. 199.

[6] S. W. Hawking. "Black Holes and Thermodynamics". In: *Phys. Rev. D* 13 (1976), pp. 191–197.

[7] S. W. Hawking. "Breakdown of Predictability in Gravitational Collapse". In: *Phys. Rev. D* 14 (1976), pp. 2460–2473.

[8] G. 't Hooft. "Dimensional reduction in quantum gravity". In: (1993). eprint: `gr-qc/9310026`.

[9] Leonard Susskind. "The World as a hologram". In: *J. Math. Phys.* 36 (1995), pp. 6377–6396. eprint: `hep-th/9409089`.

[10] Raphael Bousso. "A covariant entropy conjecture". In: *JHEP* 07 (1999), p. 004. eprint: `hep-th/9905177`.

[11] Eanna E. Flanagan, Donald Marolf, and Robert M. Wald. "Proof of Classical Versions of the Bousso Entropy Bound and of the Generalized Second Law". In: *Phys. Rev. D* 62 (2000), p. 084035. eprint: `hep-th/9908070`.

[12] Raphael Bousso et al. "Proof of a Quantum Bousso Bound". In: *Phys.Rev.* D90.4 (2014), p. 044002. DOI: `10.1103/PhysRevD.90.044002`. arXiv: `1404.5635 [hep-th]`.

[13] Raphael Bousso et al. "Entropy on a null surface for interacting quantum field theories and the Bousso bound". In: *Phys.Rev.* D91.8 (2015), p. 084030. DOI: `10.1103/PhysRevD.91.084030`. arXiv: `1406.4545 [hep-th]`.

[14] Juan Martin Maldacena. "The Large N limit of superconformal field theories and supergravity". In: *Int. J. Theor. Phys.* 38 (1999). [Adv. Theor. Math. Phys.2,231(1998)], pp. 1113–1133. DOI: 10.1023/A:1026654312961. arXiv: hep-th/9711200 [hep-th].

[15] Raphael Bousso. "Holography in general space-times". In: *JHEP* 06 (1999), p. 028. eprint: hep-th/9906022.

[16] Raphael Bousso. "The holographic principle". In: *Rev. Mod. Phys.* 74 (2002), p. 825. eprint: hep-th/0203101.

[17] Idse Heemskerk et al. "Holography from Conformal Field Theory". In: *JHEP* 10 (2009), p. 079. DOI: 10.1088/1126-6708/2009/10/079. arXiv: 0907.0151 [hep-th].

[18] Raphael Bousso and Netta Engelhardt. "New Area Law in General Relativity". In: *Phys. Rev. Lett.* 115.8 (2015), p. 081301. DOI: 10.1103/PhysRevLett.115.081301. arXiv: 1504.07627 [hep-th].

[19] Raphael Bousso and Netta Engelhardt. "Proof of a New Area Law in General Relativity". In: *Phys. Rev.* D92.4 (2015), p. 044031. DOI: 10.1103/PhysRevD.92.044031. arXiv: 1504.07660 [gr-qc].

[20] Raphael Bousso and Mudassir Moosa. "Dynamics and Observer-Dependence of Holographic Screens". In: *Phys. Rev.* D95.4 (2017), p. 046005. DOI: 10.1103/PhysRevD.95.046005. arXiv: 1611.04607 [hep-th].

[21] Mudassir Moosa. "Non-relativistic geometry of holographic screens". In: *JHEP* 06.6 (2017), p. 038. DOI: 10.1007/JHEP06(2017)038. arXiv: 1702.06960 [hep-th].

[22] Michael A. Nielsen and Isaac L. Chuang. *Quantum Computation and Quantum Information*. Cambridge University Press, 2000.

[23] W. G. Unruh. "Notes on black hole evaporation". In: *Phys. Rev. D* 14 (1976), p. 870.

[24] Luca Bombelli et al. "A Quantum Source of Entropy for Black Holes". In: *Phys.Rev.* D34 (1986), pp. 373–383. DOI: 10.1103/PhysRevD.34.373.

[25] Mark Srednicki. "Entropy and area". In: *Phys.Rev.Lett.* 71 (1993), pp. 666–669. DOI: 10.1103/PhysRevLett.71.666. arXiv: hep-th/9303048 [hep-th].

[26] Shinsei Ryu and Tadashi Takayanagi. "Holographic derivation of entanglement entropy from AdS/CFT". In: *Phys.Rev.Lett.* 96 (2006), p. 181602. DOI: 10.1103/PhysRevLett.96.181602. arXiv: hep-th/0603001 [hep-th].

[27] Veronika E. Hubeny, Mukund Rangamani, and Tadashi Takayanagi. "A Covariant holographic entanglement entropy proposal". In: *JHEP* 0707 (2007), p. 062. DOI: 10.1088/1126-6708/2007/07/062. arXiv: 0705.0016 [hep-th].

[28] Aron C. Wall. "Maximin Surfaces, and the Strong Subadditivity of the Covariant Holographic Entanglement Entropy". In: *Class. Quant. Grav.* 31.22 (2014), p. 225007. DOI: 10.1088/0264-9381/31/22/225007. arXiv: 1211.3494 [hep-th].

[29] Aitor Lewkowycz and Juan Maldacena. "Generalized gravitational entropy". In: *JHEP* 1308 (2013), p. 090. DOI: 10.1007/JHEP08(2013)090. arXiv: 1304.4926 [hep-th].

[30] Xi Dong, Aitor Lewkowycz, and Mukund Rangamani. "Deriving covariant holographic entanglement". In: (2016). arXiv: 1607.07506 [hep-th].

[31] Mark Van Raamsdonk. "Building up spacetime with quantum entanglement". In: *Gen. Rel. Grav.* 42 (2010). [Int. J. Mod. Phys.D19,2429(2010)], pp. 2323–2329. DOI: 10.1007/s10714-010-1034-0,10.1142/S0218271810018529. arXiv: 1005.3035 [hep-th].

[32] Thomas Faulkner et al. "Gravitation from Entanglement in Holographic CFTs". In: *JHEP* 03 (2014), p. 051. DOI: 10.1007/JHEP03(2014)051. arXiv: 1312.7856 [hep-th].

[33] Ning Bao et al. "The Holographic Entropy Cone". In: *JHEP* 09 (2015), p. 130. DOI: 10.1007/JHEP09(2015)130. arXiv: 1505.07839 [hep-th].

[34] Stefan Leichenauer and Mudassir Moosa. "Entanglement Tsunami in (1+1)-Dimensions". In: *Phys. Rev.* D92 (2015), p. 126004. DOI: 10.1103/PhysRevD.92.126004. arXiv: 1505.04225 [hep-th].

[35] Stefan Leichenauer, Mudassir Moosa, and Michael Smolkin. "Dynamics of the Area Law of Entanglement Entropy". In: *JHEP* 09 (2016), p. 035. DOI: 10.1007/JHEP09(2016)035. arXiv: 1604.00388 [hep-th].

[36] Leonard Susskind. "Computational Complexity and Black Hole Horizons". In: *Fortsch. Phys.* 64 (2016). [Fortsch. Phys.64,24(2016)], pp. 44–48. DOI: 10.1002/prop.201500093, 10.1002/prop.201500092. arXiv: 1403.5695 [hep-th].

[37] Scott Aaronson. "The Complexity of Quantum States and Transformations: From Quantum Money to Black Holes". In: 2016. arXiv: 1607.05256 [quant-ph]. URL: https://inspirehep.net/record/1476631/files/arXiv:1607.05256.pdf.

[38] Douglas Stanford and Leonard Susskind. "Complexity and Shock Wave Geometries". In: *Phys. Rev.* D90.12 (2014), p. 126007. DOI: 10.1103/PhysRevD.90.126007. arXiv: 1406.2678 [hep-th].

[39] Adam R. Brown et al. "Holographic Complexity Equals Bulk Action?" In: *Phys. Rev. Lett.* 116.19 (2016), p. 191301. DOI: 10.1103/PhysRevLett.116.191301. arXiv: 1509.07876 [hep-th].

[40] Adam R. Brown et al. "Complexity, action, and black holes". In: *Phys. Rev.* D93.8 (2016), p. 086006. DOI: 10.1103/PhysRevD.93.086006. arXiv: 1512.04993 [hep-th].

[41] Norman Margolus and Lev B. Levitin. "The Maximum speed of dynamical evolution". In: *Physica* D120 (1998), pp. 188–195. DOI: 10.1016/S0167-2789(98)00054-2. arXiv: quant-ph/9710043 [quant-ph].

[42] S. Lloyd. "Ultimate physical limits to computation". In: *Nature* 406 (Aug. 2000). DOI: 10.1038/35023282. eprint: quant-ph/9908043.

[43] Mudassir Moosa. "Evolution of Complexity Following a Global Quench". In: (2017). DOI: 10.1007/JHEP03(2018)031. arXiv: 1711.02668 [hep-th].

[44] Mudassir Moosa. "Divergences in the rate of complexification". In: (2017). arXiv: 1712.07137 [hep-th].

[45] Raphael Bousso and Netta Engelhardt. "Generalized Second Law for Cosmology". In: *Phys. Rev.* D93.2 (2016), p. 024025. DOI: 10.1103/PhysRevD.93.024025. arXiv: 1510.02099 [hep-th].

[46] W. Fischler and L. Susskind. "Holography and cosmology". In: (1998). eprint: hep-th/9806039.

[47] Raphael Bousso et al. "A Quantum Focussing Conjecture". In: (2015). arXiv: 1506.02669 [hep-th].

[48] Raphael Bousso et al. "Proof of the Quantum Null Energy Condition". In: (2015). arXiv: 1509.02542 [hep-th].

[49] Jason Koeller and Stefan Leichenauer. "Holographic Proof of the Quantum Null Energy Condition". In: (2015). arXiv: 1512.06109 [hep-th].

[50] Fabio Sanches and Sean J. Weinberg. "A Holographic Entanglement Entropy Conjecture for General Spacetimes". In: *Phys. Rev.* D94.8 (2016), p. 084034. DOI: 10.1103/PhysRevD.94.084034. arXiv: 1603.05250 [hep-th].

[51] Fabio Sanches and Sean J. Weinberg. "Refinement of the Bousso-Engelhardt Area Law". In: *Phys. Rev.* D94.2 (2016), p. 021502. DOI: 10.1103/PhysRevD.94.021502. arXiv: 1604.04919 [hep-th].

[52] Yasunori Nomura et al. "Spacetime Equals Entanglement". In: (2016). DOI: 10.1016/j.physletb.2016.10.045. arXiv: 1607.02508 [hep-th].

[53] Abhay Ashtekar and Badri Krishnan. "Dynamical horizons: Energy, angular momentum, fluxes and balance laws". In: *Phys. Rev. Lett.* 89 (2002), p. 261101. DOI: 10.1103/PhysRevLett.89.261101. arXiv: gr-qc/0207080 [gr-qc].

[54] Sean A. Hayward. "General laws of black-hole dynamics". In: *Phys. Rev. D* 49 (12 June 1994), pp. 6467–6474. DOI: 10.1103/PhysRevD.49.6467. URL: http://link.aps.org/doi/10.1103/PhysRevD.49.6467.

[55] Abhay Ashtekar and Badri Krishnan. "Dynamical horizons and their properties". In: *Phys. Rev.* D68 (2003), p. 104030. DOI: 10.1103/PhysRevD.68.104030. arXiv: gr-qc/0308033 [gr-qc].

[56] Abhay Ashtekar and Badri Krishnan. "Isolated and dynamical horizons and their applications". In: *Living Rev. Rel.* 7 (2004), p. 10. DOI: 10.12942/lrr-2004-10. arXiv: gr-qc/0407042 [gr-qc].

[57] Eric Gourgoulhon. "A Generalized Damour-Navier-Stokes equation applied to trapping horizons". In: *Phys. Rev.* D72 (2005), p. 104007. DOI: 10.1103/PhysRevD.72.104007. arXiv: gr-qc/0508003 [gr-qc].

[58] Eric Gourgoulhon and Jose Luis Jaramillo. "Area evolution, bulk viscosity and entropy principles for dynamical horizons". In: *Phys. Rev.* D74 (2006), p. 087502. DOI: 10.1103/PhysRevD.74.087502. arXiv: gr-qc/0607050 [gr-qc].

[59] Eric Gourgoulhon and Jose Luis Jaramillo. "New theoretical approaches to black holes". In: *New Astron. Rev.* 51 (2008), pp. 791–798. DOI: 10.1016/j.newar.2008.03.026. arXiv: 0803.2944 [astro-ph].

[60] Sean A. Hayward. "Energy conservation for dynamical black holes". In: *Phys. Rev. Lett.* 93 (2004), p. 251101. DOI: 10.1103/PhysRevLett.93.251101. arXiv: gr-qc/0404077 [gr-qc].

[61] Sean A. Hayward. "Energy and entropy conservation for dynamical black holes". In: *Phys. Rev.* D70 (2004), p. 104027. DOI: 10.1103/PhysRevD.70.104027. arXiv: gr-qc/0408008 [gr-qc].

[62] Ivan Booth and Stephen Fairhurst. "Horizon energy and angular momentum from a Hamiltonian perspective". In: *Class. Quant. Grav.* 22 (2005), pp. 4515–4550. DOI: 10.1088/0264-9381/22/21/006. arXiv: gr-qc/0505049 [gr-qc].

[63] Ivan Booth et al. "Marginally trapped tubes and dynamical horizons". In: *Class. Quant. Grav.* 23 (2006), pp. 413–440. DOI: 10.1088/0264-9381/23/2/009. arXiv: gr-qc/0506119 [gr-qc].

[64] R. Bousso and S. W. Hawking. "Pair Creation of Black Holes During Inflation". In: *Phys. Rev. D* 54 (1996), pp. 6312–6322. eprint: gr-qc/9606052.

[65] Dam Thanh Son. "Newton-Cartan Geometry and the Quantum Hall Effect". In: (2013). arXiv: 1306.0638 [cond-mat.mes-hall].

[66] Kristan Jensen. "On the coupling of Galilean-invariant field theories to curved spacetime". In: (2014). arXiv: 1408.6855 [hep-th].

[67] Michael Geracie, Kartik Prabhu, and Matthew M. Roberts. "Fields and fluids on curved non-relativistic spacetimes". In: *JHEP* 08 (2015), p. 042. DOI: 10.1007/JHEP08(2015)042. arXiv: 1503.02680 [hep-th].

[68] Richard H. Price and Kip S. Thorne. "Membrane viewpoint on black holes: Properties and evolution of the stretched horizon". In: *Phys. Rev. D* 33 (4 Feb. 1986), pp. 915–941. DOI: 10.1103/PhysRevD.33.915. URL: http://link.aps.org/doi/10.1103/PhysRevD.33.915.

[69] T. Damour. "Quelques propriétés mécaniques, électromagnétiques, thermodynamiques et quantiques des trous noirs". In: *Thése de Doctorat d'Etat, Université Pierre et Marie Curie, Paris VI* (1979).

[70] Irene Bredberg et al. "From Navier-Stokes To Einstein". In: *JHEP* 07 (2012), p. 146. DOI: 10.1007/JHEP07(2012)146. arXiv: 1101.2451 [hep-th].

[71] Sean A. Hayward. "Gravitational wave dynamics and black hole dynamics: Second quasispherical approximation". In: *Class. Quant. Grav.* 18 (2001), pp. 5561–5582. DOI: 10.1088/0264-9381/18/24/316. arXiv: gr-qc/0102013 [gr-qc].

[72] J. R. Oppenheimer and H. Snyder. "On continued gravitational contraction". In: *Phys. Rev.* 56 (1939), pp. 455–459. DOI: 10.1103/PhysRev.56.455.

[73] P.C. Vaidya. "The gravitational field of a radiating star". In: *Proc. Indian Acad. Sci. (Math. Sci.)* (1951). DOI: 10.1007/BF03173260.

[74] W.B. Bonnor and P.C. Vaidya. "Spherically symmetric radiation of charge in Einstein-Maxwell theory". In: *Gen Relativity and Gravitation* (1970). DOI: 10.1007/BF00756891.

[75] Robert M. Wald. *General Relativity*. 1984. DOI: 10.7208/chicago/9780226870373.001.0001.

[76] Yasunori Nomura et al. "Toward a Holographic Theory for General Spacetimes". In: (2016). arXiv: 1611.02702 [hep-th].

[77] D. Bigatti and Leonard Susskind. "Review of matrix theory". In: *Strings, branes and dualities. Proceedings, NATO Advanced Study Institute, Cargese, France, May 26-June 14, 1997*. 1997, pp. 277–318. arXiv: hep-th/9712072 [hep-th]. URL: http://alice.cern.ch/format/showfull?sysnb=0264145.

[78] J. David Brown and James W. York Jr. "Quasilocal energy and conserved charges derived from the gravitational action". In: *Phys. Rev.* D47 (1993), pp. 1407–1419. DOI: 10.1103/PhysRevD.47.1407. arXiv: gr-qc/9209012 [gr-qc].

[79] E. Poisson. *A Relativist's Toolkit: The Mathematics of Black-Hole Mechanics*. Cambridge University Press, 2004. DOI: https://doi.org/10.1017/CBO9780511606601.

[80] Elie Cartan. "Sur les variétés à connexion affine et la théorie de la relativité généralisée (première partie)". fre. In: *Annales scientifiques de l'École Normale Supérieure* 40 (1923), pp. 325–412. URL: http://eudml.org/doc/81417.

[81] Elie Cartan. "Sur les variétés à connexion affine, et la théorie de la relativité généralisée (deuxième partie)". fre. In: *Annales scientifiques de l'École Normale Supérieure* 42 (1925), pp. 17–88. URL: http://eudml.org/doc/81430.

[82] Michael Geracie et al. "Spacetime Symmetries of the Quantum Hall Effect". In: *Phys. Rev.* D91 (2015), p. 045030. DOI: 10.1103/PhysRevD.91.045030. arXiv: 1407.1252 [cond-mat.mes-hall].

[83] Rabin Banerjee, Arpita Mitra, and Pradip Mukherjee. "Localization of the Galilean symmetry and dynamical realization of Newton-Cartan geometry". In: *Class. Quant. Grav.* 32.4 (2015), p. 045010. DOI: 10.1088/0264-9381/32/4/045010. arXiv: 1407.3617 [hep-th].

[84] Jelle Hartong, Elias Kiritsis, and Niels A. Obers. "Schrödinger Invariance from Lifshitz Isometries in Holography and Field Theory". In: *Phys. Rev.* D92 (2015), p. 066003. DOI: 10.1103/PhysRevD.92.066003. arXiv: 1409.1522 [hep-th].

[85] Rabin Banerjee and Pradip Mukherjee. "Torsional Newton–Cartan geometry from Galilean gauge theory". In: *Class. Quant. Grav.* 33.22 (2016), p. 225013. DOI: 10.1088/0264-9381/33/22/225013. arXiv: 1604.06893 [gr-qc].

[86] Kristan Jensen. "Aspects of hot Galilean field theory". In: *JHEP* 04 (2015), p. 123. DOI: 10.1007/JHEP04(2015)123. arXiv: 1411.7024 [hep-th].

[87] Arpita Mitra. "Weyl rescaled Newton-Cartan geometry and non-relativistic conformal hydrodynamics". In: (2015). arXiv: 1508.03207 [hep-th].

[88] Jelle Hartong and Niels A. Obers. "Hořava-Lifshitz gravity from dynamical Newton-Cartan geometry". In: *JHEP* 07 (2015), p. 155. DOI: 10.1007/JHEP07(2015)155. arXiv: 1504.07461 [hep-th].

[89] Petr Horava. "Quantum Gravity at a Lifshitz Point". In: *Phys. Rev.* D79 (2009), p. 084008. DOI: 10.1103/PhysRevD.79.084008. arXiv: 0901.3775 [hep-th].

[90] Morten H. Christensen et al. "Torsional Newton-Cartan Geometry and Lifshitz Holography". In: *Phys. Rev.* D89 (2014), p. 061901. DOI: 10.1103/PhysRevD.89.061901. arXiv: 1311.4794 [hep-th].

[91] Morten H. Christensen et al. "Boundary Stress-Energy Tensor and Newton-Cartan Geometry in Lifshitz Holography". In: *JHEP* 01 (2014), p. 057. DOI: 10.1007/JHEP01(2014)057. arXiv: 1311.6471 [hep-th].

[92] Jelle Hartong, Elias Kiritsis, and Niels A. Obers. "Lifshitz space–times for Schrödinger holography". In: *Phys. Lett.* B746 (2015), pp. 318–324. DOI: 10.1016/j.physletb.2015.05.010. arXiv: 1409.1519 [hep-th].

[93] Geoff Hayward. "Gravitational action for spacetimes with nonsmooth boundaries". In: *Phys. Rev. D* 47 (8 Apr. 1993), pp. 3275–3280. DOI: 10.1103/PhysRevD.47.3275. URL: http://link.aps.org/doi/10.1103/PhysRevD.47.3275.

[94] C. Robin Graham and Edward Witten. "Conformal anomaly of submanifold observables in AdS / CFT correspondence". In: *Nucl. Phys.* B546 (1999), pp. 52–64. DOI: 10.1016/S0550-3213(99)00055-3. arXiv: hep-th/9901021 [hep-th].

[95] Pasquale Calabrese and John L. Cardy. "Evolution of entanglement entropy in one-dimensional systems". In: *J.Stat.Mech.* 0504 (2005), P04010. DOI: 10.1088/1742-5468/2005/04/P04010. arXiv: cond-mat/0503393 [cond-mat].

[96] Pasquale Calabrese and John Cardy. "Entanglement entropy and conformal field theory". In: *J.Phys.* A42 (2009), p. 504005. DOI: 10.1088/1751-8113/42/50/504005. arXiv: 0905.4013 [cond-mat.stat-mech].

[97] Javier Abajo-Arrastia, Joao Aparicio, and Esperanza Lopez. "Holographic Evolution of Entanglement Entropy". In: *JHEP* 1011 (2010), p. 149. DOI: 10.1007/JHEP11(2010)149. arXiv: 1006.4090 [hep-th].

[98] V. Balasubramanian et al. "Thermalization of Strongly Coupled Field Theories". In: *Phys.Rev.Lett.* 106 (2011), p. 191601. DOI: 10.1103/PhysRevLett.106.191601. arXiv: 1012.4753 [hep-th].

[99] V. Balasubramanian et al. "Holographic Thermalization". In: *Phys.Rev.* D84 (2011), p. 026010. DOI: 10.1103/PhysRevD.84.026010. arXiv: 1103.2683 [hep-th].

[100] Thomas Hartman and Juan Maldacena. "Time Evolution of Entanglement Entropy from Black Hole Interiors". In: *JHEP* 1305 (2013), p. 014. DOI: 10.1007/JHEP05(2013)014. arXiv: 1303.1080 [hep-th].

[101] Hong Liu and S. Josephine Suh. "Entanglement Tsunami: Universal Scaling in Holographic Thermalization". In: *Phys.Rev.Lett.* 112 (2014), p. 011601. DOI: 10.1103/PhysRevLett.112.011601. arXiv: 1305.7244 [hep-th].

[102] Hong Liu and S. Josephine Suh. "Entanglement growth during thermalization in holographic systems". In: *Phys.Rev.* D89.6 (2014), p. 066012. DOI: 10.1103/PhysRevD.89.066012. arXiv: 1311.1200 [hep-th].

[103] V. Balasubramanian et al. "Thermalization of mutual and tripartite information in strongly coupled two dimensional conformal field theories". In: *Phys.Rev.* D84 (2011), p. 105017. DOI: 10.1103/PhysRevD.84.105017. arXiv: 1110.0488 [hep-th].

[104] Curtis T. Asplund and Alice Bernamonti. "Mutual information after a local quench in conformal field theory". In: *Phys.Rev.* D89.6 (2014), p. 066015. DOI: 10.1103/PhysRevD.89.066015. arXiv: 1311.4173 [hep-th].

[105] Andrea Allais and Erik Tonni. "Holographic evolution of the mutual information". In: *JHEP* 1201 (2012), p. 102. DOI: 10.1007/JHEP01(2012)102. arXiv: 1110.1607 [hep-th].

[106] Pasquale Calabrese and John L. Cardy. "Entanglement entropy and quantum field theory". In: *J.Stat.Mech.* 0406 (2004), P06002. DOI: 10.1088/1742-5468/2004/06/P06002. arXiv: hep-th/0405152 [hep-th].

[107] Pasquale Calabrese, John Cardy, and Erik Tonni. "Entanglement entropy of two disjoint intervals in conformal field theory". In: *J.Stat.Mech.* 0911 (2009), P11001. DOI: 10.1088/1742-5468/2009/11/P11001. arXiv: 0905.2069 [hep-th].

[108] Thomas Hartman. "Entanglement Entropy at Large Central Charge". In: (2013). arXiv: 1303.6955 [hep-th].

[109] Thomas Faulkner. "The Entanglement Renyi Entropies of Disjoint Intervals in AdS/CFT". In: (2013). arXiv: 1303.7221 [hep-th].

[110] Pasquale Calabrese and John Cardy. "Quantum Quenches in Extended Systems". In: *J.Stat.Mech.* 0706 (2007), P06008. DOI: 10.1088/1742-5468/2007/06/P06008. arXiv: 0704.1880 [cond-mat.stat-mech].

[111] Pasquale Calabrese and John L. Cardy. "Time-dependence of correlation functions following a quantum quench". In: *Phys.Rev.Lett.* 96 (2006), p. 136801. DOI: 10.1103/PhysRevLett.96.136801. arXiv: cond-mat/0601225 [cond-mat].

[112] John L. Cardy. "Boundary conformal field theory". In: (2004). arXiv: hep-th/0411189 [hep-th].

[113] P. Di Francesco, P. Mathieu, and D. Senechal. *Conformal field theory*. 1997.

[114] Andrea Coser, Erik Tonni, and Pasquale Calabrese. "Entanglement negativity after a global quantum quench". In: *J.Stat.Mech.* 1412.12 (2014), P12017. DOI: 10.1088/1742-5468/2014/12/P12017. arXiv: 1410.0900 [cond-mat.stat-mech].

[115] Don N. Page. "Average entropy of a subsystem". In: *Phys.Rev.Lett.* 71 (1993), pp. 1291–1294. DOI: 10.1103/PhysRevLett.71.1291. arXiv: gr-qc/9305007 [gr-qc].

[116] Horacio Casini, Hong Liu, and Márk Mezei. "Spread of entanglement and causality". In: *JHEP* 07 (2016), p. 077. DOI: 10.1007/JHEP07(2016)077. arXiv: 1509.05044 [hep-th].

[117] Curtis T. Asplund et al. "Entanglement Scrambling in 2d Conformal Field Theory". In: *JHEP* 09 (2015), p. 110. DOI: 10.1007/JHEP09(2015)110. arXiv: 1506.03772 [hep-th].

[118] Mukund Rangamani, Moshe Rozali, and Alexandre Vincart-Emard. "Dynamics of Holographic Entanglement Entropy Following a Local Quench". In: (2015). arXiv: 1512.03478 [hep-th].

[119] Ling-Yan Hung, Robert C. Myers, and Michael Smolkin. "Some Calculable Contributions to Holographic Entanglement Entropy". In: *JHEP* 08 (2011), p. 039. DOI: 10.1007/JHEP08(2011)039. arXiv: 1105.6055 [hep-th].

[120] Sergey N. Solodukhin. "Entanglement entropy, conformal invariance and extrinsic geometry". In: *Phys.Lett.* B665 (2008), pp. 305–309. DOI: 10.1016/j.physletb.2008.05.071. arXiv: 0802.3117 [hep-th].

[121] Ling-Yan Hung, Robert C. Myers, and Michael Smolkin. "On Holographic Entanglement Entropy and Higher Curvature Gravity". In: *JHEP* 1104 (2011), p. 025. DOI: 10.1007/JHEP04(2011)025. arXiv: 1101.5813 [hep-th].

[122] Dmitri V. Fursaev, Alexander Patrushev, and Sergey N. Solodukhin. "Distributional Geometry of Squashed Cones". In: *Phys.Rev.* D88.4 (2013), p. 044054. DOI: 10.1103/PhysRevD.88.044054. arXiv: 1306.4000 [hep-th].

[123] Xi Dong. "Holographic Entanglement Entropy for General Higher Derivative Gravity". In: *JHEP* 1401 (2014), p. 044. DOI: 10.1007/JHEP01(2014)044. arXiv: 1310.5713 [hep-th].

[124] Joan Camps. "Generalized entropy and higher derivative Gravity". In: *JHEP* 03 (2014), p. 070. DOI: 10.1007/JHEP03(2014)070. arXiv: 1310.6659 [hep-th].

[125] Andrea Allais and Márk Mezei. "Some results on the shape dependence of entanglement and Rényi entropies". In: (2014). arXiv: 1407.7249 [hep-th].

[126] Mark Mezei. "Entanglement entropy across a deformed sphere". In: (2014). arXiv: 1411.7011 [hep-th].

[127] Thomas Faulkner, Robert G. Leigh, and Onkar Parrikar. "Shape Dependence of Entanglement Entropy in Conformal Field Theories". In: (2015). arXiv: 1511.05179 [hep-th].

[128] Lorenzo Bianchi et al. "Renyi Entropy and Conformal Defects". In: (2015). arXiv: 1511.06713 [hep-th].

[129] Vladimir Rosenhaus and Michael Smolkin. "Entanglement Entropy for Relevant and Geometric Perturbations". In: *JHEP* 02 (2015), p. 015. DOI: 10.1007/JHEP02(2015)015. arXiv: 1410.6530 [hep-th].

[130] Thomas Faulkner. "Bulk Emergence and the RG Flow of Entanglement Entropy". In: *JHEP* 05 (2015), p. 033. DOI: 10.1007/JHEP05(2015)033. arXiv: 1412.5648 [hep-th].

[131] Vladimir Rosenhaus and Michael Smolkin. "Entanglement Entropy: A Perturbative Calculation". In: (2014). arXiv: 1403.3733 [hep-th].

[132] S. S. Gubser, Igor R. Klebanov, and Alexander M. Polyakov. "Gauge theory correlators from noncritical string theory". In: *Phys. Lett.* B428 (1998), pp. 105–114. DOI: 10.1016/S0370-2693(98)00377-3. arXiv: hep-th/9802109 [hep-th].

[133] Edward Witten. "Anti-de Sitter space and holography". In: *Adv. Theor. Math. Phys.* 2 (1998), pp. 253–291. arXiv: hep-th/9802150 [hep-th].

[134] Igor R. Klebanov and Edward Witten. "AdS / CFT correspondence and symmetry breaking". In: *Nucl. Phys.* B556 (1999), pp. 89–114. DOI: 10.1016/S0550-3213(99)00387-9. arXiv: hep-th/9905104 [hep-th].

[135] Andrea Cappelli, Daniel Friedan, and Jose I. Latorre. "C theorem and spectral representation". In: *Nucl.Phys.* B352 (1991), pp. 616–670. DOI: 10.1016/0550-3213(91)90102-4.

[136] Joseph J. Bisognano and Eyvind H. Wichmann. "On the duality condition for a Hermitian scalar field". In: *Journal of Mathematical Physics* 16.4 (1975), pp. 985–1007. DOI: http://dx.doi.org/10.1063/1.522605. URL: http://scitation.aip.org/content/aip/journal/jmp/16/4/10.1063/1.522605.

[137] Joseph J. Bisognano and Eyvind H. Wichmann. "On the duality condition for quantum fields". In: *Journal of Mathematical Physics* 17.3 (1976), pp. 303–321. DOI: http://dx.doi.org/10.1063/1.522898. URL: http://scitation.aip.org/content/aip/journal/jmp/17/3/10.1063/1.522898.

[138] Daniel N. Kabat and M.J. Strassler. "A Comment on entropy and area". In: *Phys.Lett.* B329 (1994), pp. 46–52. DOI: 10.1016/0370-2693(94)90515-0. arXiv: hep-th/9401125 [hep-th].

[139] Luis C.B. Crispino, Atsushi Higuchi, and George E.A. Matsas. "The Unruh effect and its applications". In: *Rev.Mod.Phys.* 80 (2008), pp. 787–838. DOI: 10.1103/RevModPhys.80.787. arXiv: 0710.5373 [gr-qc].

[140] Mark P. Hertzberg and Frank Wilczek. "Some Calculable Contributions to Entanglement Entropy". In: *Phys.Rev.Lett.* 106 (2011), p. 050404. DOI: 10.1103/PhysRevLett.106.050404. arXiv: 1007.0993 [hep-th].

[141] Marina Huerta. "Numerical Determination of the Entanglement Entropy for Free Fields in the Cylinder". In: *Phys.Lett.* B710 (2012), pp. 691–696. DOI: 10.1016/j.physletb.2012.03.044. arXiv: 1112.1277 [hep-th].

[142] Aitor Lewkowycz, Robert C. Myers, and Michael Smolkin. "Observations on entanglement entropy in massive QFT's". In: *JHEP* 1304 (2013), p. 017. DOI: 10.1007/JHEP04(2013)017. arXiv: 1210.6858 [hep-th].

[143] Horacio Casini, F. D. Mazzitelli, and Eduardo Testé. "Area terms in entanglement entropy". In: *Phys. Rev.* D91.10 (2015), p. 104035. DOI: 10.1103/PhysRevD.91.104035. arXiv: 1412.6522 [hep-th].

[144] Omer Ben-Ami, Dean Carmi, and Michael Smolkin. "Renormalization group flow of entanglement entropy on spheres". In: *JHEP* 08 (2015), p. 048. DOI: 10.1007/JHEP08(2015)048. arXiv: 1504.00913 [hep-th].

[145] Chris Akers et al. "Entanglement and RG in the $O(N)$ vector model". In: (2015). arXiv: 1512.00791 [hep-th].

[146] Hong Liu and Mark Mezei. "A Refinement of entanglement entropy and the number of degrees of freedom". In: *JHEP* 1304 (2013), p. 162. DOI: 10.1007/JHEP04(2013)162. arXiv: 1202.2070 [hep-th].

[147] H. Osborn and A.C. Petkou. "Implications of conformal invariance in field theories for general dimensions". In: *Annals Phys.* 231 (1994), pp. 311–362. DOI: 10.1006/aphy.1994.1045. arXiv: hep-th/9307010 [hep-th].

[148] J. Erdmenger and H. Osborn. "Conserved currents and the energy momentum tensor in conformally invariant theories for general dimensions". In: *Nucl.Phys.* B483 (1997), pp. 431–474. DOI: 10.1016/S0550-3213(96)00545-7. arXiv: hep-th/9605009 [hep-th].

[149] Michael Smolkin and Sergey N. Solodukhin. "Correlation functions on conical defects". In: *Phys. Rev.* D91.4 (2015), p. 044008. DOI: 10.1103/PhysRevD.91.044008. arXiv: 1406.2512 [hep-th].

[150] Vladimir Rosenhaus and Michael Smolkin. "Entanglement entropy, planar surfaces, and spectral functions". In: *JHEP* 09 (2014), p. 119. DOI: 10.1007/JHEP09(2014)119. arXiv: 1407.2891 [hep-th].

[151] Stephen H. Shenker and Douglas Stanford. "Black holes and the butterfly effect". In: *JHEP* 03 (2014), p. 067. DOI: 10.1007/JHEP03(2014)067. arXiv: 1306.0622 [hep-th].

[152] Run-Qiu Yang. "Strong energy condition and complexity growth bound in holography". In: *Phys. Rev.* D95.8 (2017), p. 086017. DOI: 10.1103/PhysRevD.95.086017. arXiv: 1610.05090 [gr-qc].

[153] Mohammad M. Qaemmaqami. "On Complexity Growth in Minimal Massive 3D Gravity". In: (2017). arXiv: 1709.05894 [hep-th].

[154] Shira Chapman, Hugo Marrochio, and Robert C. Myers. "Complexity of Formation in Holography". In: *JHEP* 01 (2017), p. 062. DOI: 10.1007/JHEP01(2017)062. arXiv: 1610.08063 [hep-th].

[155] Dean Carmi et al. "On the Time Dependence of Holographic Complexity". In: (2017). arXiv: 1709.10184 [hep-th].

[156] Keun-Young Kim et al. "Comparison of holographic and field theoretic complexities by time dependent thermofield double states". In: (2017). arXiv: 1710.00600 [hep-th].

[157] Josiah Couch et al. "Holographic complexity and non-commutative gauge theory". In: (2017). arXiv: 1710.07833 [hep-th].

[158] Dean Carmi, Robert C. Myers, and Pratik Rath. "Comments on Holographic Complexity". In: *JHEP* 03 (2017), p. 118. DOI: 10.1007/JHEP03(2017)118. arXiv: 1612.00433 [hep-th].

[159] Koji Hashimoto, Norihiro Iizuka, and Sotaro Sugishita. "Time Evolution of Complexity in Abelian Gauge Theories - And Playing Quantum Othello Game -". In: (2017). arXiv: 1707.03840 [hep-th].

[160] Robert A. Jefferson and Robert C. Myers. "Circuit complexity in quantum field theory". In: *JHEP* 10 (2017), p. 107. DOI: 10.1007/JHEP10(2017)107. arXiv: 1707.08570 [hep-th].

[161] Shira Chapman et al. "Towards Complexity for Quantum Field Theory States". In: (2017). arXiv: 1707.08582 [hep-th].

[162] Run-Qiu Yang. "A Complexity for Quantum Field Theory States and Application in Thermofield Double States". In: (2017). arXiv: 1709.00921 [hep-th].

[163] Tameem Albash and Clifford V. Johnson. "Evolution of Holographic Entanglement Entropy after Thermal and Electromagnetic Quenches". In: *New J. Phys.* 13 (2011), p. 045017. DOI: 10.1088/1367-2630/13/4/045017. arXiv: 1008.3027 [hep-th].

[164] Vaios Ziogas. "Holographic mutual information in global Vaidya-BTZ spacetime". In: *JHEP* 09 (2015), p. 114. DOI: 10.1007/JHEP09(2015)114. arXiv: 1507.00306 [hep-th].

[165] Mohammad Reza Tanhayi. "Thermalization of Mutual Information in Hyperscaling Violating Backgrounds". In: *JHEP* 03 (2016), p. 202. DOI: 10.1007/JHEP03(2016)202. arXiv: 1512.04104 [hep-th].

[166] Allic Sivaramakrishnan. "Localized Excitations from Localized Unitary Operators". In: *Annals Phys.* 381 (2017), pp. 41–67. DOI: 10.1016/j.aop.2017.03.012. arXiv: 1604.00965 [hep-th].

[167] Márk Mezei and Douglas Stanford. "On entanglement spreading in chaotic systems". In: *JHEP* 05 (2017), p. 065. DOI: 10.1007/JHEP05(2017)065. arXiv: 1608.05101 [hep-th].

[168] Eyal Leviatan et al. "Quantum thermalization dynamics with Matrix-Product States". In: (2017). arXiv: 1702.08894 [cond-mat.stat-mech].

[169] Sagar F. Lokhande, Gerben W. J. Oling, and Juan F. Pedraza. "Linear response of entanglement entropy from holography". In: *JHEP* 10 (2017), p. 104. DOI: 10.1007/JHEP10(2017)104. arXiv: 1705.10324 [hep-th].

[170] M. Mestyán et al. "Exact solution for the quench dynamics of a nested integrable system". In: *J. Stat. Mech.* 1708.8 (2017), p. 083103. DOI: 10.1088/1742-5468/aa7df0.

[171] Mario Flory et al. "Time dependence of entanglement for steady state formation in AdS_3/CFT_2". In: *3rd Karl Schwarzschild Meeting on Gravitational Physics and the Gauge/Gravity Correspondence (KSM 2017) Frankfurt am Main, Germany, July 24-28, 2017*. 2017. arXiv: 1709.08614 [hep-th]. URL: http://inspirehep.net/record/1625285/files/arXiv:1709.08614.pdf.

[172] J. David Brown. "Action functionals for relativistic perfect fluids". In: *Class. Quant. Grav.* 10 (1993), pp. 1579–1606. DOI: 10.1088/0264-9381/10/8/017. arXiv: gr-qc/9304026 [gr-qc].

[173] Jiri Bicak and Karel V. Kuchar. "Null dust in canonical gravity". In: *Phys. Rev.* D56 (1997), pp. 4878–4895. DOI: 10.1103/PhysRevD.56.4878. arXiv: gr-qc/9704053 [gr-qc].

[174] Luis Lehner et al. "Gravitational action with null boundaries". In: *Phys. Rev.* D94.8 (2016), p. 084046. DOI: 10.1103/PhysRevD.94.084046. arXiv: 1609.00207 [hep-th].

[175] Alan Reynolds and Simon F. Ross. "Divergences in Holographic Complexity". In: *Class. Quant. Grav.* 34.10 (2017), p. 105004. DOI: 10.1088/1361-6382/aa6925. arXiv: 1612.05439 [hep-th].

[176] Leonard Susskind and Ying Zhao. "Switchbacks and the Bridge to Nowhere". In: (2014). arXiv: 1408.2823 [hep-th].

[177] Seyed Ali Hosseini Mansoori and Mohammad M. Qaemmaqami. "Complexity Growth, Butterfly Velocity and Black hole Thermodynamics". In: (2017). arXiv: 1711.09749 [hep-th].

[178] William Cottrell and Miguel Montero. "Complexity is Simple". In: (2017). arXiv: 1710.01175 [hep-th].

[179] Ofer Aharony et al. "Large N field theories, string theory and gravity". In: *Phys. Rept.* 323 (2000), pp. 183–386. DOI: 10.1016/S0370-1573(99)00083-6. arXiv: hep-th/9905111 [hep-th].

[180] Alex Buchel, Luis Lehner, and Robert C. Myers. "Thermal quenches in N=2* plasmas". In: *JHEP* 08 (2012), p. 049. DOI: 10.1007/JHEP08(2012)049. arXiv: 1206.6785 [hep-th].

[181] Alex Buchel et al. "Quantum quenches of holographic plasmas". In: *JHEP* 05 (2013), p. 067. DOI: 10.1007/JHEP05(2013)067. arXiv: 1302.2924 [hep-th].

[182] Alex Buchel, Robert C. Myers, and Anton van Niekerk. "Universality of Abrupt Holographic Quenches". In: *Phys. Rev. Lett.* 111 (2013), p. 201602. DOI: 10.1103/PhysRevLett.111.201602. arXiv: 1307.4740 [hep-th].

[183] G. W. Gibbons and S. W. Hawking. "Action Integrals and Partition Functions in Quantum Gravity". In: *Phys. Rev.* D15 (1977), pp. 2752–2756. DOI: 10.1103/PhysRevD.15.2752.

[184] Pablo Minces and Victor O. Rivelles. "Scalar field theory in the AdS / CFT correspondence revisited". In: *Nucl. Phys.* B572 (2000), pp. 651–669. DOI: 10.1016/S0550-3213(99)00833-0. arXiv: hep-th/9907079 [hep-th].

[185] Massimo Bianchi, Daniel Z. Freedman, and Kostas Skenderis. "Holographic renormalization". In: *Nucl. Phys.* B631 (2002), pp. 159–194. DOI: 10.1016/S0550-3213(02)00179-7. arXiv: hep-th/0112119 [hep-th].

[186] Charles Fefferman and C. Robin Graham. "The ambient metric". In: (2007). arXiv: 0710.0919 [math.DG].

[187] Sean A. Hayward. "Quasilocal gravitational energy". In: *Phys. Rev.* D49 (1994), pp. 831–839. DOI: 10.1103/PhysRevD.49.831. arXiv: gr-qc/9303030 [gr-qc].